



This is to certify that the

thesis entitled

EXCHANGE KINETICS OF THE SOLIUM ION WITH SOME CROWN ETHERS IN TETRANY DROFURAN SOLUTIONS.

presented by

PATRICE SZCZYGIEL

has been accepted towards fulfillment of the requirements for

M.S. degree in Chemi, stry

M-I--

Date_ 12/06/84

0-7639

MSU is an Affirmative Action/Fauel Onner



RETURNING MATERIALS:
Place in book drop to remove this checkout from your record. FINES will be charged if book is returned after the date stamped below.

EXCHANGE KINETICS OF THE SODIUM ION WITH SOME CROWN ETHERS IN TETRAHYDROFURAN SOLUTIONS

By

Patrice Szczygiel

A DISSERTATION

Submitted to

Michigan State University
in partial fulfillment of the requirements

for the degree of

MASTER OF SCIENCE

Department of Chemistry

ABSTRACT

EXCHANGE KINETICS OF THE SODIUM ION WITH SOME CROWN ETHERS IN TETRAHYDROFURAN SOLUTIONS

By

Patrice Szczygiel

The exchange kinetics of the sodium cation with 18 member ring crown ethers in tetrahydrofuran (THF) solutions were investigated.

The dependence of the exchange on the counteranion and on ligand substitution were studied by sodium-23 NMR spectroscopy and by electrical conductance. The anions used were tetraphenylborate (BPh₄⁻), thiocyanate (SCN⁻), iodide (I⁻), perchlorate (ClO₄⁻), hexafluoroarsenate (AsF₆⁻) and pentamethylcyclopentadienide (Cp(CH₃)₅⁻) and the ligands used were 18-crown-6 (18C6), dibenzo-18-crown-6, dicyclohexyl-18-crown-6 (DC18C6) cis-anti-cis and cis-syn-cis, diaza-18-crown-6 (DA18C6) and dithia-18-crown-6 (DT18C6). For ligands containing only oxygens as the donor atoms, the results indicate that strong ion pairing of the free and complexed salts observed with SCN⁻, I⁻, ClO₄⁻, AsF₆⁻, Cp(CH₃)₅⁻ gives fast exchange on the NMR time scale at room temperature while the loose ion pairing of the free and complexed salt observed with BPh₄⁻ gives slow exchange under the same conditions, showing the 18C6 analogs to have the same kinetic behavior. Upon substitution of oxygens by softer donor atoms, such as in DA18C6

and DT18C6, only room temperature fast exchanges are observed that are better explained in terms of complex stabilities rather than ionic association.

The parameters characterizing the exchange kinetics of sodium thiocyanate with the two isomers of DC18C6 and with DA18C6 in THF were obtained from a quantitative lineshape analysis of the sodium-23 NMR signals. With DC18C6 cis-anti-cis and cis-syn-cis, the cation exchanges via the bimolecular exchange mechanism with fast rates of decomplexation: 19.83 x 10^4 and 10.88 x 10^5 M^{-1} .sec⁻¹ respectively. The activation parameters are very similar with both crowns and an averaged Arrhenius activation energy of 2.75 kcal/mol and an averaged free energy of activation (ΔG^{\ddagger}) of 10.02 kcal/mol were obtained. With DA18C6 the associative dissociative exchange mechanism, with $\Delta G^{\ddagger}=12.85$ kcal/mol at 25°C, is predominant down to -20°C while the bimolecular exchange mechanism, offering a lower energy barrier for decomplexation with $\Delta G^{\ddagger}=8.53$ kcal/mol at -40°C, becomes predominant below -35°C.

To My Parents

ACKNOWLEDGEMENTS

The author wishes to express his deepest appreciation to Professor Alexander I. Popov for his guidance and encouragement throughout the course of this research program.

Gratitude is also extended to the Department of Chemistry, Michigan State University and to the National Science Foundation for financial aid.

Deep appreciation is given to Mr. Bonnet, director of the Ecole Supérieure de Chimie Industrielle de Lyon (France), for making all that I have done possible on a certain day of July, 1979.

Many thanks go to Mr. Nicolaon, Scientific Attaché at the French Ambassy, for his last-minute help and recommendations before I left France and to Professor Huet for his help during his visits at MSU.

Special thanks go to all the past and present members of the research group for their friendship, help and suggestions and in particular to Bruce for catalyzing several of my rate limiting steps.

Many thanks go to Sharon Corner for typing this thesis.

Finally, I wish to thank all my friends (from New York City to California) for making my stay in this country more enjoyable.

TABLE OF CONTENTS

Chapter				Page
LIST OF 7	TABLES			
LIST OF I	FIGURES	5		
INTRODU	CTION.	•••••		1
CHAPTEI	R I – HIS	TORICAI	REVIEW	5
1.1	The Phy	ysicochen	nical Methods	6
1.2	The Me	chanisms	of Exchange	15
1.3	The Kir	netic Res	ults	22
CHAPTE	R II – EX	PERIME	NTAL PART	45
2.1	Salts ar	nd Ligand	s Purification	46
2.2	Solvent	Purifica	tion	50
2.3	Sample	Preparat	ion	53
	2.3.1	Kinetic	Measurements	53
	2.3.2	Formati	on Constants Measurements	55
	2.3.3	Conduct	ance Measurements	55
2.4	NMR M	leasureme	ents	56
	2.4.1	Proton N	NMR Measurements	56
	2.4.2	Sodium-	23 NMR Measurements	56
		2.4.2.1	Instrumentation	56
		2.4.2.2	Reference Solution	56
		2.4.2.3	Field-Frequency Lock and Temperature Control	57
		2.4.2.4	Measurements of the Sodium-23 Chemical Shifts at High and Low Temperature	58

Chapte	er				Page
		2.4.2.5	Data Acq	uisition and Signal Processing	58
			2.4.2.5.1	Signal Averaging	59
			2.4.2.5.2	Zero-Filling Technique	59
			2.4.2.5.3	Sensitivity Enhancement	60
	2.4.3	Data Ha	indling		60
2.9	5 Condu	ctance Me	easurement	s	62
	2.5.1	Conduct	ance Equip	ments	62
	2.5.2	Data Ha	ındling		63
CHAPT	(OF THE E	XCHANGE 6 AND SON	RE SODIUM-23 NMR STUDY OF SOME SODIUM SALTS ME SUBSTITUTED ANALOGS	
	j	N THF	••••••		66
3.	l Introd	uction	••••••		67
3.5	2 Result	s and Disc	cussion		68
3.3	3 Conclu	usion	••••••		91
CHAPT	7	TION BET	WEEN THE	JDY OF THE IONIC ASSOCIA- SOLVATED AND COMPLEXED OME ANIONS IN THF	93
4.1	l Introd	uction	•••••		94
4.5	2 Result	s and Disc	cussion		94
4.:	B Conclu	usion	•••••		105
CHAPT	C	YANATE IS AND T	WITH DA18 HE CIS-SYI	EXATION OF SODIUM THIO- 8C6 AND WITH THE CIS-ANTI- N-CIS ISOMERS OF DC18C6 3 NMR SPECTROSCOPY	106
5. 1					107
5.2					107
•••	5.2.1	Sodium-	23 NMR of	Solvated and Complexed nce of Chemical Exchange	107
	5.2.2	Betweer	NaSCN So	anism for the Exchange Divated and Complexed by	118

Chapter				Page
		5.2.2.1	Sodium-23 NMR Study of the Stability of the DA18C6 Complex of NaSCN in THF at Various Temperatures	118
		5.2.2.2	The Kinetic Results	124
	5.2.3		s and Mechanism for the Exchange Between Solvated and Complexed by DC18C6 in THF	138
	5.2.4		Discussion: Rates and Activation ters	143
5.3	Conclu	sion		149
5.4	Future	Work		150
APPEND	N' SP	CFTB-1 PECTRA	IE NTCDTL SUBROUTINE OF THE NICOLET 180 PROGRAM FOR TRANSFERING NMR FROM THE BRUKER WH-180 NMR SPEC- R ONTO A FLOPPY DISK	153
APPEND	Г	APE INT	R OF NMR SPECTRA FROM A MAGNETIC O PERMANENT MEMORY ON A CIBER COMPUTER	155
APPEND	IX III -	KINFIT S LORENT TIME, LI DEPHAS	SUBROUTINE EQUATION FOR AN NMR ZIAN LINESHAPE CORRECTED FOR DELAY NE BROADENING AND ZERO-ORDER ING IN THE ABSENCE OF CHEMICAL IGE	157
APPEND		SHAPE C GOING C NONEQU TIME, LI	SUBROUTINE EQUATION FOR AN NMR LINE- OF AN UNCOUPLED SPIN SYSTEM UNDER- CHEMICAL EXCHANGE BETWEEN TWO UIVALENT SITES CORRECTED FOR DELAY NE BROADENING AND ZERO-ORDER ING	159
APPEND	IX V - A	APPLICA'	TION OF THE COMPUTER PROGRAM KINFIT CALCULATION OF COMPLEX FORMATION ITS FROM THE NMR DATA	161
APPEND	IX VI -	CALCUL	ATION AND PROPAGATION OF ERRORS	164
APPEND		TION PA FOR DEI ZERO-O	TION OF THE LINESHAPE OF THE ABSORP- RT OF THE NMR SPECTRUM CORRECTED LAY TIME DE, LINE BROADENING LB AND RDER DEPHASING IN THE ABSENCE OF AL EXCHANGE	167
REFERE				

LIST OF TABLES

Table		Page
1	Rate Constants for the Formation of Some Cryptates	
	in Propylene Carbonate at 25°C	23
2	Rate Constants of Cryptand Exchange at 25°C	24
3	Rate Constants for the Cryptate (Ag·C222)+ in	
	Acetonitrile-Water Mixtures at 25°C	25
4	Rate Constants for the Formation of Some Cryptates	
	at 25°C	27
5	Rate Constants and Activation Parameters of Some	
	Crown Complexes in Methanol	32
6	Rate Constants for the Complexation of 18C6 in Various	
	Solvents	36
7	Rate Constants and Activation Parameters for the	
	Change of Conformation of 18C6 in Various Solvents	38
8	Activation Parameters for the Complexation of 18C6	
	in DMF According to a Three Steps Eigen-Winkler	
	Mechanism	39
9	Activation Parameters and Exchange Rates for Some	
	Crown Complexes in Various Solvents	41
10	Cells Constants for Various Frequencies at 25.00°C	
	± 0.05°C	64
11	Key Properties of Tetrahydrofuran	69

Table		Page
12	Sodium-23 Chemical Shifts and Linewidths at Half-Height	
	of Some Sodium Salts Undergoing Chemical Exchange	
	with Some 18 Member Ring Crown Ethers in THE	70
13	Equivalent Conductances of Some Sodium Salts Solvated	
	and Complexed by 18C6 and DA18C6 at a Concentration	
	of 0.010 <u>M</u> and at 25.00 ± 0.05°C in THF	96
14	Transverse Relaxation Times and Sodium-23 NMR	
	Frequencies for NaSCN Solvated or Complexed in THF	
	Solutions at Various Temperatures	109
15	Activation Energy, E _r , for Solvent Reorganization and	
	Transverse Relaxation Time T ₂ at 25°C for NaSCN 0.0100	
	$\underline{\mathtt{M}}$ Solvated and Complexed in THF	117
16	Sodium-23 Chemical Shifts of Solutions Containing	
	NaSCN and DA18C6 at Various Mole Ratios and	
	Temperatures in THF	121
17	Temperature Dependence of the Relaxation Time of	
	the Exchange Between NaSCN Solvated and Complexed	
	by DA18C6 in THF	130
18	Values of $1/[Na^+]_{eq}$ and $1/(\tau \times C_{Na}^+)$ at Various	
	Temperatures for NaSCN Solutions Containing DA18C6	
	at Two Different Concentrations in THF	136
19	Values of the Dissociation Rates and of $1/\tau_{NaC}^+$ for	
	a THF Solution Containing NaSCN and DA18C6 at a	
	Ligand/Na ⁺ Mole Ratio of 0.53 and at Different	
	Temperatures	137

Table		Page
20	Temperature Dependence of the Relaxation Time of	
	the Exchange Between NaSCN Solvated and Complexed	
	by DC18C6 in THF	139
21	Activation Parameters and Rates for the Dissociation	
	of NaSCN Complexes in THF	145
22	Activation Parameters and Rates for the Formation	
	of the NaSCN·DA18C6 Complex in THF	148

LIST OF FIGURES

Figure		Page
1	Structures of some naturally occuring and some	
	synthetic macrocyclic compounds	3
2	Possible ionic associations in low dielectric solvents;	
	(a) Contact ion pair; (b) Solvent shared ion pair; (c)	
	Solvent separated ion pair; (d) Triple ions; (e)	
	Quadrupoles; (f) Higher aggregates such as octopoles	
	(n = $4,27$). The species M^+ , X^- and S are the metal	
	ion, the counter anion and the solvent molecule	
	respectively. All the species presented are solvated	
	although, for more clarity, it is omitted. In equation	
	(a) the two ionic species are in contact, in equation	
	(b) at least one solvent molecule is shared by both	
	ions in their first solvation sphere and in equation	
	(c) the two ions have their first solvation sphere either	
	in contact or separated by solvent molecules	7
3	Chemical Kinetics "Time Line" (approximate)	8
4	Semilog plots of potassium-39 relaxation rates vs.	
	1/T for 1,3-dioxolane solutions. Top curve: K+.18C6	
	complex (0.05 M); Middle Full curves: (●) 18C6/K+	
	= 0.5 (\blacksquare) 18C6/K ⁺ = 0.25; Lower curve: KAsF ₆ (0.1	
	\underline{M}); Dashed curves: extrapolations of $1/T_{2AV}$ (Obtained	
	from reference 25)	12

Figure		Page
5	Three possible forms of cryptand C222	21
6	Some examples of spiro-bis-crown-ethers	40
7	The five possible diastereoisomers of	
	dicyclohexyl-18-crown-6	48
8	Proton NMR spectra of (a) the cis-syn-cis and (b)	
	the cis-anti-cis isomer of dicyclohexyl-18-crown-6	
	at room temperature in CDCl ₃	51
9	NMR tubes configuration	54
10	Computer analysis of the $^{23}\mathrm{Na}$ lineshape for a THF	
	solution containing 0.01 \underline{M} NaSCN and 0.005 \underline{M} DA18C6	
	at -39.2°C. (x) experimental points. (o) calculated	
	points	61
11	Sodium-23 NMR spectrum of NaBPh ₄ (0.051 M) and	
	DC18C6 cis-anti-cis (0.025 M) in THF with NaCl	
	(0.1 \underline{M}) in D ₂ O as external reference. T = 23.6°C	74
12	Sodium-23 NMR spectrum of NaBPh ₄ (0.051 M) and	
	DC18C6 cis-syn-cis (0.024 M) in THF with NaCl (0.1	
	\underline{M}) in D_2O as external reference. $T = 23.6 ^{\circ}C$	75
13	Sodium-23 NMR spectrum of NaBPh ₄ (0.049 M) and	
	DA18C6 (0.025 \underline{M}) in THF with NaCl (0.1 \underline{M}) in D ₂ O	
	as external reference. T = 22.9°C	76
14	Sodium-23 NMR spectrum of NaSCN (0.049 M) and	
	DA18C6 (0.025 \underline{M}) in THF with NaCl (0.1 \underline{M}) in D2O	
	as external reference. T = 22.9°C	77
15	Sodium-23 NMR spectrum of NaBPh ₄ (0.0053 M)	
	and DB18C6 (0.0026 M) in THF. T = 23.6°C	78

Figure		Page
16	Sodium-23 NMR spectrum of NaI (0.050 $\underline{\text{M}}$) and DT18C6	
	(0.026 \underline{M}) in THF with NaCl (0.1 \underline{M}) in D_2O as external	
	reference. T = 24.0°C	79
17	(a) Sodium-23 NMR spectrum of NaI (0.050 $\underline{\text{M}}$) and	
	DC18C6 cis-anti-cis (0.025 \underline{M}) in THF with NaCl	
	(0.1 \underline{M}) in D_2O as external reference. $T = 23.6 ^{\circ}C$.	
	(b) Calculated spectrum. (c) Deconvoluted spectrum	80
18	(a) Sodium-23 NMR spectrum of NaI (0.052 M) and	
	DC18C6 cis-syn-cis (0.025 \underline{M}) in THF with NaCl (0.1	
	$\underline{\text{M}}$) in D ₂ O as external reference. T = 23.6°C. (b)	
	Calculated spectrum. (c) Deconvoluted spectrum	81
19	(a) Sodium-23 NMR spectrum of NaI (0.050 $\underline{\text{M}}$) and	
	DA18C6 (0.025 $\underline{\text{M}}$) in THF with NaCl (0.1 $\underline{\text{M}}$) in D ₂ O	
	as external reference. T = 24.0°C. (b) Calculated	
	spectrum. (c) Deconvoluted spectrum	82
20	Sodium-23 NMR spectrum of Me ₅ CpNa (0.050 M)	
	and 18C6 (0.026 \underline{M}) in THF with NaCl (0.1 \underline{M}) in D ₂ O	
	as external reference. T = 23.6°C	83
21	Sodium-23 NMR spectrum of Me ₅ CpNa (0.050 <u>M</u>)	
	and DA18C6 (0.025 \underline{M}) in THF with NaCl (0.1 \underline{M})	
	in D ₂ O as external reference. T = 23.6°C	84
22	Sodium-23 NMR spectrum of Me ₅ CpNa (0.050 <u>M</u>)	
	and DB18C6 (0.024 \underline{M}) in THF with NaCl (0.1 \underline{M}) in	
	D ₂ O as external reference. T = 23.6°C	85
23	Sodium-23 NMR spectrum of NaI (0.0051 M) and	
	N.N'-diethanol-DA18C6 (0.0027 M) in THF. T = 23.8°C	86

Figure		Page
24	Computer analysis of the $^{23}\mathrm{Na}$ Lorentzian lineshape	
	of a solution containing NaSCN 0.0099 \underline{M} and DA18C6	
	0.0191 <u>M</u> in THF at -41.3°C	112
25	Semilog plots of sodium-23 transverse relaxation	
	rates vs. 1/T for NaSCN (O), NaSCN·DA18C6 (■),	
	NaSCN·DC18C6 (cis-anti-cis) (♠) and NaSCN·DC18C6	
	(cis-syn-cis) (●) at 0.0100 <u>M</u> in THF	113
26	Temperature dependence of the sodium-23 angular	
	frequencies and chemical shifts $\underline{\text{vs.}}$ NaCl 0.10 $\underline{\text{M}}$ in	
	D_2O at 22.3°C for NaSCN (O), NaSCN·DA18C6 (\blacksquare),	
	NaSCN·DC18C6 (cis-anti-cis) (and NaSCN·DC18C6	
	(cis-syn-cis) (●) at 0.0100 <u>M</u> in THF	115
27	Sodium-23 chemical shifts vs. DA18C6/NaSCN mole	
	ratio in THF	122
28	Van't Hoff plot for the complexation of NaSCN 0.0100	
	M by DA18C6 in THF	125
29	Arrhenius plot of $ln(1/\tau)$ vs. (1/T) for DA18C6/NaSCN	
	in THF - (0) DA18C6/Na ⁺ = $0.72 - (\bullet)$ DA18C6/Na ⁺	
	= 0.53	131
30	Plot of $1/\pi \times C_{Na}^+$ vs. $1/[Na^+]_{eq}$ for DA18C6/NaSCN	
	systems in THF at various temperatures	135
31	Arrhenius plot of $ln(1/\tau)$ vs. (1/T) for DC18C6	
	(cis-anti-cis)/NaSCN in THF - Ligand/Na ⁺ = 0.50	140
32	Arrhenius plot of $ln(1/\tau)$ vs. (1/T) for DC18C6	
	(cis-syn-cis)/NaSCN in THF - Ligand/Na ⁺ = 0.51	141

rigure		Page
33	Sodium-23 NMR spectra for a THF solution containing	
	NaBPh ₄ (0.050 \underline{M}) and DA18C6 (0.025 \underline{M}) at various	
	temperatures	151

INTRODUCTION

Since the discoveries of the synthetic macrocyclic polyethers crown ethers by Pedersen $^{1-3}$ and cryptands by Lehn and co-workers $^{4-7}$, the ability of these compounds to strongly and selectively complex alkali and alkaline earth metal ions in solutions was soon well established. These discoveries and the recognition of the biological role of Li⁺, Na⁺ and K⁺ cations⁸⁻¹⁰ enhanced the interest of the chemists throughout the world. As a result, the coordination chemistry and the equilibrium properties of these ions associated with their interactions with the macrocycles rapidly became a major field of research during the past fifteen years. The physicochemical studies already done have been carried out with a number of different techniques¹¹ and are described in several reviews¹²⁻¹⁶. However, most of these studies dealt with the thermodynamic stability of such complexes in a large variety of nonaqueous solvents. The low solubility of the macrocyclic polyethers in water and the strong solvating power of water toward the alkali and alkaline earth metal ions lead to very low thermodynamic stabilities of the complexes in aqueous solutions.

Surprisingly, the kinetic studies and studies of exchange mechanisms have been quite sparse, despite their importance for the understanding of ion transport processes in organic and biological membranes⁸ and of catalytic phenomena¹⁷. As pointed out by J.-M. Lehn¹⁸ in the early stage of these different investigations, the overall process of molecular recognition includes a selection process with the formation of a specific complex followed by

a specific function of this complex such as specific reactions and/or transport properties and/or catalytic properties. The selectivity step can be either static (thermodynamic selectivity) or dynamic (kinetic selectivity) or both.

Therefore, it was of interest for us to improve the knowledge one already has on these complexation reactions by also determining their kinetic parameters. The species and the solvent to be studied were determined when J.D. Lin¹⁹, in this research group, found an anion dependence on the exchange kinetics of the sodium ion with the 18-crown-6 (Figure 1) in the low dielectric solvents tetrahydrofuran and 1,3-dioxolane. At room temperature, this exchange is slow on the sodium-23 NMR time scale with the tetraphenylborate anion (BPh₄⁻) but becomes fast when the counter ion is either the iodide (I⁻), the perchlorate (ClO₄⁻) or the thiocyanate (NCS⁻). These results were rather surprising since in all previous studies, most of the authors did not pay a great deal of attention to the anions, probably assuming no anion influence on their results. This might be true in high dielectric media such as the widely used methanol where no significantly strong ionic association occurs but not in solvents with low dielectric constants. Moreover, this was the first slow exchange ever observed with a crown ether at room temperature. The slow exchanges usually observed at room temperature were obtained with cryptands as macrocyclic receptors. Their tridimensional cavity, strongly encapsulating the alkali metal ions, lowers the rate of decomplexation and, as a result, room temperature exchange is slow on the NMR time $scale^{20-22}$. To explain this quite unusual slow exchange, we decided to study the kinetics of complexation of the sodium ion with a large variety of counter anions and crown ethers in tetrahydrofuran.

In this laboratory, we directly probe the chemical environment of the alkali ions by multinuclear NMR spectroscopy. This sensitive technique has

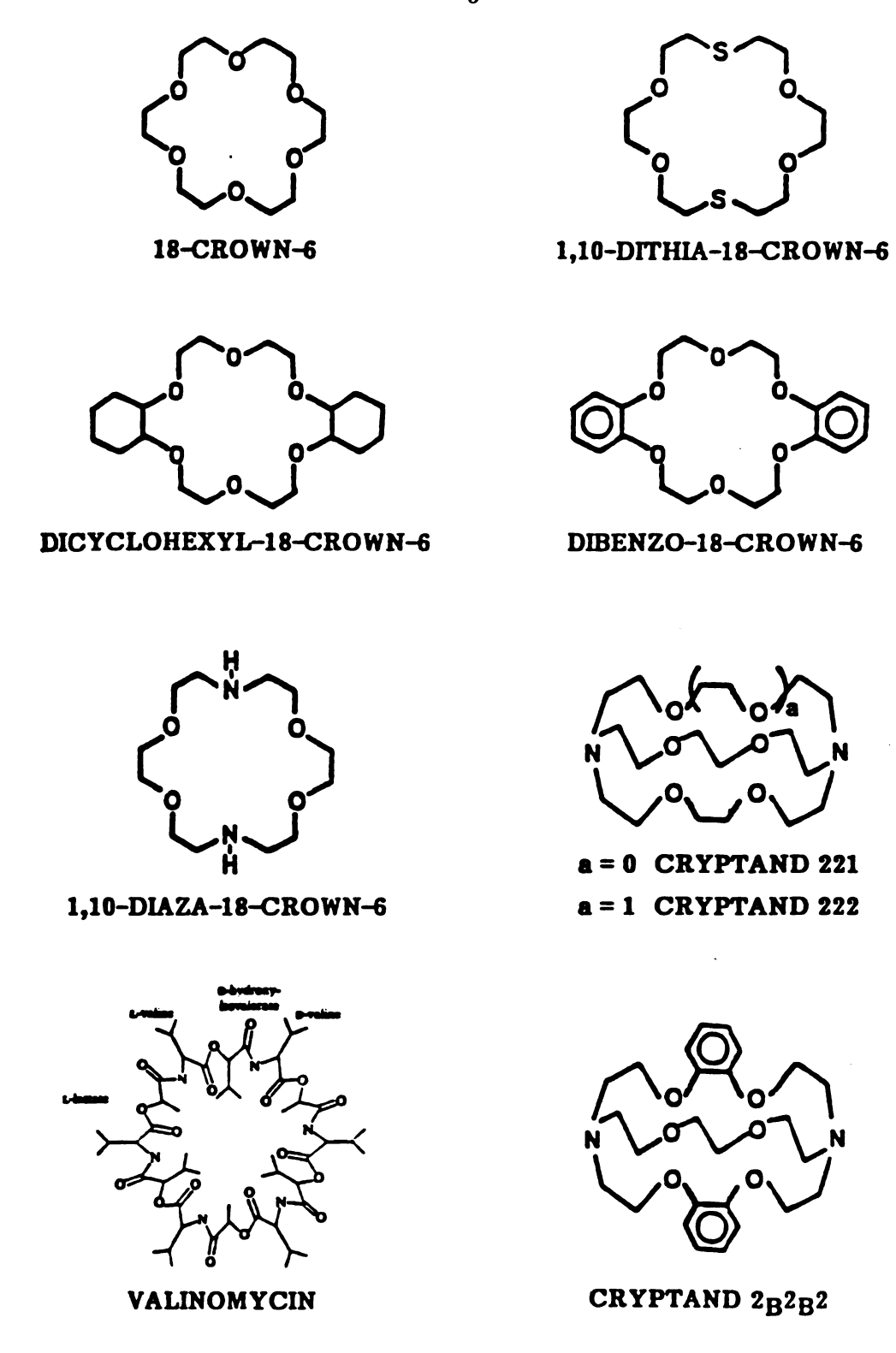


Figure 1 Structures of some naturally occuring and some synthetic macrocyclic compounds

already proved to be valuable for studying ionic solvation, thermodynamics and kinetics of complexation in nonaqueous solvents 11,20,23,24. We used sodium-23 NMR for this study and with the advance of superconducting magnets and the development of fast Fourier Transform NMR, high quality 23Na NMR spectra can be obtained even for dilute solutions, i.e., 0.01-0.001 M. In this dissertation, a kinetic study of complexation reactions of the sodium cation with some crown ethers in tetrahydrofuran is presented.

In the first part, we qualitatively investigate, by sodium-23 NMR, the anion and crown dependence on the exchange rate between the solvated and complexed sodium cation in tetrahydrofuran at room temperature. The second part is a qualitative conductance study of the ionic association of some sodium salts solvated and complexed in tetrahydrofuran. The third and last part is a quantitative study on the effect of substituent groups on the kinetics of the Na⁺ ion complexation by macrocyclic ligands containing 18-crown-6 skeleton in tetrahydrofuran.

We will first review the different physicochemical methods already used to get kinetic parameters of complexation reactions with an emphasis on multinuclear NMR spectroscopy. Then the different mechanisms of exchange observed so far will also be presented and finally the kinetics of complexation reactions involving metal ions with crown ethers and cryptands will be reviewed. For the last topic outlined above, the literature up to early 1981 has been covered in the Ph.D. Thesis of Emmanuel Schmidt²⁵.

CHAPTER I

HISTORICAL REVIEW

1.1. The Physicochemical Methods

As noted by Evring in 1978^{26} , kinetic studies of macrocyclic complexation reactions in nonaqueous solvents have been sparse in the past. High reaction rates when crown ethers are involved increase experimental difficulties and the lack of color of the complexes make spectrophotometric measurements nearly impossible. Another reason omitted by Eyring is the formation of stable ion pairs and of higher aggregates in nonaqueous solvents with low dielectric constants. Such reactions are shown in Figure 2. This ionic association limits the conductometric measurements to high dielectric media in which little or no ionic association occurs. The reasons outlined above explain why most of the kinetic studies previously reported were carried out with cryptates since their smaller decomplexation rate falls in the range observable by a number of techniques such as cyclic voltammetry²⁸, stopped-flow²⁹⁻⁴⁰, spectrophotometry⁴¹, ¹H-NMR⁴² and alkali metal NMR $spectroscopy^{20-22,43-45}$. It should be noted that for the stopped-flow measurements, the detection method is either conductometry for high dielectric media such as water, water mixtures, N,N-dimethylformamide (DMF), propylene carbonate (PC)^{29-33,37-40} or spectrophotometry when UV absorbing complexes are studied $^{34-36}$.

The transient chemical relaxation techniques developed by Eigen and co-workers 46,47 : temperature-jump, pressure-jump and electric field-jump are very good techniques to study fast reactions in solution such as those involving crown ethers since they range down to 10^{-7} sec. (See Figure 3 for a comparison of the different kinetic techniques). Unfortunately, their detection methods are still a limitation since the latter are the same as those used with the stopped-flow technique. This explains why the few studies done with these transient relaxation techniques involve benzene substituted

(a)
$$M^+ + X^- \rightleftharpoons MX$$

(b)
$$M^+ + X^- \rightleftharpoons M^+(S)X^-$$

(c)
$$M^+ + X^- + (n-2)S \rightleftharpoons M^+(S)_n X^-$$

(d)
$$\begin{cases} 2M^+ + X^- \rightleftharpoons M_2X^+ \\ M^+ + 2X^- \rightleftharpoons MX_2^- \end{cases}$$

(e)
$$2MX \rightleftharpoons (MX)_2$$

(f)
$$nMX \rightleftharpoons (MX)_n$$

Figure 2 Possible ionic associations in low dielectric solvents; (a) Contact ion pair; (b) Solvent shared ion pair: (c) Solvent separated ion pair; (d) Triple ions; (e) Quadrupoles; (f) Higher aggregates such as octopoles (n = 4,27). The species M⁺, X⁻ and S are the metal ion, the counter anion and the solvent molecule respectively. All the species presented are solvated although, for more clarity, it is omitted. In equation (a) the two ionic species are in contact, in equation (b) at least one solvent molecule is shared by both ions in their first solvation sphere and in equation (c) the two ions have their first solvation sphere either in contact or separated by solvent molecules

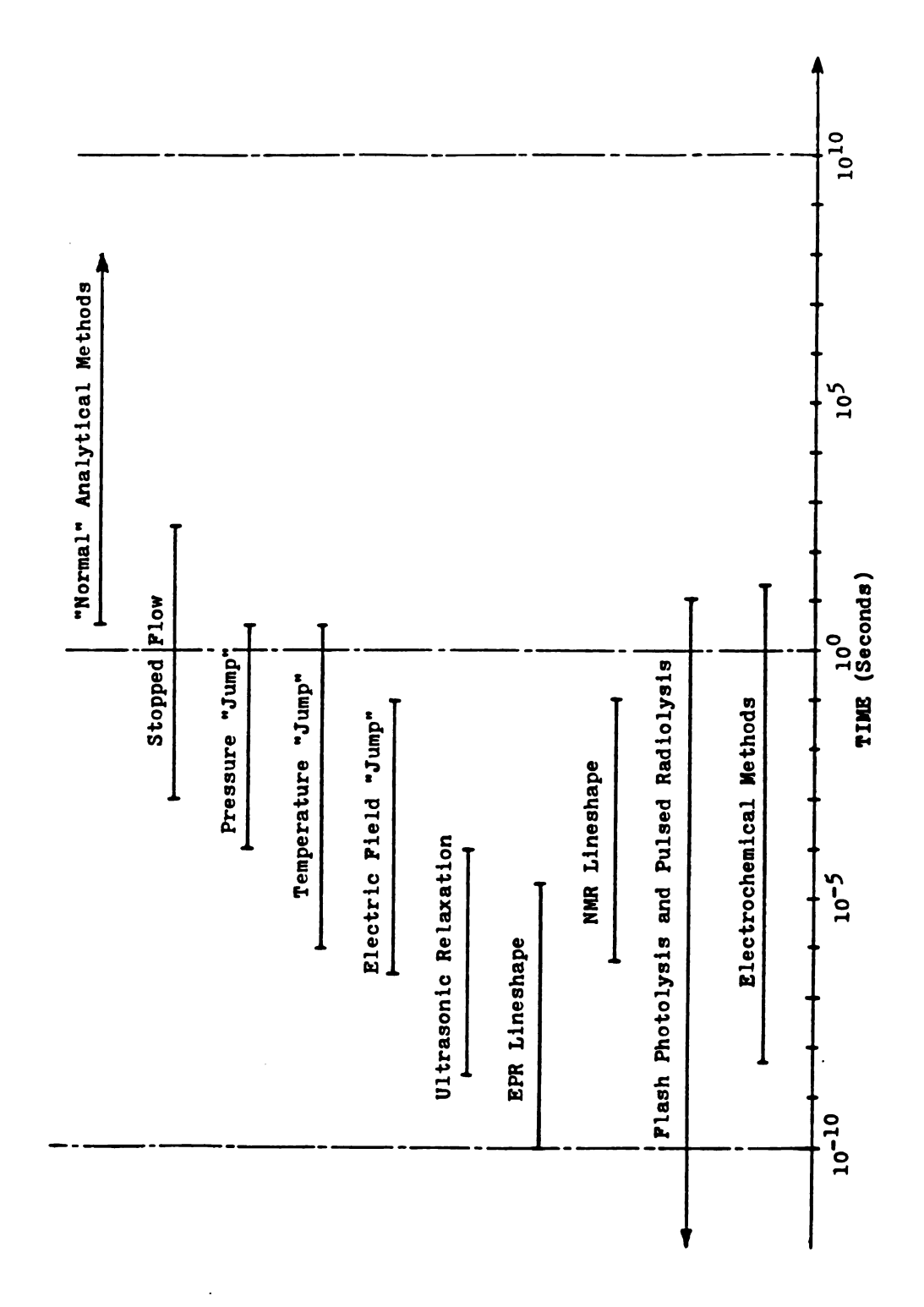


Figure 3 Chemical kinetics "Time Line" (approximate)

crown ethers absorbing in the near UV region with spectrophotometrical detection 48 or conductometric detection in water 49. Another method developed by Eigen and co-workers, the ultrasonic absorption relaxation, is a very good technique for studying the interactions of metal ions with crown ethers in solution. This technique has already been extensively used by several workers 50-57 and with the progress of X or Y-cut quartz crystals used as piezoelectric resonators, frequencies up to 500 MHz can be attained. According to the fundamental equation:

$$\tau^{-1} = 2\pi f_{rel}. \tag{1.1}$$

where τ and $f_{rel.}$ are the relaxation time and the relaxation frequency for a single exchange process respectively, one can see that relaxation times as low as 3.5 x 10^{-10} sec. can be obtained. However, most of the time this technique is much too powerful for the complexation reactions we are interested in, since it can detect conformational rearrangement of solvated crowns or complexes as well as simple ionic associations which occur to a great extent in low dielectric solvents 58-61. This high sensitivity usually makes the interpretation of the results very difficult.

Surprisingly, for a long time the dynamic NMR (DNMR) spectroscopy was thought to be limited to rate constants less than 10^4 sec⁻¹⁶². Several attempts have been made to derive kinetics of complexation by either proton or carbon-13 NMR spectroscopy for both crown ethers and cryptands but the small ¹H or ¹³C NMR chemical shift range (0.1-0.5 ppm for both nuclei, see reference 63) between the solvated and complexed forms of the ligands severely limits the sensitivity of measurements. With a few exceptions⁶⁴, the Arrhenius activation energy (E_B) of decomplexation cannot be obtained

and one is usually limited to the determination of the exchange rate and of the free energy of activation for decomplexation ΔG^{\dagger} at the coalescence temperature $T_c^{65,66}$. In many cases, T_c falls below the liquid range of common solvents and the use of very low melting freons (like freon 21 : CHCl₂F) becomes necessary⁶⁵. In some isolated cases, these techniques can lead to valuable information and suggest the mechanism of exchange^{42,64}.

Probably, the most interesting NMR technique for studying complexation reactions of cryptands and crown ethers with metal ions in solution involves measurements of the resonance of the metal ions themselves. In 1971, Schori and co-workers²⁴ published the first application of this technique to kinetic studies. Their method applies only under three conditions which are: (1) the metal ion NMR chemical shift difference between the solvated and complexed nucleus must be negligible within experimental error; (2) the linewidth at half-height of the complexed nucleus must be significantly larger than the one of the solvated nucleus; (3) at chemical equilibrium, the population of solvated species must be greater than or equal to the population of complexed species. The equations describing the three conditions stated above are:

$$\omega A - \omega B \simeq 0$$
 (1.2)

$$T_{2A} \gg T_{2B}$$
 with $T_2 = (\pi W_{1/2})^{-1}$ (1.3)

$$PA \gg PB$$
 (1.4)

where ω , T_2 , $W_{1/2}$ and p are the frequency, the spin-spin relaxation time, the linewidth at half-height and the population respectively and where A and B stand for the solvated and complexed site of the nucleus investigated

respectively. By solving the Block-McConnell equations for the steady-state transverse magnetization between two uncoupled magnetic environments⁷² with the approximations mentioned above, the authors derived the equation:

$$\frac{1}{\tau_{A}} = \frac{(1/T_{2B} - 1/T_{2obs})(1/T_{2obs} - 1/T_{2A})P_{B}}{(1/T_{2AV} - 1/T_{2obs})}$$
(1.5)

with

$$1/T_{2AV} = p_A/T_{2A} + p_B/T_{2B}$$
 (1.6)

and

$$T_{2obs} = (\pi W_{1/2})^{-1} \tag{1.7}$$

where $W_{1/2obs}$ is the linewidth at half-height of the multinuclear NMR signal undergoing fast exchange and τ_A is the mean lifetime of the nucleus in the solvated site. The other symbols have their usual meaning. The method consists of obtaining the spectra of the pure solvated and complexed species in order to characterize the temperature dependence of T_{2B} for the complexed site and of T_{2Aref} for the solvated site. Then by studying a solution with a mole ratio ligand to salt of at most 0.5, T_{2obs} values can be obtained at different temperatures. A typical plot is shown on Figure 4. With this method, the authors could easily derive the kinetic data as well as the mechanism of exchange as shown later. The main advantage of the method is that the necessary data for the plot can be rapidly obtained from the multinuclear NMR spectra and the data in equation (1.5) for obtaining τ_A are derived off the plot. In Figure 4, one sees that at high temperature, one population averaged NMR line is observed with $1/T_{2obs} = 1/T_{2AV}$. As the coalescence

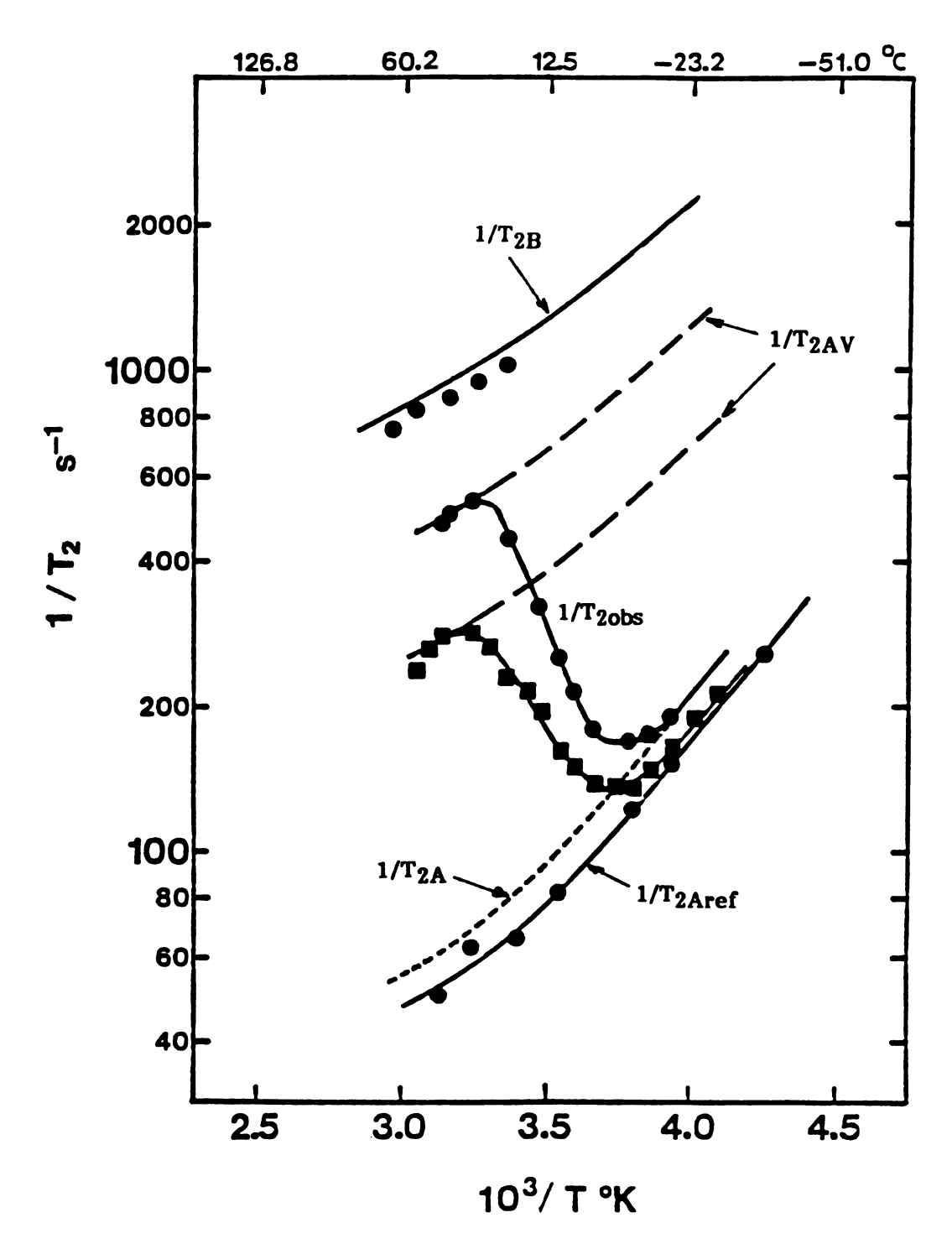


Figure 4 Semilog plots of potassium-39 relaxation rates vs. 1/T for 1,3-dioxolane solutions. Top curve: K+·18C6 complex (0.05 M); Middle Full curves: (•) 18C6/K+ = 0.5 (•) 18C6/K+ = 0.25; Lower curve: KAsF₆ (0.1 M); Dashed curves: extrapolations of 1/T_{2AV} (Obtained from reference 25)

temperature is reached, the signal corresponding to the complexed species slowly broadens out into the baseline (this is practically done by applying a large delay time DE \geq 800-1000 µsec) and only a signal corresponding to the solvated species broadened by chemical exchange is observed. Finally, at low temperature, far below the coalescence temperature, a signal corresponding to the solvated species and not significantly affected by the exchange is observed and the limiting value $1/T_{20bs} = 1/T_{2A}$ is reached. The small difference between $1/T_{20bs} = 1/T_{2A}$ and $1/T_{2Aref}$ at low temperature is attributed to a difference of viscosity due to the presence of the complex. In order to derive $1/T_{2Av}$, $1/T_{2A}$ is assumed to have the same temperature dependence as $1/T_{2Aref}$.

The main disadvantage of the above method is that the kinetic data can only be derived around coalescence temperature since it was shown that these data usually do not lend themselves to extrapolation at room temperature⁶⁷. The above method has been used by other authors^{25,67,68}.

A more precise NMR method for studying exchange kinetics was described by Ceraso and co-workers in 1973^{20,69}. It involves a complete line shape analysis of the NMR spectra of the species undergoing chemical exchange. The theoretical equation of the NMR spectrum was derived by solving the Block-McConnell equations mentioned above without approximations. The theoretical absorption (or real) part of the NMR spectrum is described by the equation:

$$I = -\gamma H_1 M_0 [(SU + TV)/(S^2 + T^2)] + B$$
 (1.8)

with

$$S = \frac{P_A}{T_{2A}} + \frac{P_B}{T_{2B}} + \frac{\tau}{T_{2A}T_{2B}} - \tau (\omega_A^{-\omega})(\omega_B^{-\omega})$$
 (1.9)

$$U = 1 + \tau(p_A/T_{2A} + p_B/T_{2B})$$
 (1.10)

$$T = (p_{A} \omega_{A} + p_{B} \omega_{B} - \omega) + \tau \left(\frac{\omega_{A} - \omega}{T_{2B}} + \frac{\omega_{B} - \omega}{T_{2A}}\right)$$
 (1.11)

$$V = \tau (p_A \omega_A + p_B \omega_B - \omega) \qquad (1.12)$$

where I is the intensity at the frequency ω , γ is the gyromagnetic ratio of the nucleus, M_0 is the macroscopic magnetization, H_1 is the magnetic induction of frequency ω , B is the baseline intensity and τ is the relaxation time of the exchange process. The other symbols have their usual meaning. The frequencies ω_A and ω_B and the relaxation times T_{2A} and T_{2B} are first obtained from solutions containing only the salt or the complex, then spectra of solutions undergoing chemical exchange, i.e., mole ratio ligand to salt between 0 and 1, are obtained and fitted to the theoretical equation (1.8) in which ω is the independent variable, I is the dependent variable and $(\gamma H_1 M_0)$, B and τ are the three unknowns to be found. The main advantage of this method is that it is not limited to a narrow temperature range like Schori's method. Moreover, it is believed to be the most versatile method for studying crown ethers interactions with alkali metal ions as it will be discussed later.

It should be noted that other approximate NMR methods can be developed by considering the NMR properties of the nucleus studied and by modifying the Block-McConnell equations accordingly. This was done by Shamsipur⁷⁰ when he studied the kinetics of complexation of Cs^+ with various crown ethers by cesium-133 NMR spectroscopy. For species undergoing fast exchange, i.e., above coalescence temperature T_c , the author derived the following equation:

$$1/T_{2obs} = p_A/T_{2A} + p_B/T_{2B} + p_A p_B(\omega_A - \omega_B)^2 \tau$$
 (1.13)

in which the quantity $p_A p_B(\omega_A - \omega_B)^2 \tau$ represents the exchange broadening (see equation (1.6) which is the limiting case for very fast exchange, <u>i.e.</u>, very small relaxation time τ). Since cesium-133 is a nucleus with narrow linewidth (about 1 Hz) and consequently long transverse relaxation time T_2 , the author assumed the linewidths at half-height of the solvated and complexed cesium to be negligible compared with that of the species undergoing fast chemical exchange as shown in the equation below:

$$1/T_{2obs} >> 1/T_{2A} \simeq 1/T_{2B} \simeq 0$$
 (1.14)

By combining equations (1.13) and (1.14), the author derived the following equation which only holds above coalescence temperature.

$$1/T_{2obs} \simeq p_{A}p_{B}(\omega_{A}-\omega_{B})^{2}\tau \qquad (1.15)$$

1.2. The Mechanisms of Exchange

In 1969, Wong et al.⁶⁴ reported a proton NMR kinetic study of the complexation of dimethyl-dibenzo-18-crown-6 with the fluorenyl sodium ion pair (Na⁺Fl⁻) in THF-d₈ solutions. As noted in section 1.1., this study is a special case in which the fluorenyl ring delocalized electrons cause large chemical shifts of the ligand protons between solvated and complexed forms of the macrocycle allowing the authors to observe coalescence temperatures for each set of the crown protons within the liquid range of THF-d₈ when using a 2:1 ligand to salt ratio. The authors assumed the exchange process

to be the bimolecular process shown below:

$$Fl^-Na^+C^* + C \Longrightarrow Fl^-Na^+C + C^*$$
 (1.16)

This is one of the few cases in which the Arrhenius activation energy $(E_{\rm a})$ could be derived with either proton or carbon-13 NMR spectroscopy. the value of $E_{\rm a}$ is 12.5 kcal/mole.

The most interesting mechanisms for us were first proposed by Schori and co-workers²⁴ who studied the kinetics of complexation of sodium thiocyanate with dibenzo-18-crown-6 (DB18C6) in N,N-dimethylformamide (DMF) using dynamic multinuclear NMR spectroscopy. Assuming no significant chemical shift difference on the sodium-23 NMR frequency scale between the solvated and complexed sodium ion, they modified the Block-McConnell equations developing the method described in section 1.1. The authors proposed two possible routes for the exchange of sodium between the solvated and complexed forms according to the equations:

$$M(S)_{n}^{+} + C = \frac{k_{1}}{k'_{-1}} \qquad MC^{+} + nS$$
 (1.17)

*
$$M(S)_n^+ + MC^+ = {k_2 \over m} * MC^+ + M(S)_n^+$$
 (1.18)

where S is the solvent, M⁺ is the metal ion and C is the macrocyclic polyether. It should be noted, however, that MC⁺ and C are undoubtedly also solvated to some extent. Equation (1.17) represents a first order associative mechanism and equation (1.18) is a bimolecular mechanism between the solvated and complexed species. In this dissertation, these mechanisms will be called associative-dissociative and bimolecular respectively. The authors found

the associative-dissociative mechanism to be predominant with an upper limit of 10^3 M^{-1} sec⁻¹ for k_2 . They also observed a strong ionic strength dependence on the observed rate constant of the decomplexation reaction k'_{-1} which in terms of the transition-state theory is given by the equation

$$k_{-1}^{\dagger} = K_{-1}(k_BT/h)(y_S^ny_C/y^{\dagger})$$
 (1.19)

and

$$K_{-1}^{\dagger} = \exp(-\Delta G_{-1}^{\dagger}/RT)$$
 (1.20)

where K_{-1}^{\ddagger} is the "equilibrium" constant for the formation of the activated complex from the complexed species, ΔG_{-1}^{\ddagger} is the free energy of activation associated with this process and the y's are molar activity coefficients. They found the best results by keeping the ionic strength constant with lithium thiocyanate which they assumed not to compete effectively with sodium ions for DB18C6. They extrapolated their data to infinite dilution and room temperature and found k_{-1}° (25°C) = 1.0 x 10⁵ sec⁻¹ which is consistent for a decomplexation rate of crown ethers. However, 12 years later Schmidt and Popov⁶⁷ ruled out such extrapolation to room temperature invoking that the Arrhenius activation energy (Ea) may vary with temperature as noted by Liesegang et al.⁵⁰ and that another mechanism may contribute at a different temperature. Also, the same authors⁶⁷ reported the first bimolecular mechanism (equation (1.18)) ever observed by studying the kinetics of exchange of potassium hexafluoroarsenate with 18-crown-6 in 1,3-dioxolane solutions. Schori et al. 24 observed a strong anion dependence on the exchange rate τ_A^{-1} (see Section 1.1) which drops from 800 sec⁻¹ to 445 sec⁻¹ when the small thiocyanate anion (SCN⁻, $a \simeq 2.4$ Å) is replaced by the bulky tetraphenylborate anion (BPh₄⁻, a $\simeq 5.0$ Å). This anion influence will be discussed later.

Mechanisms (1.16) and (1.17) were also proposed in 1970 by Lehn and co-workers⁴² when they studied the formation of M+·C222 complexes in D₂O with proton NMR spectroscopy. However, the authors could not determine unambiguously which of the mechanisms was involved.

In 1972, Chock⁴⁸ reported a relaxation study of complex formation of dibenzo-30-crown-10 (DB30C10) with Na $^+$, K $^+$, Rb $^+$, Cs $^+$, NH $_4^+$ and Tl $^+$ cations in methanol temperature-jump relaxation solutions using spectrophotochemical detection at a near-UV wavelength. According to the author, the simplest mechanism consistent with the relaxation amplitude data is the two-step process represented by the equations:

$$C_1 = \frac{k_{12}}{k_{21}} = C_2$$
 (1.21)

$$C_1 = \frac{k_{12}}{k_{21}} \quad C_2$$
 (1.21)
 $M^+ + C_2 = \frac{k_{23}}{k_{32}} \quad MC_2^+$ (1.22)

where \mathbf{C}_1 and \mathbf{C}_2 are the unreactive and reactive form of the crown respectively. the Joule heating temperature-jump apparatus he utilized did not permit measurement of relaxation times under a microsecond so that he was unable to measure the kinetics of the fast preequilibrium. According to the author, C2 has an open configuration and is the predominant species. After complexation this form has a closed configuration which is stabilized by the monovalent cation in a "wrap-around" type complex. However, it was not mentioned whether the conformational rearrangement of C_2 from the open to the closed configuration occurs during the cation binding step or after this step has been completed. Very possibly this last case could apply here since conformational rearrangements of complexes have been reported as it will be discussed below. The author found that the rates of formation are all equal and diffusion controlled while the decomplexation rate ranges between 10^4 and 10^5 sec⁻¹ for all ions.

Grell et al.⁷¹ reported a study of the formation of the M⁺-valinomycin complexes in methanol using ultrasonic absorption method. The data indicated that the uncomplexed ligand undergoes some fast conformational equilibria, and the mechanism could be simply described as shown below

$$M^+ + V = \frac{k_{12}}{k_{21}} = M^+ \cdots V = \frac{k_{23}}{k_{32}} = MV^+$$
 (1.23)

where MV⁺ is the final form of the complex, M⁺····V is an intermediate encounter complex and M⁺ and V are the solvated cation and ligand respectively. A diffusion controlled bimolecular collision, between a reactive form of the ligand and the solvated cation is followed by the rate-determining conformational change of the ligand around the cation leading to the compact final structure of the MV⁺ complex. Mechanism (1.23) is usually referred as the Eigen-Winkler mechanism.

Very recently, Petrucci et al.⁵⁶ reported a study of the complexation of lithium, sodium and potassium thiocyanates with 18-crown-6 in DMF solutions using ultrasonic absorption method. They observed and characterized the fast crown ether rearrangement originally proposed by Chock⁴⁸ and the data indicated that the Eigen-Winkler mechanism was the predominant one. They also observed a new relaxation process occuring above 45°C at low frequencies only if the cation (Na⁺ or K⁺) and the 18C6 are simultaneously present in solution. They attributed this new process to a two step rearrangement of the complex described by the equation shown below:

$$M^{+} + C \xrightarrow{k_{1}} M^{+} \cdots C \xrightarrow{k_{2}} MC^{+} \xrightarrow{k_{3}} (MC)^{+} (1.24)$$

where M⁺····C is a solvent separated pair, MC⁺ is a contact pair and (MC)⁺ is an included metal complex in the final "wrap-around" configuration. Steps 2 and 3 are attributed to a multistep ligand rearrangement around the cation and/or to the desolvation process. The mechanical resonator used for this study did not allow them to get enough informations at very low frequencies (f < 30 MHz) in order to fully explain the observed new relaxation process.

Using Raman spectroscopy, they also investigated the competition between SCN⁻ and the crown ether for the metal ion as shown below:

$$M^{+} + SCN^{-} \stackrel{K}{\longrightarrow} M^{+}NCS^{-}$$
 (1.25)

$$M^{+} + C \stackrel{K_{F}}{=} (MC)^{+}$$
 (1.26)

It appears that K < K_F for NaSCN/18C6 and KSCN/18C6 but the converse situation K > K_F appears to be the case for LiSCN/18C6 as well as for LiSCN/15C5 and LiSCN/12C4 systems. The intermediate situation $K \simeq K_F$ appears to occur for NH₄SCN/18C6, NH₄SCN/15C5 and NaSCN/15C5 systems. This again demonstrates the role played by the cation-anion association which should not be ignored when studying cation-ligand interactions.

Although kinetics of cryptates formation is not of direct interest for our study, it should be noted that these ligands undergo the same mechanisms of exchange as the one reported above for the crown ethers but in the case of cryptates, rearrangements appear to be somewhat more complicated. In their early studies, Lehn and co-workers⁴² proposed three conformations which hold for both the solvated cryptands and the complexed cryptates and which can be represented as shown below

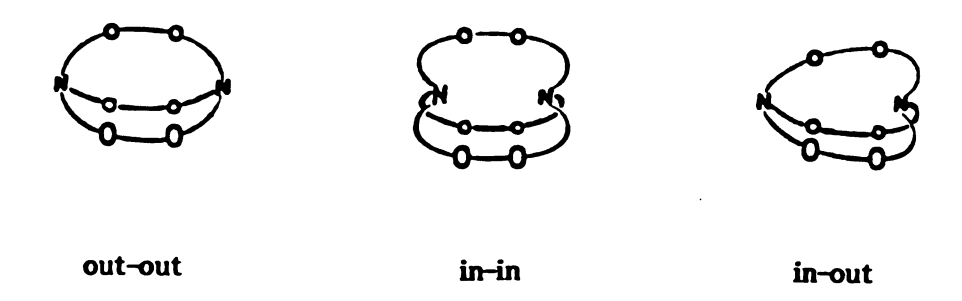


Figure 5. Three possible forms of cryptand C222.

Both lone pairs of the N atoms point away from the cavity in the "out-out" conformation, both point into the interior of the cavity in the "in-in" conformation and "in-out" is the obvious intermediate case. The authors noted that the exchange between the solvated and complexed ligand may occur in any one of these forms. In addition to these rather complicated features, the cryptate complexes can also exist in three different forms depending on the metal ion position relative to the cryptand cavity. The complex may be either exclusive when the metal ion is inside the cavity or exclusive when the metal ion is outside the cavity and interacting with several oxygen atoms or external when the metal ion interacts with one nitrogen atom³⁵. The exchange processes between all these possible forms usually lead to rather difficult interpretations of the kinetic data^{35,44}.

In conclusion, we can classify these mechanisms of exchange into two main groups, the first containing the bimolecular processes which can be described by either equation (1.16) when the ligand is in excess or equation (1.18) when the metal ion is in excess. The second group contains the associative-dissociative processes in which several ligand and complex

rearrangements can occur and which are best represented by their rate limiting step, <u>i.e.</u>, equation (1.22). For our multinuclear DNMR studies of kinetics of complexation, we will only retain mechanisms (1.18) and (1.22) since this technique is not sensitive enough to observe very fast relaxation processes.

1.3. The Kinetic Results

In this section, we do not intend to present an exhaustive review of the kinetic studies of the complex formations with crown ethers and cryptands. This part is to be considered more as an update of the review done by Schmidt in 1981²⁵. Before describing in some detail the crown kinetics, we will review the cryptate kinetics which has been described by Lehn¹⁸, Cox et al.³² and more recently by Schmidt²⁵. All the data summarized in Tables 1-4 have been obtained by Cox, Schneider and co-workers³³⁻⁴⁰ and confirm the typical trends already observed for cryptate kinetics which are worth being recalled.

- The exchange mechanism between the solvated and the complexed sites of the metal ion is the associative-dissociative one (Equation (1.22)) and not the bimolecular one (Equation (1.18)).
- 2. The association rates in water tend to be smaller than the association rates in nonaqueous solvents and are usually much lower than the diffusion controlled rates ($10^{10} \ \text{M}^{-1} \text{sec}^{-1}$).
- 3. For a given solvent, variations in the formation constant are essentially reflected in the dissociation rates.
- 4. The dissociation rates increase with the donor ability of the solvent (a few exceptions are given in reference 22).
 - 5. The dissociation of the cryptates is acid catalyzed.

These general features were mostly derived from rate data since very few activation parameters have been reported.

Table 1 - Rate Constants for the Formation of Some Cryptates in Propylene Carbonate at $25^{\circ}\mathrm{C}^{33}$

Cation	Cryptand	k _d (sec ⁻¹)(a)	kf (<u>M</u> ⁻¹ sec ⁻¹)
Na+	C222	(9)	(9)
	C2B22	(p)	(p)
	C2B2B2	$\langle 2 \times 10^{-1} \rangle$	< 10 ⁹
K ⁺	C222	$3 (\pm 1) \times 10^{-3}$	$4.5 (\pm 1.5) \times 10^{8}$
	C2B22	5.7×10^{-3}	5.8×10^7
	${ m C2B^2B^2}$	2.03×10^{-2}	2.9×10^7
Rb⁺	C222	1.7×10^{-1}	1.8 x 108
	$C2_B22$	3.32	1.3 x 108
	C2B2B2	18.8	8.0×10^7

 k_d ± 5% unless otherwise noted Strongly acid-catalyzed dissociation

(B)

Table 2 - Rate Constants of Cryptand Exchange at $25^{\circ}\mathrm{C}^{36}$

MCry ₁ n+	Cry ₂	Solvent	k _e (sec ⁻¹)(a)	k _d (sec ⁻¹)(b)
(Ca·C2B22) ²⁺	C221	Н2О	0.54 ± 0.04	0.55
(T1.C222) ⁺	C221	Н2О	5.2 ± 0.2	5.5 ± 0.5
(T1.C222) ⁺	C221	MeOH-H ₂ O (90:10)	0.14	0.12 ± 0.01
$(Pb \cdot C211)^{2+}$	C221	МеОН	1.45 (±0.10) x 10^{-1}	6×10^{-3}
$(Pb \cdot C211)^{2+}$	C222	МеОН	$(3.5 \times 10^4) \times [C222]^{(c)}$	6×10^{-3}

 $MCry_2^{n+} + Cry_1$ k e (a) Rate for the exchange MCry₁n⁺ + Cry₂

(b) Rate for the dissociation $MCry_1^{n+}$ $\stackrel{k_d}{=}$ $M^{n+} + Cry_1$

(c) At $[C222] < ca. 10^{-2} M$

Table 3 - Rate Constants for the Cryptate (Ag-C222)⁺ in Acetonitrile - Water Mixtures at 25°C³⁸

XAN	k _d (sec ⁻¹)(a)	10 ⁻⁸ x kf (M ⁻¹ ·sec ⁻¹)	Method
0.00	0.46 ± 0.01	15.6	(Ag·C222) ⁺ + HC10 ₄
0.05	0.69	2.5	(Ag·C222) ⁺ + HC10 ₄
0.1	0.80	1.3	$(Ag \cdot C222)^+ + HC10_4$
0.2	1.00	1.1	$(Ag \cdot C222)^+ + HC10_4$
0.3	1.04	1.1	$(Ag \cdot C222)^+ + HC10_4$
0.5	1.06	1.5	(Ag·C222) ⁺ + HC10 ₄
2.0	1.18	2.4	$(Ag \cdot C222)^+ + HC10_4$
6.0	0.78	4.3	(Ag·C222) ⁺ + HC10 ₄
0.95	0.70	5.4	$(Ag \cdot C222)^+ + HC10_4$
0.98	0.5 ± 1.2	ı	$(Ag \cdot C222)^+ + HC10_4$
1.0	0.60 ± 0.15	5.0	$(Ag \cdot C222)^+ + CF_3SO_3H$
1.0	0.5 ± 0.1	4.2	$(Ag \cdot C222)C1O_4 + CH_3SO_3H$
1.0	0.45 ± 0.10	3.8	$(Ag \cdot C222)CF_3SO_3 + Pb(CF_3SO_3)_2$

rable 3 - cont

XAN	k _d (sec ⁻¹)(a)	$10^{-8} \times k_f (\overline{M}^{-1} \cdot sec^{-1})$	Method
1.0	0.50 ± 0.15	4.2	(Ag·C222)C1O ₄ + Pb(CF ₃ SO ₃) ₂
1.0	0.60 ± 0.10	5.0	$(Ag \cdot C222)C10_4 + Pb(C10_4)_2$
1.0	0.4 ± 0.2	3.3	$(Ag \cdot C222)C1O_4 + NaC1O_4$
1.0	0.9 ± 0.5	7.5	$(Ag \cdot C222)C1O_4 + FSO_3H$

(a) $k_d \pm 15\%$ if not otherwise stated

Table 4. Rate Constants for the Formation of Some Cryptates at 25°C(a)

				1, /vr-1		
				Krim -sec - July		
Cation	Cryptand	H ₂ O(c)	MeOH(f)	DMSO	DMF	PC
Ca ²⁺	C211	2.6 x 10 ² (d)	9.0 x 10 ³	1	1.05 x 10 ³	2.2 x 104
Ca^{2+}	C221	$5.9 \times 10^{3}(d)$	1.9×10^4	2.0×10^{1}	1.3×10^3	1.1×10^{5}
Sr^{2+}	C221	$3.3 \times 10^{4}(d)$	9.2×10^4	5.3×10^{2}	1.4×10^4	1
Ba ²⁺	C221	$1.2 \times 10^{5(d)}$	1.9 x 10 ⁶	7.6×10^3	1.8×10^{5}	1
Pb2+	C221	I	$9.2(\pm 1.0) \times 10^{5(e)}$	ı	ı	1
Ca^{2+}	C222	$7.8 \times 10^{3}(d)$	3.4×10^4	ı	2.2×10^3	ca. 6 x 10 ⁵
Sr^{2+}	C222	$1.4 \times 104(d)$	3.1×10^5	6.6×10^{2}	2.9×10^4	ı
Ba ²⁺	C222	$9.0 \times 104(d)$	ca. 5 x 10 ⁶	2.3×10^4	6.1×10^{5}	ı
Ca^{2+}	$C2_{B}22$	3.9×10^3	6.4×10^3	ı	1.9×10^{2}	1.8×10^{5}
Sr ²⁺	$C2_{B22}$	9.2×10^3	4.6×10^4	1.6×10^{2}	3.8×10^3	ı
Ba ²⁺	C2B22	4.5×10^4	4.1×10^5	5.8×10^{3}	6.7×10^4	ı

Table 4 - cont.

P.C.	4.4 x 104 -
DMP	- 4.2 x 10 ² 1.1 x 10 ⁴
- k _f (<u>M</u> -1 _{.sec} -1)(b) DMSO	2.5 x 10 ¹
MeOH(f)	5.0 x 10 ² 4.8 x 10 ³ 5.6 x 10 ⁴
H ₂ O(c)	5.1 x 10 ² 1.4 x 10 ³ 6.4 x 10 ³
Cryptand	$\begin{array}{c} \text{C2B}^2\text{B2} \\ \text{C2B}^2\text{B2} \\ \text{C2B}^2\text{B2} \end{array}$
Cation	Ca ²⁺ Sr ²⁺ Ba ²⁺

Table 4 - cont.

				. , -1,(a)		
				kd(sec_1)/8/		
Cation	Cryptand	H ₂ O	MeOH(f)	DMSO	DMF	PC
Ca ²⁺	C211	8.2 x 10-1(d)	3.6 x 10 ⁻²	ı	8.0 x 10 ⁻¹	4.9 x 10-5(h)
Ca^{2+}	C221	$6.4 \times 10^{-4}(d)$	2.3×10^{-6}	1.9×10^{-3}	8.3×10^{-4}	$3.4 \times 10^{-7}(h)$
Sr ²⁺	C221	$1.4 \times 10^{-3}(d)$	8.2×10^{-7}	4.2×10^{-4}	3.5×10^{-4}	1
Ba ²⁺	C221	$6.1 \times 10^{-2}(d)$	4.6×10^{-5}	5.4×10^{-2}	1.4×10^{-2}	ı
Pb ²⁺	C221	I	$6 \times 10^{-3}(e)$	I	ı	1
Ca^{2+}	C222	$2.1 \times 10^{-1}(d)$	2.2×10^{-4}	1	3.0×10^{-1}	$1.0 \times 10^{-5}(h)$
Sr^{2+}	C222	$8.4 \times 10^{-5}(d)$	5.5×10^{-7}	5.2×10^{-3}	2.0×10^{-3}	ı
Ba ²⁺	C222	$1.8 \times 10^{-5}(d)$	6.3×10^{-7}	8.0×10^{-3}	2.5×10^{-3}	ı
Ca2+	$C2_B22$	5.2×10^{-1}	5.0×10^{-4}	I	6.0×10^{-1}	$1.4 \times 10^{-5}(h)$
Sr^{2+}	$C2_B22$	2.9×10^{-4}	1.4×10^{-6}	9.6×10^{-3}	4.5×10^{-3}	ı
Ba ²⁺	$C2_{B}22$	5.5×10^{-4}	3.5×10^{-6}	1.0×10^{-1}	2.2×10^{-2}	ı

Table 4 - cont.

				- k _d (sec ⁻¹)(g)		
Cation	Cryptand	Н2О	MeOH(f)	DMSO	DMF	PC
Ca2+	C2B2B2	1.9 x 10 ⁻¹	4.7 x 10 ⁻⁴	ı	ı	1.1 x 10 ⁻⁵
Sr^{2+}	C2B2B2	5.8×10^{-4}	4.3×10^{-6}	9.1×10^{-3}	7.9×10^{-3}	I
Ba ²⁺	$C_{2}B_{2}B_{2}$	1.5×10^{-2}	1.8×10^{-4}	4.0×10^{-1}	2.2×10^{-1}	ı

(a) Data from reference 40 unless otherwise noted; (b) $k_f \pm 5\%$ unless otherwise indicated; (c) $k_f \pm 20\%$; (d) Reference 29; (e) Reference 35; (f) Reference 39; (g) $k_d \pm 10\%$ unless otherwise indicated; (h) $k_d \pm 20\%$ obtained from $k_d = k_f/K_F$.

Kinetic studies of crown ether complexes have been rather sparse because they require very accurate work and also because, as noted earlier, most of the classical relaxation methods are not applicable. Since 1981, Cox, Firman and Schneider^{34,37} studied the thermodynamics and kinetics of complex formation involving some alkaline earth metal ions with substituted 18-crown-6 crown ethers in methanol by using stopped-flow conductometry or stopped-flow spectrophotometry methods. They obtained the stability constants with their competitive potentiometric titration using the Ag/Ag⁺ electrode to monitor the silver concentration in the reaction

$$ML^{n+} + Ag^{+} \Longrightarrow AgL^{+} + M^{n+}$$
 (1.27)

By knowing the equilibrium constant of the AgL⁺ complex, they could calculate the equilibrium constant of the MLn+ complexes. The results obtained are given in Table 5. For the diaza-18-crown-6 (2,2)and N,N'-dimethyl-diaza-18-crown-6 (2,2-Me₂), they observed that the kinetic behavior of these crowns is quite different from that of the cryptates presented above although their dissociation is also acid catalyzed and the differences in the stability constants (KF) are reflected in the rates of decomplexation (kd) which are considerably faster than those obtained with the cryptates. The data showed more similarities to the corresponding data for the 18C6 complexes and, according to the authors, solvation of the metal complexes should make a major contribution to the differences between the (2,2) and the (2,2-Me₂) complex since the N-H bond of (2,2) is strongly polarized in the presence of a metal ion in the crown cavity, thus leading to significant interactions involving the hydrogen atom and solvent molecules.

Petrucci et al. made a major contribution to the understanding of kinetics

Rate Constants and Activation Parameters of Some Crown Complexes in Methanol^(a) Table 5.

Ion	Ligand(f)	$k_{\mathbf{d}}(\mathbf{sec^{-1}})(\mathbf{b})$	$k_{\mathbf{f}}(\underline{\mathbf{M}}^{-1}.\mathrm{sec}^{-1})$	$\Delta H_{\rm d}^{\rm \#} ({ m c}) \Delta S_{ m d}^{\rm \#} ({ m d})$ (kJ.mol ⁻¹) (J.mol ⁻¹ .deg ⁻	$\Delta H_{\rm d}^{\dagger}$ (c) $\Delta S_{\rm d}^{\dagger}$ (d) (kJ.mol ⁻¹) (J.mol ⁻¹ .deg ⁻¹)
Sr ²⁺	(2,2)	4.2	2.1 x 10 ⁶	72.7	+11
	$(2, 2-Me_2)$	0.58	1.8 x 10 ⁶	51.8	92-
	C222	$6.8 \times 10^{-9}(e)$	$5.4(\pm 1.0) \times 104(e)$	ı	ı
	DB18C6	$2.7(\pm 0.3) \times 10^{1}(e)$	$9.6(\pm 0.5) \times 104(e)$	ı	ı
Ca2+	(2,2)	80.3	2.5×10^5	42.8	-65
	$(2, 2-Me_2)$	38.4	6.1×10^{5}	38.7	-85
Ba ²⁺	(2,2)	8.0	6.4×10^6	45.0	-77
	$(2, 2-Me_2)$	1.4	1.1×10^7	59.1	-44

(b) $k_d \pm 5\%$; (i) Error $\langle 2.5 \text{ kJ.mol}^{-1}$ (f) $(2.2) = \text{diaza-18-crown-6 and } (2,2-\text{Me}_2) =$ (a) Results from reference 37 at 25°C unless otherwise noted; (d) Error $\langle \pm 10 \text{ J.mol}^{-1}.\text{deg}^{-1};$ (e) Reference 34 at -15°C; N,N'-dimethyl-diaza-18-crown-6.

of macrocyclic complexation reaction. They studied complexation reactions of 18-crown-6 with several alkali metal ions in nonaqueous solvents using ultrasonic or dielectric relaxation methods. For most of their studies, the simplest mechanisms consistent with their relaxation data were either the Chock mechanism (Equations (1.21) and (1.22)) or the Eigen-Winkler mechanism (Equation (1.23)). For a better understanding of their results, it is worth recalling these mechanisms

$$C_1 \stackrel{k_0}{=} C_2 \tag{1.21}$$

$$M^+ + C_2 = \frac{k_2}{k_{-2}} = MC_2^+$$
 (1.22)

$$M^{+} + C = \frac{k_{1}}{k_{-1}} \qquad M^{+} \cdots C = \frac{k_{2}}{k_{-2}} \qquad MC^{+}$$
 (1.23)

They first investigated the interactions of LiClO₄ with 18C6 in 1,3-dioxolane and 1,2-dimethoxyethane (DME) solutions⁵⁴. In 1,3-dioxolane, they observed a relaxation without solute proving that this solvent exists in at least two conformations, then by replacing LiClO₄-18C6 with LiClO₄-15C5, they observed relaxation at a different frequency showing the different kinetic behavior at these two crowns toward LiClO4. At room temperature and with 18C6, the Chock and Eigen-Winkler mechanisms were kinetically indistinguishable and they reported an overall formation constant $K_{\mathbf{F}}$ = 1.56 \underline{M}^{-1} . However, they observed a relaxation process at -19.8°C for an 18C6 solution indicating at least two conformations for this crown and leading the authors to favor the Chock mechanism with a crown conformational rearrangement prior complexation in 1,3-dioxolane. In DME, they previously reported that $LiClO_4$ is mainly present as contact ion pairs and quadrupoles⁶¹. They observed the relaxation corresponding to the quadrupole formation represented by the equation shown below:

$$\begin{array}{ccc}
 & k_4 \\
2 \text{ LiClO}_4 & & k_4 \\
\hline
k_4 & & (\text{LiClO}_4)_2
\end{array} (1.28)$$

Assuming no competition between the complex and the quadrupole formation they derived $k_{-4} = 8.1 \times 10^7 \text{ sec}^{-1}$, $k_4 = 1.2 \times 10^9 \text{ M}^{-1} \text{ sec}^{-1}$ and $K_4 = 14 \text{ M}^{-1}$ according to the following equation.

$$K_4 = k_4/k_{-4} \tag{1.29}$$

Here, the assumption of no competition can be subject to criticism since the stability constant of the quadrupole is large enough to assume that the quadrupole formation and the complex formation affect each other to a certain extent. The results for both solvents are presented in Table 6.

The above authors also studied the complexation of LiClO₄, NaClO₄ and KClO₄ with 18C6 in methanol (MeOH) solutions⁵⁵. They observed the change of conformation of 18C6 at -20°C and proposed that this reaction implies the exchange of one molecule of MeOH with the bulk solvent. They proposed the simple two steps Eigen-Winkler mechanism between the reactive form of the crown and the metal ions, the second step being rate determining and reflecting the rearrangement of the open crown around the ion, not a desolvation process. By considering the insolubility of KClO₄ in MeOH, they proposed that the first form of the potassium complex represented as M⁺·····C in Equation (1.23) or (1.24) is not a solvent separated complex but more probably a different configurational entity of the final complex. The results are shown

in Tables 6-7. In ethanol, they also observed, at -15°C, the 18C6 rearrangement followed by the two steps Eigen-Winkler mechanism with NaClO₄ and LiClO₄⁵⁷. The results are given in Table 6-7. The authors proposed a third step in the Eigen-Winkler mechanism (see section 1.2., equation (1.24)) when they studied the complexation of Na⁺ and K⁺ with 18C6 in DMF^{56,57}. No interaction was observed between LiSCN and 18C6 in DMF probably because SCN⁻ is more competitive for Li⁺ than 18C6 whose cavity is rather large for this ion. They observed the 18C6 isomerization at -10°C. The rate constants and the activation parameters are given in Tables 6-8. From the data discussed above, we see that 18-crown-6 in solution can undergo a relaxation indicating at least two different conformations for the solvated crown probably due to its great flexibility.

Several attempts have been made to derive the conformations of this ligand in the solid sate 73 as well as in the liquid state 74 . Recently, Perrin et al. 75 studied the theoretical and experimental conformations of 18-crown-6 by dipole moment measurements. Within the six possible theoretical conformations, three of them with low dipole have been observed in the solid state complexed or uncomplexed. The authors observed a high dipole moment in cyclohexane solutions ($\mu \simeq 2.66$ Debye at 20°C) showing that the three other conformations having a high dipole moment are possible in solution.

By using the dynamic NMR method first published by Schori et al. 24 , Schmidt and Popov⁶⁷ studied the complexation of KAsF₆ with 18-crown-6 in various nonaqueous solvents; Lazlo et al. 68 studied the interactions of NaClO₄ with a variety of spiro-bis-crown ethers in pyridine. This new group of crown ethers, first synthetized by Weber⁷⁶ have a spiro-linked assembly of two crown ether like macrorings. They are usually referred to as O_n-O_m, n and m being the number of oxygen atoms in each ring. Some of these

Table 6 - Rate Constants for the Complexation of 18C6 in Various Solvents 54-57

			$k_2/(1+K_{-0})^{(8)}$			
			or $k_2K_1^{(b)}$	k ₂ (c)	k-2	
Ions	Solvent	Temperature	$(\underline{M}^{-1} \cdot \sec^{-1})$	(sec ⁻¹)	(sec^{-1})	Mechanism
	1,3-dioxolane	25°C	8.5 x 10 ⁷	1	5.4 x 107	Chock
	DME	25°C	2.4×10^{8}	ı	6.6 x 10 ⁶	
LiC104	1,3-dioxolane	25°C	8.5×10^7	ı	5.4×10^7	
LiC104	МеОН	25°C	ı	6.0×10^7	ı	Eigen-Winkler
NaC104	МеОН	25°C	ı	2.8 x 108	ı	(2 steps)
KC104	МеОН	25°C	ı	1.8 x 108	ı	
NaC104	ЕtОН	25°C	ı	3.2×10^{8}	ı	
NaSCN	DMF	25°C	ı	3.7×10^8	ı	Eigen-Winkler
KSCN	DMF	25°C	1	1.6 x 108	ı	(3 steps)
KC104	DMF	40°C	ı	1.3×10^7	ı	1

cont. Table 6 -

(a) If the Chock mechanism applies, see text; (b) If the Eigen-Winkler mechanism applies, see text; (c) Except the last value at 40°C which represents k3 in the three-step Eigen-Winkler mechanism (Equation (1.24)).

Table 7 - Rate Constants and Activation Parameters for the Change of Conformation of 18C6 in Various Solvents⁵⁵⁻⁵⁷

Solvent	Solvent Temperature	$\frac{k_0}{(\sec^{-1})}$	k-0 (sec ⁻ 1)	ΔH [‡] (kcal/mol)	ΔS [‡] (e.u.)	AHo (kcal/mol)
МеОН	-20°C	1	3.14 x 108	5.8 ± 0.4	3.54 ± 0.01	-2.6 ± 0.4
МеОН	25°C	ı	2.09×10^9	1	I	ı
DMF	-10°C	9.9 x 106	5.5 x 108	7.5	10.2	-3.7
DMF	40°C	2.8×10^7	ı	l	I	1
Етон	-15°C	I	4.8 x 108	4.8	ı	-3.7

Table 8 - Activation Parameters for the Complexation of 18C6 in DMF According to a Three-Step Eigen-Winkler Mechanism⁵⁶⁻⁵⁷

Ions	Temperature	ΔΗ ₂ (kcal/mol)	ΔS ₂ [‡] (e.u.)	$(\Delta H_2 + \Delta H_3)$	$(M_2 + \Delta H_3)$ ΔH_3^{\ddagger} (kcal/mol)	ΔS ₃ [‡] (e.u.)	ΔH ₃ (kcal/mol)
NaSCN	25°C	2.4	-11.4	1.3	-	1	1
KSCN	25°C	3.55	- 9.1	-2.45	1	ı	ı
NaSCN	40°C	3.4	- 7.5	1.4	ı	ı	1
KC104	40°C	3.9	7.7 -	-0.91	3.4	-15.3	-5.4

macrocycle are shown in the Figure 6 below.

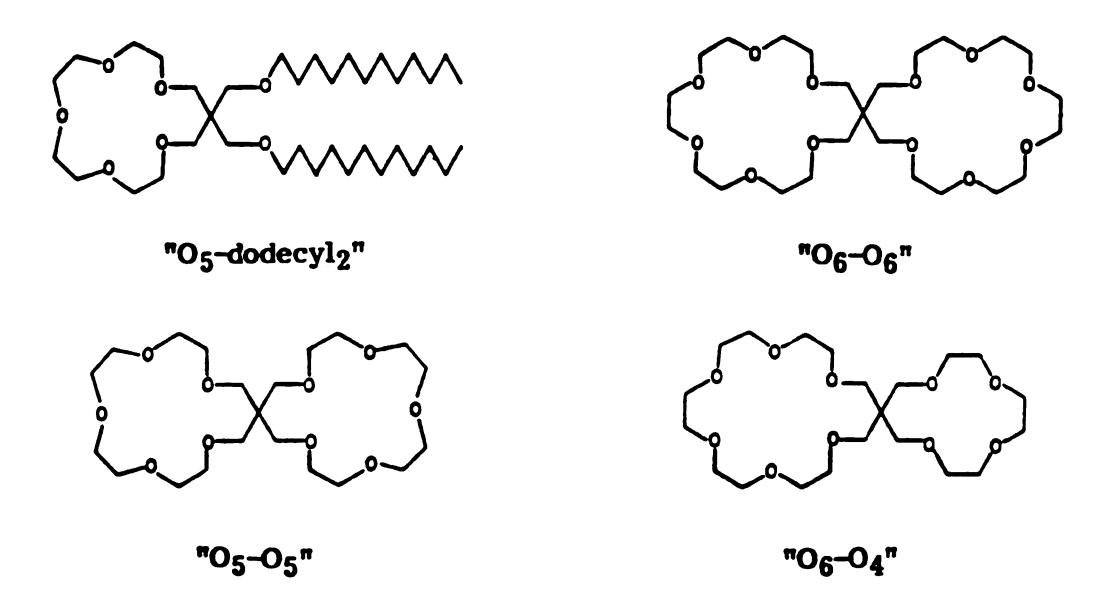


Figure 6. Some examples of spiro-bis-crown-ethers.

Since these ligands have two possible sites for the sodium ion, the authors could not derive any result with the method used which only applies for a two-sites exchange (see section 1.1). However, the "O₅-dodecyl₂" ligand with a single cavity could lead to the kinetic parameters which are shown in Table 9 along with those obtained by Schmidt and Popov.

McLain⁷⁷ reported a kinetic study of the complexation of NaPF₆ with a N-substituted monoaza-15-crown-5 in methylene chloride solutions using phosphorus-31 NMR spectroscopy. With an excess of crown, the author observed the bimolecular mechanism (Equation (1.16)). At 3°C, the rate of exchange dropped from 37.2 x 10^4 M⁻¹sec⁻¹ down to 3.86 x 10^4 M⁻¹sec⁻¹ when the substituent -P(Ph)₂[Fe(Cp)(CO)Me] is replaced by -P(Ph)₂[Fe(Cp)(CO) COMe] indicating that the oxygen of the extra carbonyl group in the second

Table 9 - Activation Parameters and Exchange Rates for Some Crown Complexes in Various Solvents^{67–68}

So I vent	8ystem	E _a (a) (kcal/mol)	AH _d (b) (kcal/mol)	[‡] (b) (ε.u.)	AGd (c) (298K) (kcal/mol)	$k_{\mathbf{d}}(\mathbf{d})$ $(\underline{\mathbf{M}}^{-1}.\mathbf{sec}^{-1})$	Mechanism(e)
acetone	K+.18C6	9.2 ± 0.5	8.6 ± 0.5	- 4 ± 2	9.8 ± 0.1	(4.1 ± 0.9) x 10 ⁵	-
acetone/ 1,3-dioxolane	K ⁺ ·18C6	13.8 ± 0.5	13.2 ± 0.5	12 ± 2	9.6 ± 0.1	$(5.7 \pm 1.1) \times 10^5$	-
Methanol	K+.18C6	9.2 ± 0.7	8.6 ± 0.7	- 3 ± 3	9.5 ± 0.2	$(6.8 \pm 2.7) \times 10^5$	_
				8 + 3	10.9 ± 0.2	$(6.8 \pm 2.7) \times 10^4$	=
И2О	K+.18C6	10.8	10.2	+ 3.1		3.7 x 10 ⁶	=
1,3-dioxolane	K+.18C6	16.8 ± 0.3	16.2 ± 0.3	15 ± 1	11.70 ± 0.01	$(1.65 \pm 0.04) \times 10^4$	1
		15.5 ± 0.7	14.9 ± 0.7	11 ± 2	11.67 ± 0.03	$(1.74 \pm 0.09) \times 10^4$	- 1
Pyridine	Na ⁺ · (O ₅ -dodecyl ₂)	9.44	8.85	-10	11.7	1.52 x 104	=

(a) Arrhenius activation energy; (b) ΔH_0^{\dagger} and ΔS_1^{\dagger} are the activation enthalpy and entropy, respectively; (c) $\Delta G_0^{\dagger} = \Delta H_0^{\dagger} - T_{\Delta} S_0^{\dagger}$; (d) Rate of decomplexation in sec⁻¹ when mechanism II applies; (e) I = bimolecular mechanism and II = associative-dissociative mechanism.

substituent is also bonded to the sodium ion giving an hexacoordinated sodium complex while the first substituent gives a pentacoordinated sodium complex. This conclusion was confirmed by infrared data obtained for the acylic carbonyl stretch in the 1500-1600 cm⁻¹ region. This result is in excellent agreement with those already obtained for the "lariat" ethers⁷⁸⁻⁸³. This new group of ligands, first synthesized by Gokel and co-workers⁸⁴ are crown ethers having one or more side chains with donor heteroatoms which can also bind to the cation. These side chains are attached either to a carbon or a nitrogen (for monoaza or diaza-crown ethers) of the ring, i.e., a carbon pivot or a nitrogen pivot respectively. Recently, Gokel et al.85 showed that the solid disubstituted diaza-18-crown-6.Na+ complex shown later (see Experimental Part), has a crystalline structure which is intermediate between those found for cryptate complexes (Na·C222)+ and (Na·C221)+. The arrangement of the macroring donor atoms is a twist-boat structure while the two hydroxyethyl side arms are bent on the same side of the ring. This cryptate like configuration in which the sodium ion is strongly encapsuled explains the decrease in the rate of exchange observed by McLain and discussed above.

Krane et al.65 reported a dynamic NMR study of lithium cation complexes with small crowns and could only report free energy barriers at coalescence which range from 9 kcal/mole at -93°C in CHCl₂F (Freon 21) to 17 kcal/mole at +42°C in 1,2-dichloroethane.

By analyzing the results presented above, along with those reviewed by Schmidt²⁵, the following picture emerges.

1. As with the cryptates, within a given solvent, variations in the stability constant, whether resulting from changes in cation or ligand, are essentially reflected in the dissociation rate of the complex, the association rate being diffusion controlled. We also see in Table 6 that when the cation

is too small to fit into the ligand cavity, there is complexation with fast decomplexation rate rather than no cation ligand interactions as it was believed in the early investigations of crowns complexation.

- 2. The dissociation rates are much higher in aqueous solutions reflecting the low stability of the crown complexes.
- 3. The energy barrier for decomplexation is lower for crown complexes than for the cryptates. This fact is directly related to the rate constants of decomplexation.
- 4. The flexibility of the crowns, as well as the substituents on it, influence the kinetic results to a great extent.
- 5. The cation exchange between the solvated and complexed sites can proceed either via the associative-dissociative mechanism or via the bimolecular mechanism. This means that for kinetics of crown ether complexation reactions, the kinetic parameters can no longer be derived from the kinetic parameters of decomplexation and the thermodynamic parameters without knowing the mechanism.
- 6. For a given cation and ligand, the relative change in the dissociation rate is less sensitive to the donor ability of the solvent with crowns than it is with cryptates.

In summary, stabilities of macrocyclic complexes can be viewed in terms of the following factors: radius-charge density of the metal ion, cation-ligand interactions including electrostatic (cation-anion, ligand-cation, ligand-anion) interactions, polarization and ligand field effects such as electrostatic ligand-ligand repulsion. Ion size specificity for a given ligand is usually explained in terms of compensation between binding energy, solvation of cation, ligand and complex and ligand conformational rearrangement energy upon complexation. As we see, the complexity of such systems is difficult

to overcome and the data interpretations as well as the proposed mechanisms are a very simplified picture of the actual phenomena. As explained earlier, a single technique is not sufficient enough and electronic spectroscopy, NMR spectroscopy of several nuclei, electrical conductance, electrochemical techniques and ultrasonic relaxation must all be used to derive all the species which are present and which undergo chemical exchange in solutions and to lead to a possible good understanding of macrocyclic complexation reactions in liquid solutions.

CHAPTER II

EXPERIMENTAL PART

2.1. Salts and Ligands Purification

Sodium salts were of analytical reagent grade quality. Sodium tetraphenylborate (Aldrich Gold Label), sodium iodide (Matheson, Coleman and Bell, MCB), sodium perchlorate (G. Frederick Smith) and sodium hexafluoroarsenate (Ozark Chemicals) were sufficiently pure for our purposes and were not further purified except for drying under vacuum at room temperature for a least two days. Sodium pentamethylcyclopentadienide (Alfa Products) was purchases as a 0.86 M solution in tetrahydrofuran (THF) and was diluted to the desired concentration. Sodium thiocyanate (Mallinckrodt) was recrystallized from acetonitrile (Fisher Scientific, certified ACS). The method consists of making a hot saturated solution (just below the boiling point of this solution), filter it in order to remove the insoluble impurities and then allow it to cool down to room temperature followed by a slow immersion into an isopropanol-dry ice bath. After ten to fifteen minutes, the crystallization was completed and the solvent was removed by filtration. This filtration was done fast enough so that the solution did not warm up to room temperature, so as not to redissolve the salt. The final product was a fine white crystalline powder. The resulting salt was finally dried on a vacuum line at a pressure less than 10^{-5} torr and at room temperature for at least two days.

The macrocyclic polyether 18-crown-6 (18C6, Aldrich) was recrystallized twice from acetonitrile⁸⁶. The dried 18C6 melts at 36-37°C [lit. m.p. 36.5-38.0°C⁸⁶, 39.5-40.5°C⁸⁷, 39-40°C¹]. Dibenzo-18-crown-6 (DB18C6, Parish) was recrystallized twice from benzene. The dried DB18C6 melts at 164-166°C [lit. m.p. 164°C¹]. Diaza-18-crown-6 (DA18C6 or [22], MCB) was recrystallized from n-heptane. The above three crowns were dried under vacuum at room temperature for at least two days. Dithia-18-crown-6 (DT18C6, Parish) was simply dried under vacuum at 50°C for at least two

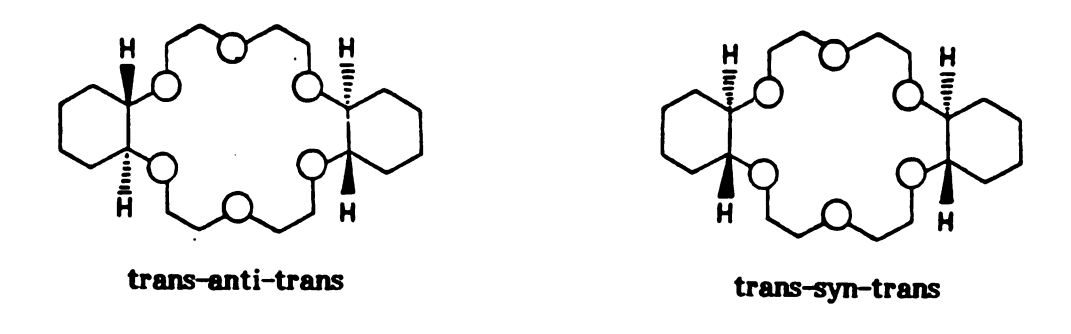
days.

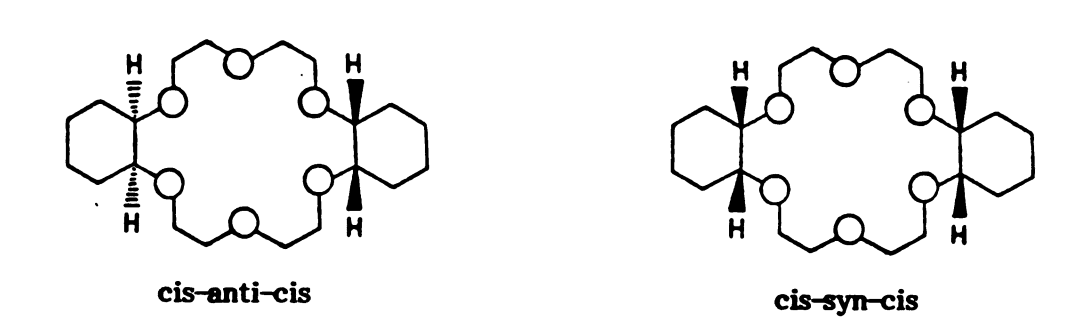
The mixed dicyclohexyl-18-crown-6 diastereoisomers (DC18C6, Aldrich) were separated into two principal components by Izatt and co-workers⁸⁸ who had previously identified the two major isomers as the cis-anti-cis (Isomer A, m.p. 83-84°C) and cis-syn-cis (Isomer B, m.p. 61-62°C) isomers. The structure of the five possible diastereoisomers is shown in Figure 7. It should be noted that isomer A also exists in a second crystalline form with m.p. 69-70°C⁸⁹. The two major isomers were separated by following the procedure developed by Izatt and co-workers⁸⁸. The method consists of taking advantage of the great solubility differences between the lead perchlorate (Pb(ClO₄)₂) and oxonium perchlorate (H₃OClO₄) complexes of isomers A and B.

Ia + Ib + Pb(ClO₄)₂
$$\xrightarrow{\text{H}_2\text{O}}$$
 [PbIa][ClO₄]₂·H₂O_(s) + [PbIb]²⁺ (2.1)

Ia + Ib + HClO₄
$$\stackrel{\text{H}_2\text{O}}{=}$$
 [H₃OIb][ClO₄]_(S) + [H₃OIa]⁺ (2.2)

The mixture of diastereoisomers is first dissolved in distilled water and isomer A precipitated as the lead perchlorate complex followed by filtration of the precipitate. The filtrate is then treated with hydrogen sulfide gas until the precipitation of the lead sulfide (PbS) is complete. The solid PbS is filtered off and the filtrate is treated with enough perchloric acid to precipitate isomer B as the oxonium perchlorate complex. Pure isomer A is isolated by dissolving the lead perchlorate complex in a mixture of N,N-dimethylformamide and water (50% by volume) followed by the precipitation of PbS with hydrogen sulfide gas. The precipitate is filtered off and the solvents removed under vacuum. Water is then added to the resulting viscous oil and this mixture is extracted with n-hexane. Pure isomer B is isolated by dissolving the oxonium





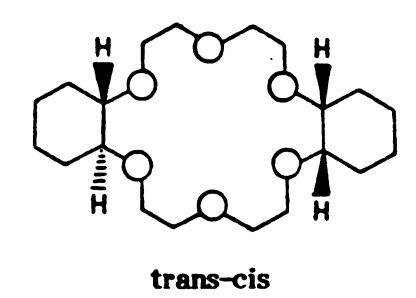


Figure 7 The five possible diastereoisomers of dicyclohexyl-18-crown-6

perchlorate complex in a mixture of acetone and water followed by extraction of this solution by n-hexane. For both isomers the n-hexane extracts are dried over anhydrous magnesium sulfate. The n-hexane is removed under vacuum and the solid isomers A and B are recrystallized from n-hexane and diethyl ether respectively. In our case, the hydrogen sulfide gas was obtained by the decomposition of sodium sulfide with a 30% phosphoric acid solution in a concentrated aqueous solution. The acid solution was allowed to drip slowly from a separatory funnel into the sodium sulfide solution. In the extraction and recrystallization steps, a mixture of hexanes was used instead of n-hexane as recommended in reference 88. The two diastereoisomers were then dried at room temperature on a vacuum line at a pressure less than 10^{-5} torr for at least two days. By using this method, 24% of isomer A (m.p. 67-68°C) and 20% of isomer B (m.p. 60-61°C) were obtained. These resulting yields, compared with those of reference 4 (39% and 44% respectively) are very low. This might be due either to the use of a mixture of hexanes instead of n-hexane as mentioned earlier or to diethyl ether for the recrystallization of isomer B which is definitely not appropriate. It should also be noted that, as shown above, the melting point of isomer A is not as good as the one of isomer B. This is very probably due to the separation step in which isomer A was first precipitated with aqueous lead perchlorate as the lead(II) complex. This aqueous lead perchlorate was made by dissolving 14.4 g of lead carbonate in a mixture of 14.8 g of 70% perchloric acid and 15 ml of water. The resulting solution has a pH = 3, therefore it also precipitated a small amount of isomer B as the oxonium perchlorate complex and affected the purity of isomer A. For future work, it would certainly be better to precipitate isomer B first.

Literature has been checked to see if it exists a significant spectroscopic

difference between the two major isomers in order to check quantitatively their purity. Unfortunately, the only difference ever observed thus far is the width of the proton NMR multiplet in the 3.3-4.0 ppm region⁹⁰. This difference is small as shown on Figure 8. The two isomers have also been separated by column chromatography on Woelm alumina (activity grade 1) using n-hexane-diethyl ether solvent mixtures as eluents⁸⁹. However, this separation method is costly and very time consuming with a low yield for each isomer⁸⁸.

The macrocyclic polyether N,N'-bis(2-hydroxyethyl)-1,4,10,13-tetraoxa-7,16-diaza-cyclooctadecane complexed with sodium iodide was a gift from Professor Gokel, its structure is shown below. It was dried at room temperature for two days.

Its purity was previously checked by proton NMR, carbon-13 NMR, infrared spectroscopy and elemental analysis by G.W. Gokel and his research group. The anhydrous complex melts at 131-132°C. It should be noted that the macrocyclic polyether can easily be obtained uncomplexed from DA18C6⁹¹.

All the melting points mentioned above were taken on a Thomas-Hoover melting point apparatus and are uncorrected. All salts and ligands were constantly kept in separate desiccators.

2.2. Solvent Purification

Tetrahydrofuran (THF, Mallinckrodt) was refluxed over magnesium metal

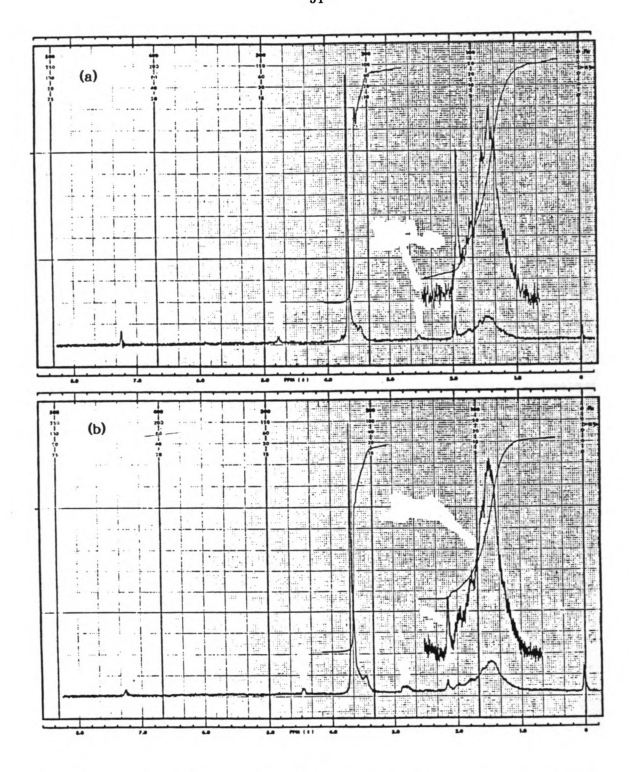


Figure 8 Proton NMR spectra of (a) the cis-syn-cis and (b) the cis-anti-cis isomer of dicyclohexyl-18-crown-6 at room temperature in CDCl₃

and benzophenone (an indicator which turns dark blue in the absence of water) for one week, fractionally distilled and then transferred into a dry box under dry nitrogen atmosphere and further dried over freshly activated 3 Å or 4 A molecular sieves. These sieves were previously washed with distilled water, then dried at 110°C for several days and finally activated at 500°C under a flux of dry nitrogen for 24 hours. It was found that, like methanol⁹², THF slowly decomposes after a prolonged standing over molecular sieves. Therefore, only a small quantity (100 ml) was stored over sieves while the remaining stock solvent was kept in a closed 500 ml flask in a dry box under nitrogen atmosphere. The water content of purified THF was determined by using a Varian Aerograph Model 920 gas chromatograph connected with a Sargent Welch Model SRG recorder. The method previously used in this laboratory was the standard additions method which was tedious and time consuming. A new method was developed, it consists of comparing the water peak of the solvent with the water peak of carbon tetrachloride (CCl₄, Mallinckrodt) saturated with water which contains 100 ppm of H₂O at 24°C⁹³. the water content of THF was always found to be less than 10 ppm by both methods. The experimental conditions were as follow:

Column: 80/100 Porapak QS; 5' x 1/4" SS

Carrier gas: Helium

Sample size: 5 microliters

Flow rates: Reference = 30 ml/min.

Carrier = 30 ml/min.

Temperature: Column = 200°C

Injection = 300°C

Detector = 245°C

53

Filament current:

90 mA

Attenuation:

1

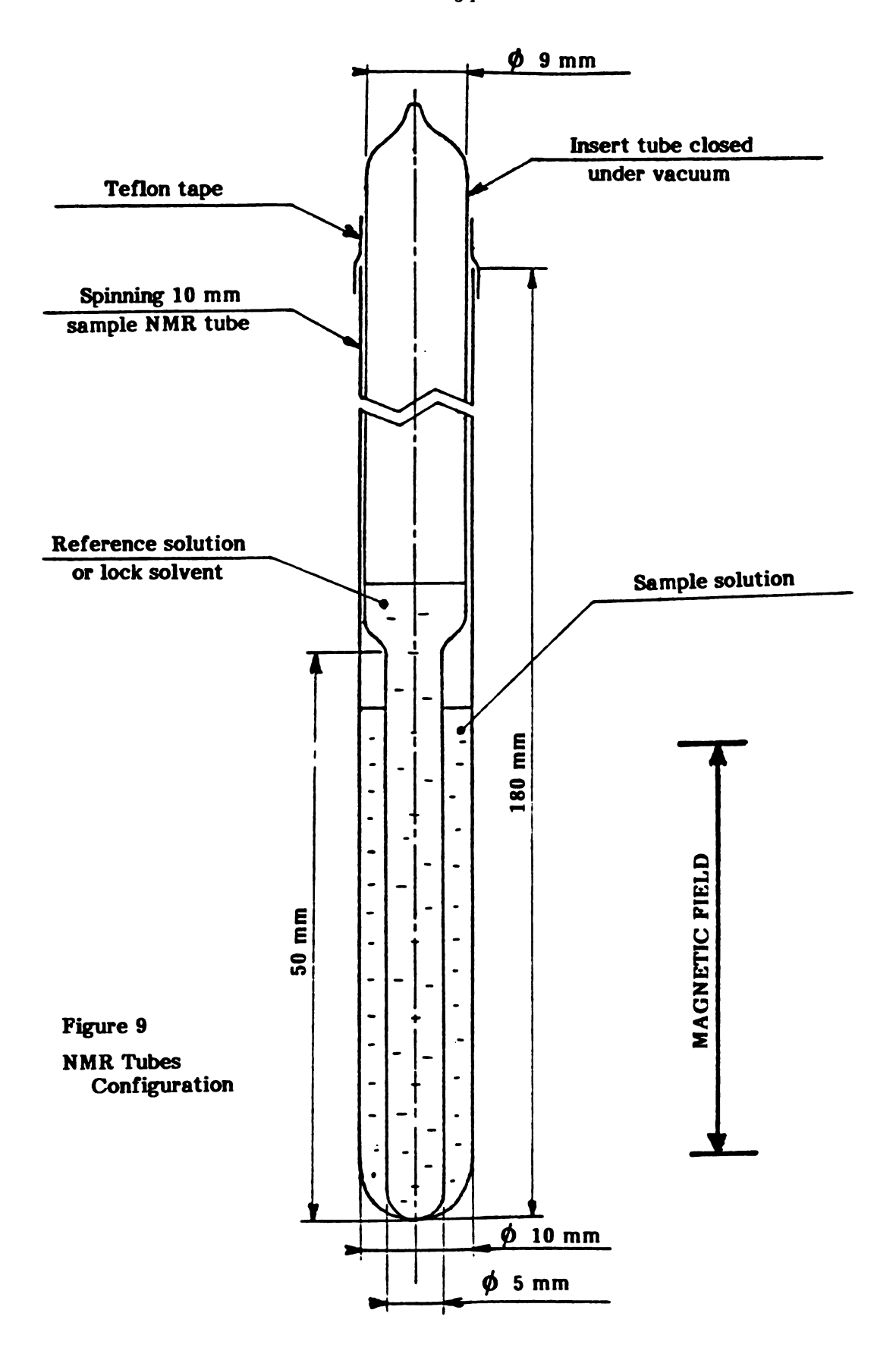
The deuterated solvents chloroform-d, acetone- d_6 (Stohler Isotopes) and deuterium oxide (D_2O , KOR Isotopes) were used as received.

2.3. Sample Preparation

In view of the hygroscopic nature of the nonaqueous solvents and of the reagents, all nonaqueous solutions were prepared either in a glove bag under dry nitrogen atmosphere or in a dry box under dry argon atmosphere. Flasks and NMR tubes were rinsed with distilled water, cleaned with hot concentrated nitric acid for at least 30 minutes in order to remove the sodium ion adsorbed at the surface of the Pyrex glass, rinsed again with distilled and deionized water, dried at 150°C for three days and then transferred into a desiccator All the flasks used for this study are class A Pyrex volumetric flasks.

2.3.1 Kinetic Measurements

Samples were prepared by weighing out various amounts of complexing ligand and salt either into 2 ml volumetric flasks for the qualitative kinetic study of the exchange (fast or slow on the NMR time scale) or into 10 ml volumetric flasks for the samples used to obtain the spin-spin relaxation time, T_2 , or the exchange relaxation time, τ , in the quantitative study. It was followed by dilution with THF. After dissolution, the solutions were transferred into 10 mm NMR tubes. The insert tube containing either the reference sodium chloride solution in D_2O for room temperature studies or a lock solvent (D_2O for high temperature studies or acetone- d_6 for low temperature studies) was then introduced in the NMR tube, which was wrapped with teflon tape (see Figure 9) to prevent contamination by atmospheric moisture as well as solvent



evaporation (major problem with THF solutions).

The reference solutions were made by dissolving an accurately weighed amount of dried sodium chloride in 99.75% D_2O in a 5 ml volumetric flask. After dissolution, each solution was transferred to an insert for 10 mm NMR tubes and frozen in a dry ice-isopropanol bath. This insert was then connected onto a vacuum line under rough vacuum (760 torr > P > 0.01 torr). The solution was degased by bringing it back to room temperature and freezing it again. The vacuum line was then connected to high vacuum (P < 10^{-5} torr) and the insert tube closed under vacuum to prevent any change in the reference solution concentration.

2.3.2. Formation Constants Measurements

Samples were prepared in 5 ml volumetric flasks as described above. They were transferred into 5 mm NMR tubes which were closed under rough vacuum without degasing. Because of the high vapor pressure of THF, as little empty volume as possible was left at the top of each tube to prevent large solvent evaporation which would change the solution concentration. The 5 mm tubes were individually introduced in a 10 mm tube with two spacers. The outer tube contained a reference solution of NaCl in D₂O whose concentration was adjusted by dilution until two sodium-23 NMR signals of about the same height were obtained. The 10 mm tube was then capped and wrapped with teflon tape. The reference concentration, although not known, was constant for a complete mole ratio study (12 samples) at a given temperature.

2.3.3. Conductance Measurements

The Erlenmeyer type conductance cells with a side arm for the introduction of the sample have been described elsewhere⁹⁴. They were cleaned with running distilled water for 2 hours, filled with hot nitric acid

for 30 minutes, cleaned again with running distilled water for 30 minutes, steamed with water vapors at 100°C for one hour and put into an oven at 120°C for at least one day. The sample were prepared, as described above, in 50 ml volumetric flasks and then transferred into a conductance cell which was then capped and wrapped with teflon tape.

2.4. NMR Measurements

2.4.1. Proton NMR Measurements

This technique was only used to check the purity of the two isomers of DC18C6, therefore a routine Varian T-60 NMR spectrometer was of sufficient quality for this purpose.

2.4.2. Sodium-23 NMR Measurements

2.4.2.1. Instrumentation

Sodium-23 NMR measurements were obtained with a Bruker WH-180 spectrometer operating at a field of 42.3 kG and a frequency of 47.610 MHz in the pulsed Fourier transform mode. A Nicolet 1180 data system equipped with a Nicolet 293B Programmable Pulser and a Nicolet NTCFTB-1180 program was used to carry out the time averaging of spectra and the Fourier transformation of the data. The high frequency probe (21-75 MHz) has a core diameter of 20 mm. A Tektronix 475A oscilloscope was used to tune the probe to the appropriate resonance frequency.

2.4.2.2. Reference Solution

0.1 \underline{M} and 0.5 \underline{M} solutions of NaCl in D₂O at 23°C were used as external standards. Since the chemical shifts of these solutions versus an aqueous sodium salt solution at infinite dilution are not known, the reported sodium-23 chemical shifts will be referred to either the 0.10 \underline{M} or the 0.50 \underline{M} solution of NaCl in D₂O. Live and Chan⁹⁵ reported chemical shifts

corrections due to differences in bulk diamagnetic susceptibilities between sample and reference solvents for a cylindrical sample placed in a magnetic field parallel to the main axis of the sample (superconducting magnets) under continuous wave conditions, according to the equation:

$$\delta_{\text{corr}} = \delta_{\text{obs}} - \frac{4\pi}{3} (K_V^{\text{ref}} - K_V^{\text{sample}})$$
 (2.3)

where K_V^{ref} and K_V^{sample} are the unitless volumetric susceptibilities 96 of the reference and the sample solvent respectively and $^{\delta}_{corr}$ and $^{\delta}_{obs}$ are the corrected and observed chemical shifts in ppm respectively. It should be noted than with pulsed experiments utilizing a superconducting magnet, the equation becomes:

$$\delta_{\text{corr}} = \delta_{\text{obs}} + \frac{4\pi}{3} (K_V^{\text{ref}} - K_V^{\text{sample}})$$
 (2.4)

where the symbols have the same meaning. Equations (2.3) and (2.4) are correct for chemical shifts when downfield (paramagnetic shift) is assigned as the positive shift. It was also shown by Templeman and Van Geet⁹⁷ that for low salt concentration, such as the ones used in this study, the contribution of the added salt to the volumetric susceptibility of the solutions can be neglected. Thus, the correction is constant for a given sample solvent and is meaningful only when chemical shifts of a given species are compared in different solvents. The volumetric susceptibility correction between D₂O and THF remains constant and does not affect, to any significant extent, our results.

2.4.2.3. Field-Frequency Lock and Temperature Control

Since THF-dg was not available in adequate quantities, the lock

solvents were never used as internal lock. The sample NMR tubes configurations have already been described in section 2.3.1 and 2.3.2. For each variable temperature study, the field was locked at a temperature close to the middle of the temperature range studied with either D_2O for high temperature studies or acetone- d_6 for low temperature studies.

Temperature was controlled with a Bruker B-ST 100/700 temperature control unit and measured to within \pm 0.1°C with a calibrated Doric digital thermocouple placed in the probe about 1 cm below the sample. A large flow of N_2 gas and a spin rate of 16-18 Hz were maintained in order to minimize the temperature gradient across the sample.

2.4.2.4. Measurements of the Sodium-23 Chemical Shifts at High and Low Temperature.

Measurements were first made at room temperature using a 0.10 \underline{M} sodium chloride solution in D_2O as the external reference. This reference was then replaced by the pure lock solvent and the spectra were obtained again without the reference. The temperature was changed to the desired one without loosing the lock. The chemical shifts were obtained by comparing the position of the signals versus one edge of the spectrum. Since the sweep width was not changed for a given variable temperature study, the chemical shifts of the species at different temperatures could be obtained versus 0.1 \underline{M} NaCl in \underline{D}_2O at room temperature.

2.4.2.5. Data Acquisition and Signal Processing

Although the receptivity of the sodium-23 nucleus is high (9.25 x) 10^{-2} relative to the proton⁹⁸), high quality spectra required for lineshape analysis were difficult to obtain because of the low concentration of the solutions and also because of a 20 mm core diameter for the probe used which implies 5 mm of "dead" space around the 10 mm NMR tubes. To overcome

this problem, we used a high magnetic field but it was still necessary to carefully optimize every step of the data acquisition in order to obtain spectra with good signal to noise (S/N).

2.4.2.5.1. Signal Averaging

In dilute solutions (0.01 \underline{M} in Na⁺) sodium-23 NMR signals cannot be obtained in one scan and signal averaging is necessary. At room temperature the typical number of scans (NS) to obtain adquate spectra using a 10 mm NMR tube are:

NS = 15,000 if $W_{1/2} = 80$ Hz and LB = 15 Hz

NS = 40,000 if $W_{1/2}$ = 300 Hz and LB = 50 Hz

where LB is the artificial line broadening (see below) and $W_{1/2}$ the width of the NMR signal at half-height. Fortunately, sodium-23 spin-spin relaxation times, T_2 , are short so that many signals can be accumulated in a short time. Typical experiment times are 10 minutes for narrow lines ($\simeq 100$ Hz) and 20 minutes for broad lines ($\simeq 300$ Hz). However, care must be taken to avoid both truncation of the free induction decay (FID) and saturation which distort the line shape⁹⁹. All measurements were done in such a way that the FID decayed completely during the acquisition time which should always be greater than $5T_1$, T_1 being the spin-lattice relaxation time of the nucleus being investigated. Even when this condition applies, a fast acquisition often leads to some baseline distorsion.

2.4.2.5.2. Zero Filling Technique

The theoretical and practical aspects of this technique were reviewed by Lindon and Ferridge¹⁰⁰. They consist of increasing the point to point resolution and sometimes improving lineshapes and positions by adding more than N zeros to an N-point FID prior to Fourier transformation. This technique was used for all kinetic studies and, typically, the spectra accumulated using

No points of memory were zerofilled to 4No or 8No points 100,101 . With a spectrum width of 6500 Hz the chemical shifts were accurate to \pm 0.1 ppm for narrow lines and to \pm 0.3 ppm for broad lines and the line widths to \pm 10%. For broad signals, the zerofilling technique saves a considerable amount of time.

2.4.2.5.3. Sensitivity Enhancement

The FID's were multiplied by a negative exponential weighing function $f(t) = \exp(-LB/t)$ so that the line shape remains Lorentzian after transformation. This method improves the S/N ratio and does not affect the line shape 100. For each spectrum a compromise must be found between the sensitivity enhancement and undesirable line broadening. A typical artificial line broadening which was found to apply well for this study is about $0.2 W_{1/2}$.

2.4.3. Data Handling

All the FID's for the quantitative kinetic studies were stored on a high density disk prior to Fourier transformation. They could be recalled at will and Fourier transformed until the correct artifical line broadening was found. The spectra were expanded in the region of interest by using the Nicolet NTCFTB-1180 program. At this point, care must be taken to write down the frequency scale, i.e., the number of Hz between 2 points, and not to have too many points describing the baseline and just a few points describing the NMR signal. If so, the fit of the spectra will not be good due to the lack of information contained in the transferred spectra. For example, one can see in Figure 10 the fits of two different transfers of the same spectrum with the same phasing. The difference in the relaxation time, τ , is not very big but the drop by a factor of two in the relative error leads to a better accuracy in the kinetic parameters and gives more reliability to the results obtained.

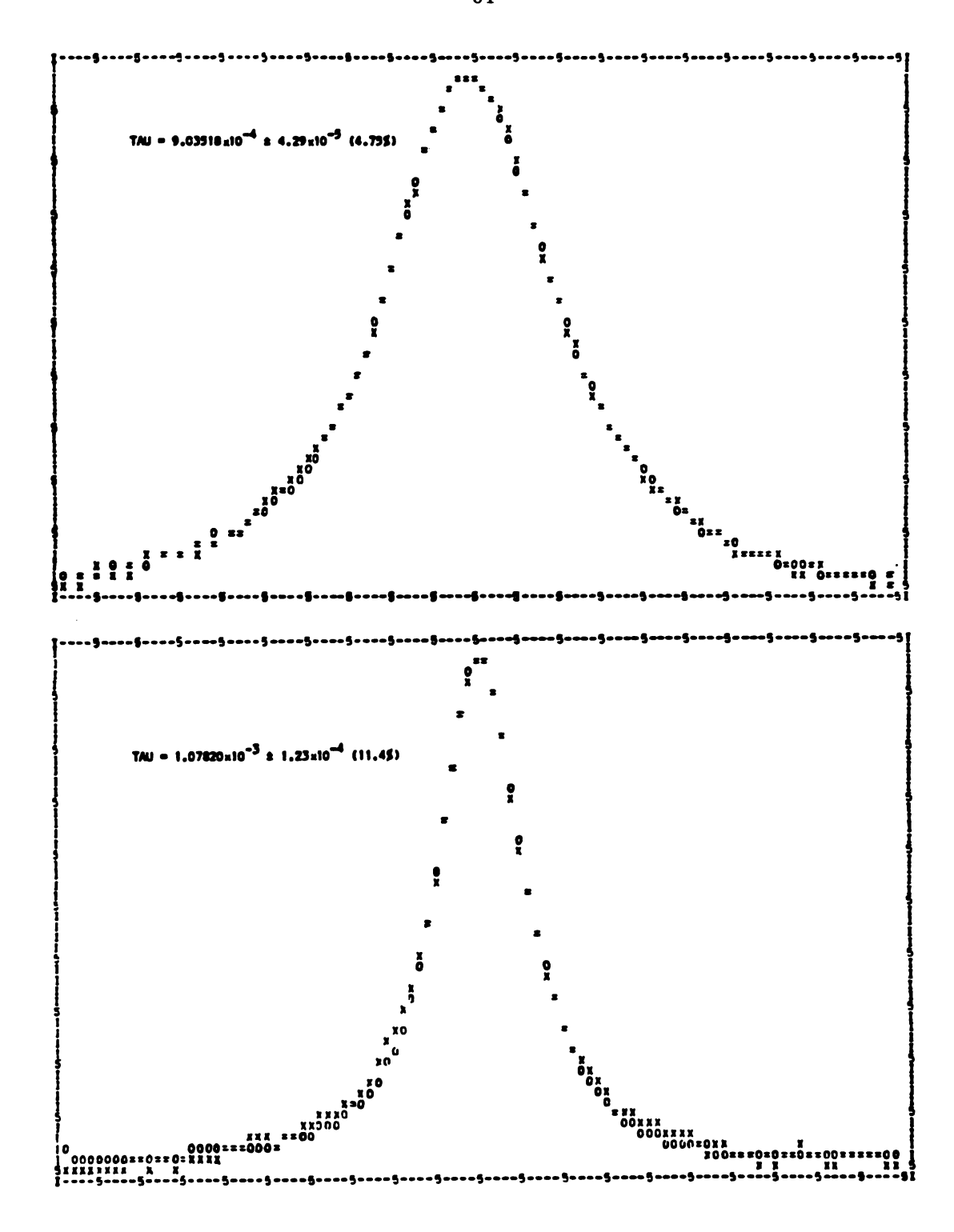


Figure 10 Computer analysis of the ²³Na lineshape for a THF solution containing 0.01 M NaSCN and 0.005 M DA18C6 at -39.2°C. (x) experimental points. (o) calculated points

The expanded region of the spectra was transferred in the ASCII format onto a floppy disk in a PDP-11 (Digital Equipment Corporation, DEC) microcomputer by using the Nicolet NTCDTL data-transfer subroutine (See Appendix I). The microcomputer was previously connected to the RS-232 CH.B outlet of the Nicolet 1180 Data System. The floppy was initialized and conditioned to accept a file in the ASCII format with the RT-11 Version 4 program 102 located on the system floppy. After the transfer of all the desired files, the floppy was taken to another PDP-11 (DEC) computer connected to a CIBER CDC-6500 computer system. Then, the files were put in the appropriate format for the non-linear least-squares curvefitting program KINFIT¹⁰³ by using the NIC-84 program¹⁰² in RSX language. The files in the KINFIT format were kept in permanent memory in the PDP-11 (DEC) computer until transferred onto a magnetic tape using the CIBER-6500 language. Finally, the magnetic tape was mounted on the CIBER CDC-6500 computer and the files put in permanent memory on the CDC-6500 (See Appendix II). At this stage, the desired file can be called (without omitting the 1 in column 70 of the control card in the KINFIT program) and fitted to the appropriate equation (See Appendices III and IV).

The stability constants of complexes were calculated by fitting the chemical shift-mole ratio data to the appropriate equation using the program KINFIT (See Appendix V).

2.5. Conductance measurements.

2.5.1. Conductance Equipments

Resistances were measured at 398 \pm 2, 629 \pm 2, 971 \pm 6, 1942 \pm 11 and 3876 \pm 18 Hz with a bridge assembly originally designed and described by Thompson and Rogers 104 which was duplicated with minor improvements

by Smith¹⁰⁵. The complete conductance circuit is described elsewhere^{105,106}. The cell was always connected in parallel with a capacitor and when the cell resistance was greater than 90,000 ohms, the cell was shunted in parallel with a 90,000 ohms standard precision resistor. This wiring was installed in a metallic box connected to the ground in order to avoid any electromagnetic and/or electrostatic interferences from the surrounding. A Heath Company laboratory oscilloscope was used as a null point detector. The Erlenmeyer type cells were thermostated to within \pm 0.05°C in a constant temperature oil bath as recommended by J. Comyn et al.¹⁰⁷.

2.5.2. Data Handling

The cell constants given in Table 10 were determined at 25.00°C. To determine these constants, aqueous potassium chloride solutions were used and the conductance equation of Barthel et al. 108 was applied as follows:

$$\Lambda = 149.873 - 95.01C^{1/2} + 38.48C \log C + 183.1C - 176.4C^{3/2}$$
 (2.5)

By examining Table 10, we see that the most reliable results were obtained at 971 Hz with the 25 ml and 30 ml cells since two reproducible cell constants are given in both cases. The 20 ml cell was used to determine the conductivity of pure THF. One might think that the oven drying of these cells changed their constants which are geometrical factors given by the equation:

$$K(cm^{-1}) = \frac{\ell(cm)}{S(cm^2)}$$
 (2.6)

where K is the cell constant, ℓ is the distance between the electrodes and S is the area of the electrodes. The 25 ml and 30 ml cells used for this study are made of Pyrex (coefficient of linear expansion = 3.5 x 10^{-6} K⁻¹)

Table 10 - Cells Constants for Various Frequencies at 25.00°C ± 0.05°C

Frequency (Hz)	20 ml cell	25 ml cell	30 ml cell
398 ± 2	(a)	2.321(c)	1.487(c)
629 ± 2	(a)	2.432(c)	1.476(c)
		2.429(b)	
971 ± 2	(a)	2.413(c)	1.464(c)
		2.416(b)	1.463(b)
1942 ± 11	0.508(b)	2.406(b)	1.450(b)
3876 ± 18	0.505(b)	2.358(c)	1.424(c)
		2.395(b)	1.443(b)

⁽a) The values could not be obtained.

⁽b) Values obtained by Bruce Strasser (personal communication)

⁽c) Values obtained by Roger Boss (personal communication)

and their electrodes are 5.4 cm and 6.4 cm apart from each other, respectively. The change in the cells constants for a 100°C change in temperature will always be less than the experimental error on the cells constants.

Also, Khazaeli⁹⁴ suggested a correction for irreversibility at the electrodes and the capacitance by-pass effect for the same experimental set-up, by using the equation:

$$R_{meas} = R_0 + af^2 + b/f^{1/2}$$
 (2.7)

in which R_{meas} and R_o are measured and corrected resistances respectively, f is the frequency and a and b are adjustable parameters. This equation was not used in this work, because it is not correctly referenced and therefore no proof is given for the validity of this equation and also because the five data points obtained at the five frequencies for each sample are not enough to get a good estimate of the three unknowns R_o , a and b. The goal of the conductance work being only a qualitative comparison of the ionic association in solution, the data will be reported at the individual frequencies for each system.

CHAPTER III ROOM TEMPERATURE SODIUM-23 NMR STUDY OF THE EXCHANGE OF SOME SODIUM SALTS WITH 18C6 AND SOME SUBSTITUTED ANALOGS IN THF

3.1. Introduction

In numerous thermodynamic and kinetic studies of crown ether and cryptand complexation with metal ions in solution, it has been usually assumed that the anions do not play a significant role in such reactions. This fact is surprising since soon after the discovery of the crown ethers by Pedersen¹, Schori and co-workers²⁴ observed a strong anion dependence on the exchange kinetics of the sodium ion with DB18C6 in DMF solutions. At -13°C, the rate of decomplexation drops from 800 sec⁻¹ to 445 sec⁻¹ and from 1800 sec⁻¹ to 1220 sec⁻¹ at a ligand to salt mole ratio of 0.17 and 0.35 respectively, when the thiocyanate anion is replaced by the tetraphenylborate. This was the first indication of slow decomplexation rates with the tetraphenylborate as well as of the dependency of exchange kinetics of macrocyclic complexation reactions on the anion.

Ten years later, J.D. Lin^{19,109} studied the interactions of the sodium ion with 18C6 in low dielectric solvents THF and 1,3-dioxolane and found unquestionable evidence of this exchange kinetics dependence on the anion. Using sodium-23 NMR spectroscopy, she observed a slow exchange, on the NMR time scale, at room temperature which is characterized by two sodium resonances on the NMR spectrum, when the counteranion is the tetraphenylborate at a ligand to salt mole ratio of 0.5 in both solvents. This exchange becomes fast, i.e., one population averaged sodium resonance, when the counteranion is either the perchlorate or the iodide. These results confirmed the ones previously obtained by Schori et al. and it became clear that the anion could no longer be ignored when studying exchange kinetics of macrocyclic complexation reactions especially in low dielectric media.

The goal of the work presented in this chapter is to use sodium-23 NMR spectroscopy for continuing the investigation of the anion effect on the

exchange kinetics of the sodium ion with crown ethers in low dielectric ethereal solvents. Since the slow exchange described above was only observed with the 18C6, we also investigate the effect of substituent groups on the ligand by using a variety of 18 member ring crown ethers.

3.2. Results and Discussion

Since the slow exchange described earlier was only observed in THF and 1,3-dioxolane, we decided to carry out this study in THF first because this solvent presents a wider range of applications such as organic synthesis, organometallic chemistry, polymer chemistry¹¹⁰⁻¹¹² and also because several studies on ionic association in THF involving some of the salts used for this study have already been reported as it will be discussed in the next chapter. Most of the salts and crowns as well as the corresponding complexes are soluble in THF allowing the study of a large variety of combinations and therefore the derivation of more interesting comparisons. The key properties of THF are given in Table 11.

For this study, a ligand to salt mole ratio of about 0.5, and a total concentration of salt of 0.05 M, was used for most of the systems investigated. These systems include the following sodium salts, NaBPh4, NaSCN, NaI, NaClO4, NaAsF6, NaCp(CH3)5 (where Cp = cyclopentadienide) and complexes of these salts with each of the following crowns, 18C6, DC18C6(cis-anti-cis), DC18C6(cis-syn-cis), DA18C6, DT18C6, DB18C6 and the N,N'-disubstituted DA18C6 earlier described in Chapter II. The measurements were carried out at room temperature. The results are presented in Table 12. Some representative spectra are shown in Figures 11-23.

Although these results describe systems undergoing chemical exchange, we can, nevertheless, deduce some general trends from these data. When

Table 11 - Key Properties of Tetrahydrofuran(a)

Density	_{0.880} (b)
	0.883(c)
dlnv/dT(d)	0.001085(b)
	0.00133(c)
Viscosity log n	-3.655 + 393/T(b)
	$-3.670 \pm 395/T(c)$
Dielectric Constant D	-1.495 + 2659/T(b)
	-1.50 + 2650/T(c)
dlnD/dlnT	-1.16(b)
	-1.19(c)
Donor number DN(e)	20.0
Melting point m.p. (°C)	-108
Boiling point b.p. (°C)	65
Dipole moment μ (Debye)	1.75

⁽a) At 25°C unless otherwise indicated; (b) Determined from -70 to 25°C, reference 113; (c) Determined from -78 to 30°C, reference 114; (d) v = molar volume; (e) The Gutmann donor number DN is defined as the negative enthalpy for the reaction $S + SbCl_5 \xrightarrow{1,2-DCE} S \cdot SbCl_5$. That is DN = $-\Delta H^{\circ}_F$ (S·SbCl₅) where S is the solvent molecule and 1,2-DCE is 1,2-dichloroethane¹¹⁵,116.

Table 12 - Sodium-23 Chemical Shifts and Linewidths at Half-Height of Some Sodium Salts Undergoing Chemical Exchange with Some 18 Member Ring Crown Ethers in THP(a)

Salt	Ligand	$C^{T_{N_{\mathbf{B}}}+(b)}$	[crown](c)	Temperature (°C)	(p) [§] (d)	W _{1/2} (d) (Hz)
NaBPh ₄	18C6	0.050	0.59	22.9	- 7.1 -15.6	65 171
	DC18C6 cis-anti-cis	0.051	0.49	23.6	- 7.2 -15.0	80 (e)
	DC18C6 cis-syn-cis	0.051	0.48	23.6	- 7.2 -13.4	55 (e)
	DA18C6	0.049	0.50	22.9	- 8.2	105
	DT18C6	0.050	0.50	24.4	8.9 -	45
	DB18C6	0.0053 ± 0.0001	0.49	23.6	(£)	(800)
NaSCN	18C6(g)	0.050	0.52	24.8	(h)	196
	DC18C6 cis-anti-cis	0.051	0.49	23.6	- 5.9	227
	DC18C6 cis-syn-cis	0.049	0.51	23.5	- 5.9	245

Table 12 - cont.

Selt	Ligand	$C^{T}_{Na}^{+}(b)$	[crown](c) [salt]	Temperature (C°)	(mdd)	W _{1/2} (d)
	DA18C6	0.049	0.50	22.9	- 4.1	130
	DT18C6	0.05	0.52	24.0	- 2.4	100
	DB18C6	(i)				
NaI	18C6(j)	0.05	0.51	(h)	- 2.1	(h)
	DC18C6 cis-anti-cis	0.050	0.50	23.6	+ 0.7(k)	104(k)
	DC18C6 cis-syn-cis	0.052	0.48	23.6	+ 0.2(k)	122(k)
	DA18C6	0.050	0.50	22.9	+ 0.9(k)	78(k)
	DT18C6	0.050	0.52	24.0	8.9 +	25
	DB18C6	(i)				
	N,N'- diethanol DA18C6	0.0051 ± 0.0001	0.52	23.8	(J)	(e) (e)
NaC104	18C6(j)	0.05	0.51	(h)	-12.8	(h)

Table 12 - cont.

Salt	Ligand	$CT_{Na}^{+}(b)$	[crown](c) [salt]	Temperature (C°)	(mdd)	W _{1/2} (d) (Hz)
	DC18C6 cis-anti-cis	0.053	0.47	23.6	-10.6	7.1
	DC18C6 cis-syn-cis	0.051	0.49	23.6	-10.4	88
	DA18C6	0.051	0.49	23.3	6.7 -	72
	DT18C6	0.049	0.52	24.0	7.7 -	22
	DB18C6	(i)				
NaAsF ₆	18C6	0.010	0.50	23.9	(f)	229
	DC18C6 cis-anti-cis	0.010	0.50	23.9	(J)	112
	DC18C6 cis-syn-cis	0.010	0.50	23.9	(J)	171
	DA18C6	0.010	0.54	23.9	(f)	102
	DT18C6	0.010	0.51	23.8	8.6	31

Table 12 - cont.

(i) 0.050 0.51 0.050 0.52 cis 0.050 0.50 0.050 0.50	$cT_{Na}^{+}(b)$ $\frac{[crown]}{[salt]}(c)$	Temperature (C°)	(mdd)	W _{1/2} (d)
18C6 0.050 0.51 DC18C6 0.050 0.52 cis-anti-cis 0.050 0.50 DC18C6 0.050 0.50 cis-syn-cis 0.050 0.50 DA18C6 0.050 0.50 DT18C6 0.050 0.51	(i)			
0.050 0.52 0.050 0.50 0.050 0.50		23.6	(-35.3)	(006)
0.050 0.50 0.050 0.50 0.050 0.51		23.6	(-35.3)	(006)
0.050 0.50		23.6	(-35.3)	(1000)
0.050 0.51		23.6	-24.6	550
		23.6	-29.6	360
0.49	0.050 0.49	23.6	-28.5	> 1000

(a) The chemical shifts are vs. NaCl (0.10 M) in D₂O and are uncorrected for bulk volumetric susceptibility; (b) C^T_{Na} + ± 0.001 M unless otherwise noted; (c) Mole ratio ± 0.01; (d) δ ± 0.2 ppm and W_{1/2} ± 10% except the values in brackets which are estimated; (e) Could not be determined; (f) The spectrum was obtained without external reference; (g) Results obtained from Bruce Strasser. Personal communication; (h) The value was not reported; (i) The complex is not soluble; (j) Results obtained from reference 109; (k) The result was obtained from the deconvolution subroutine NTCCAP of the Nicolet NTCFTB program, see Figures 17-19.

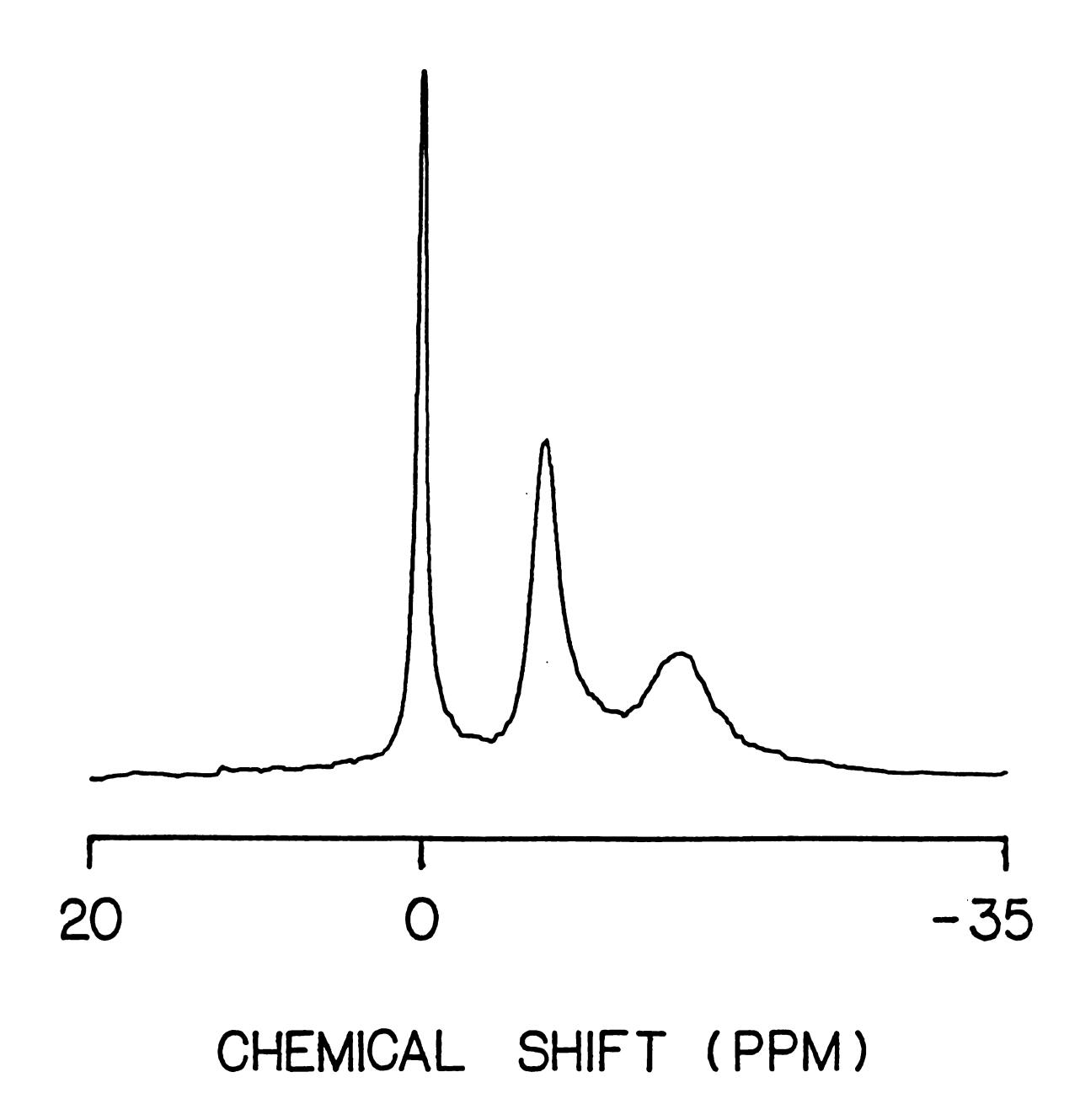


Figure 11 Sodium-23 NMR spectrum of NaBPh₄ (0.051 \underline{M}) and DC18C6 cis-anti-cis (0.025 \underline{M}) in THF with NaCl (0.1 \underline{M}) in D₂O as external reference. T = 23. $\overline{6}$ °C

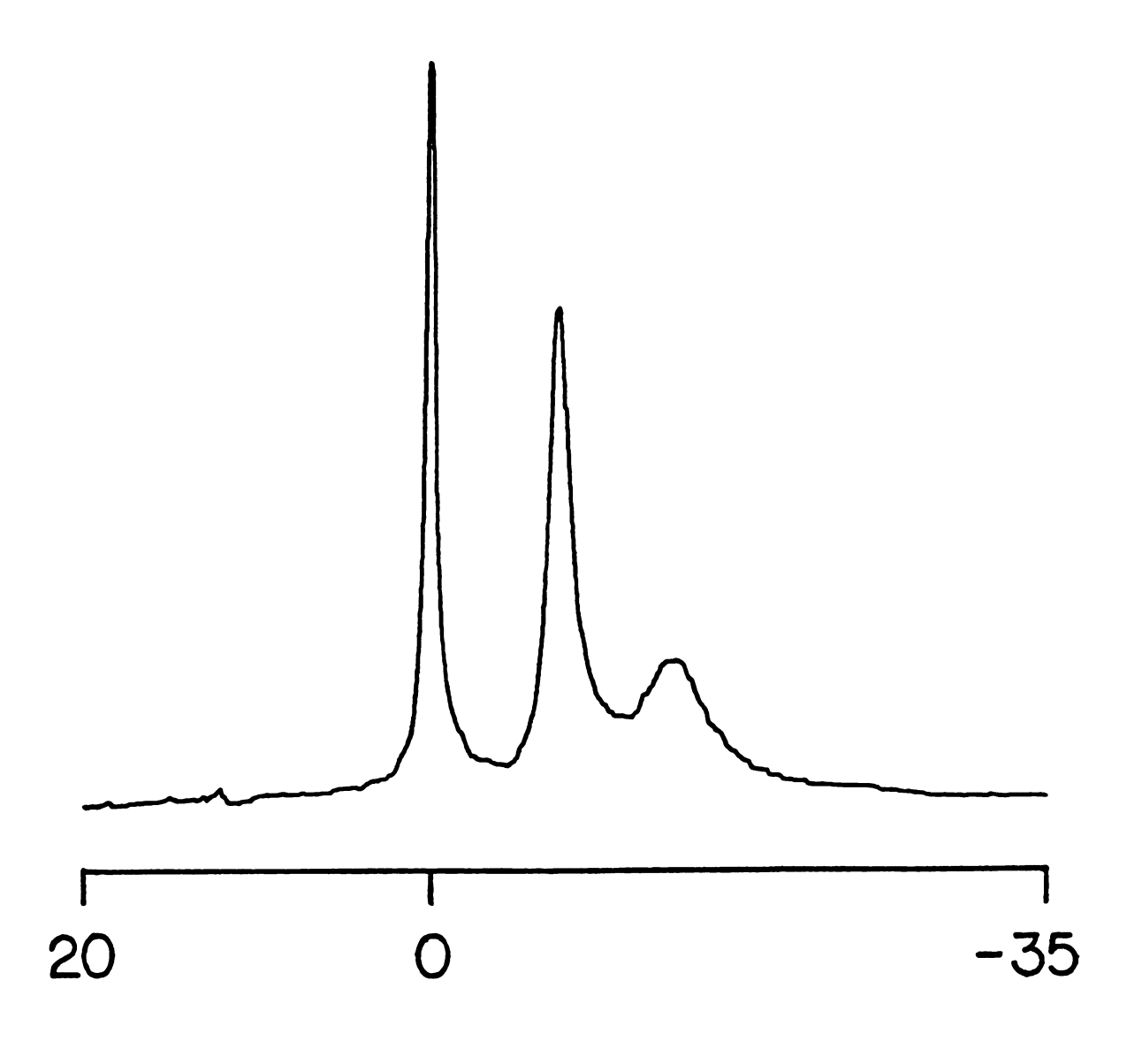


Figure 12 Sodium-23 NMR spectrum of NaBPh₄ (0.051 \underline{M}) and DC18C6 cis-syn-cis (0.024 \underline{M}) in THF with NaCl (0.1 \underline{M}) in D₂O as external reference. T = 23.6°C

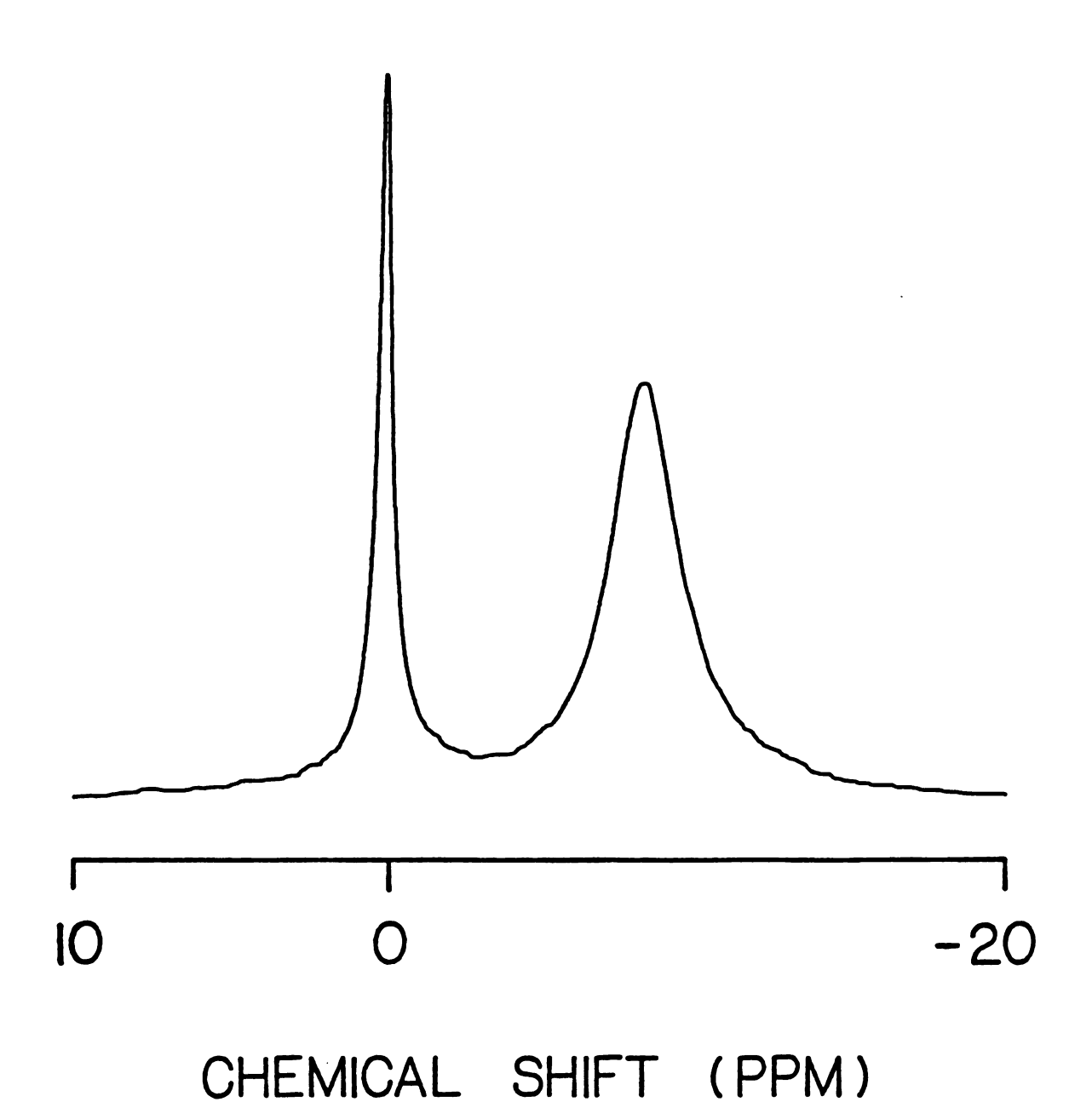


Figure 13 Sodium-23 NMR spectrum of NaBPh₄ (0.049 \underline{M}) and DA18C6 (0.025 \underline{M}) in THF with NaCl (0.1 \underline{M}) in D₂O as external reference. T = 22.9°C

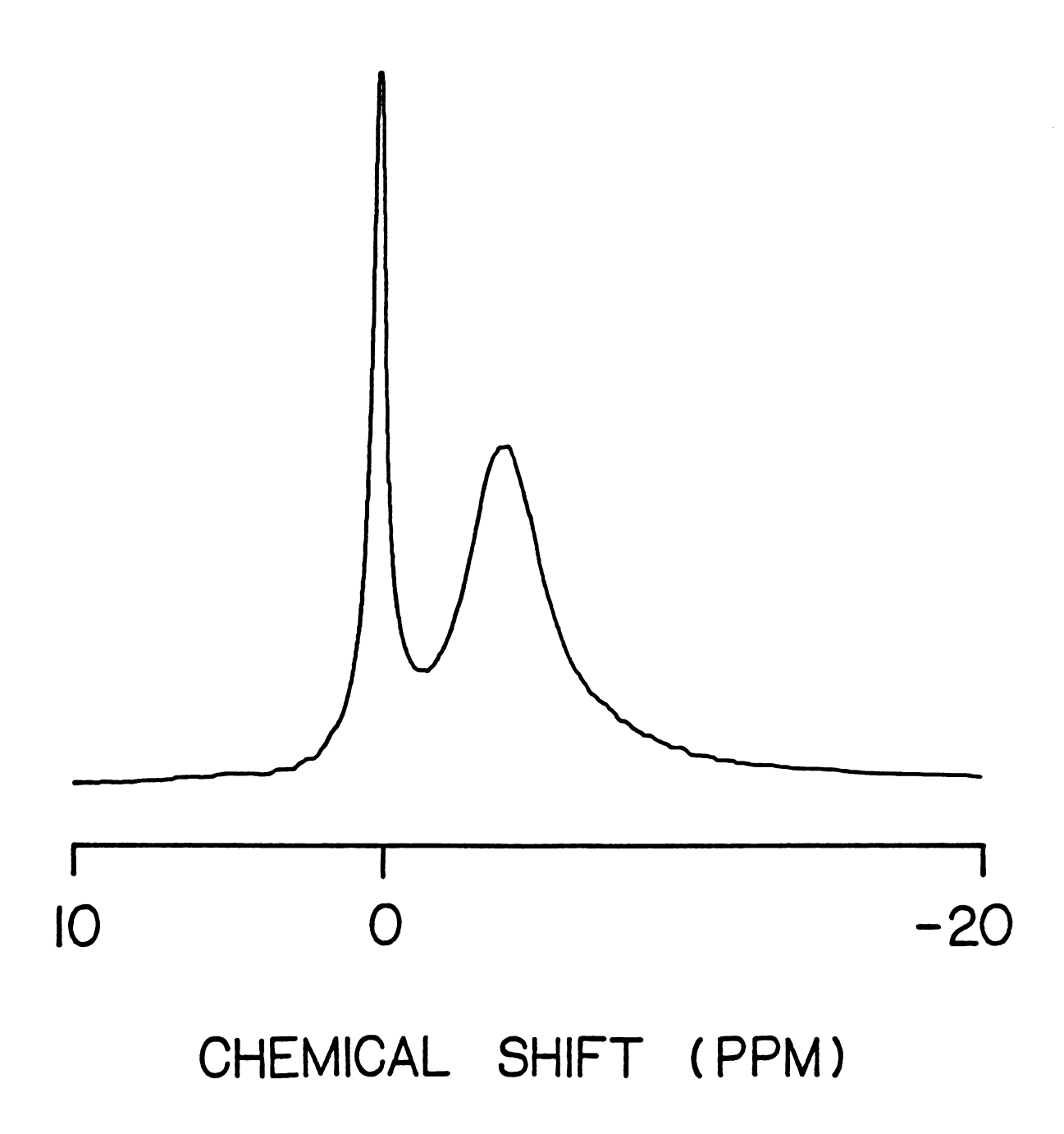


Figure 14 Sodium-23 NMR spectrum of NaSCN (0.049 \underline{M}) and DA18C6 (0.025 \underline{M}) in THF with NaCl (0.1 \underline{M}) in D₂O as external reference. T = 22.9°C

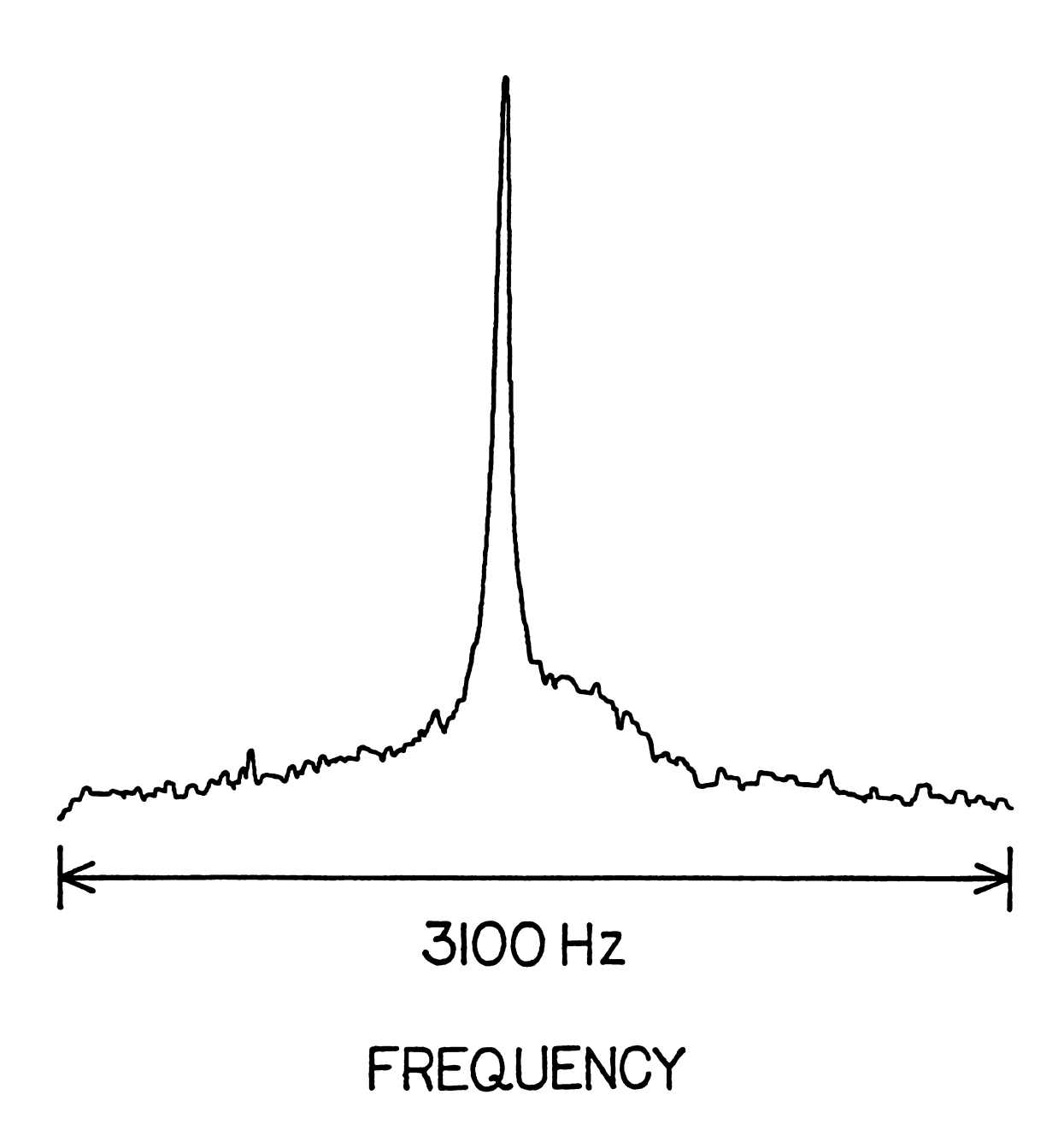


Figure 15 Sodium-23 NMR spectrum of NaBPh₄ (0.0053 \underline{M}) and DB18C6 (0.0026 \underline{M}) in THF. T = 23.6°C

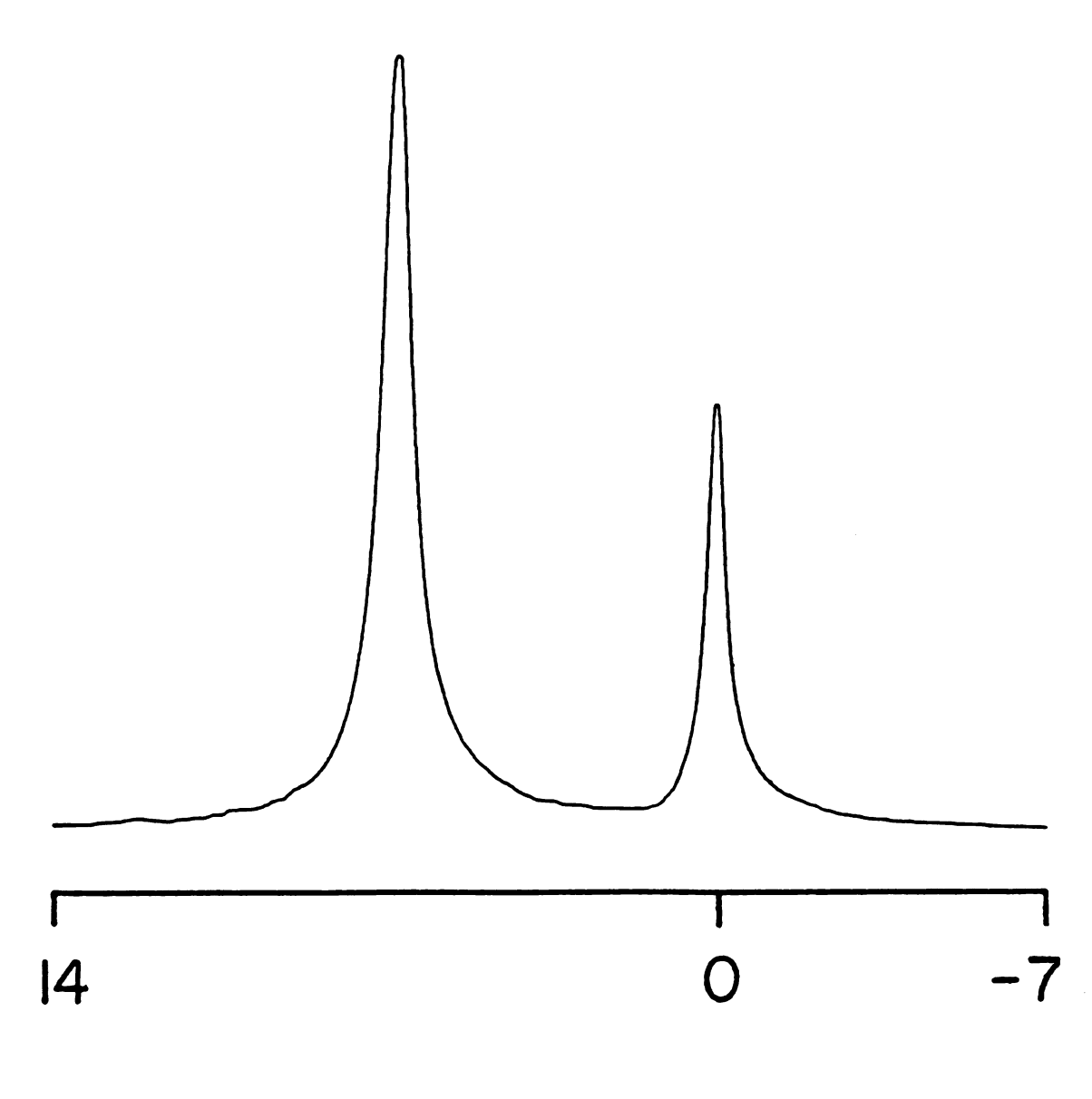


Figure 16 Sodium-23 NMR spectrum of NaI (0.050 \underline{M}) and DT18C6 (0.026 $\underline{\underline{M}}$) in THF with NaCl (0.1 $\underline{\underline{M}}$) in D₂O as external reference. $\overline{\underline{T}}$ = 24.0°C

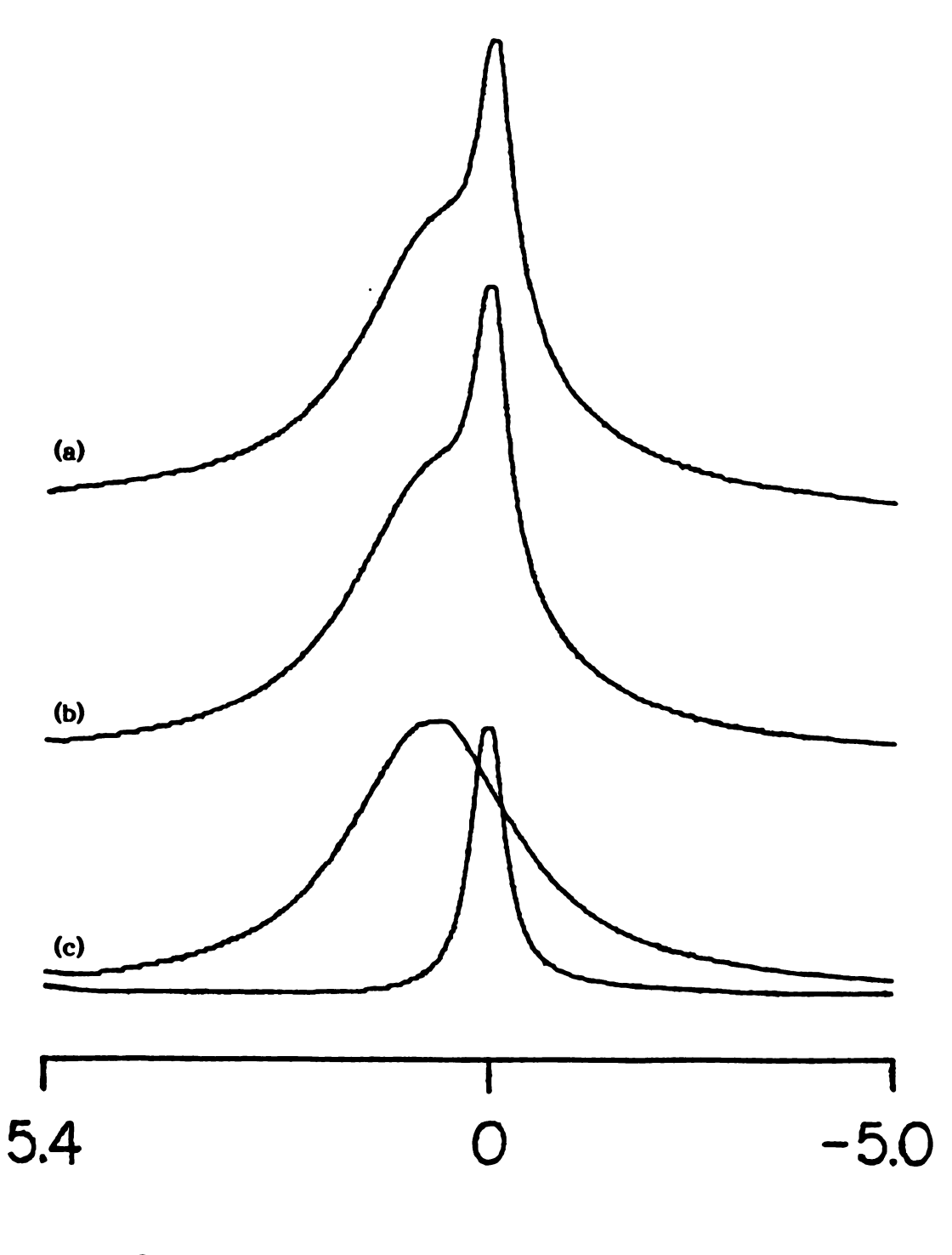


Figure 17 (a) Sodium-23 NMR spectrum of NaI (0.050 \underline{M}) and DC18C6 cis-anti-cis (0.025 \underline{M}) in THF with NaCl (0.1 \underline{M}) in D₂O as external reference. T = 23.6°C. (b) Calculated spectrum. (c) Deconvoluted spectrum

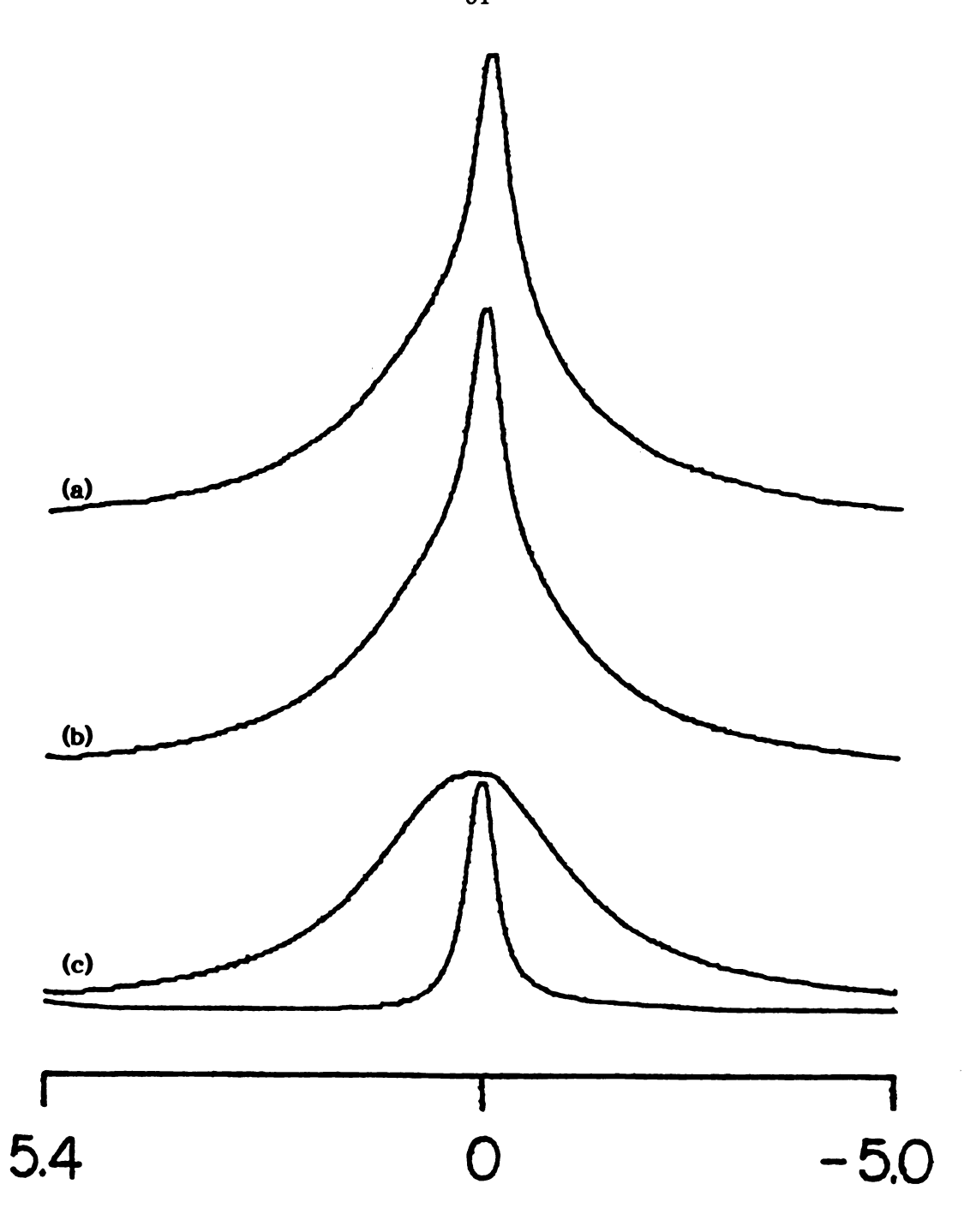


Figure 18 (a) Sodium-23 NMR spectrum of NaI (0.052 M) and DC18C6 cis-syn-cis (0.025 M) in THF with NaCl (0.1 M) in D₂O as external reference. T = 23.6°C. (b) Calculated spectrum. (c) Deconvoluted spectrum

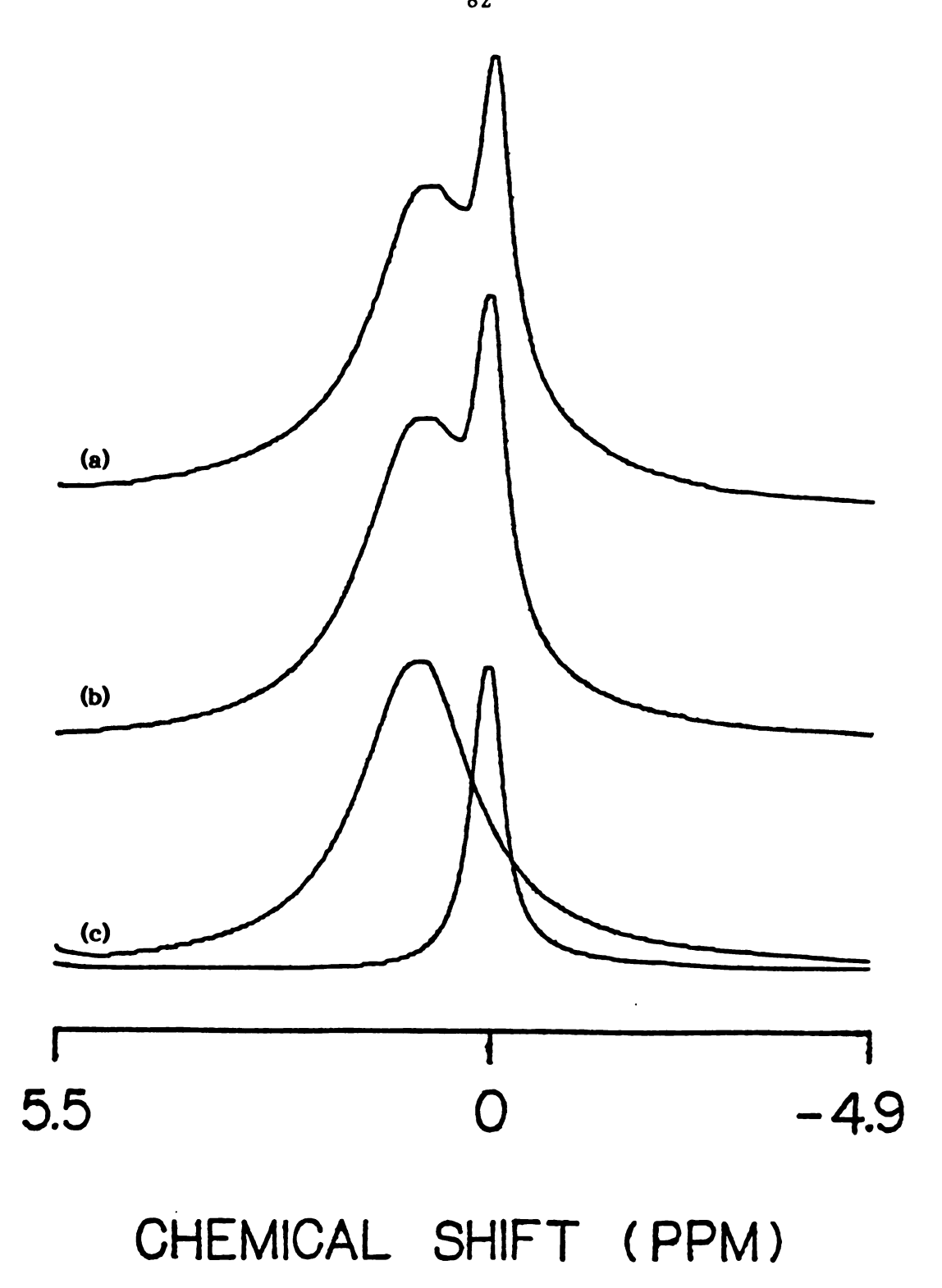


Figure 19 (a) Sodium-23 NMR spectrum of Nal (0.050 \underline{M}) and DA18C6 (0.025 \underline{M}) in THF with NaCl (0.1 \underline{M}) in D₂O as external reference. T = 24.0°C. (b) Calculated spectrum. (c) Deconvoluted spectrum

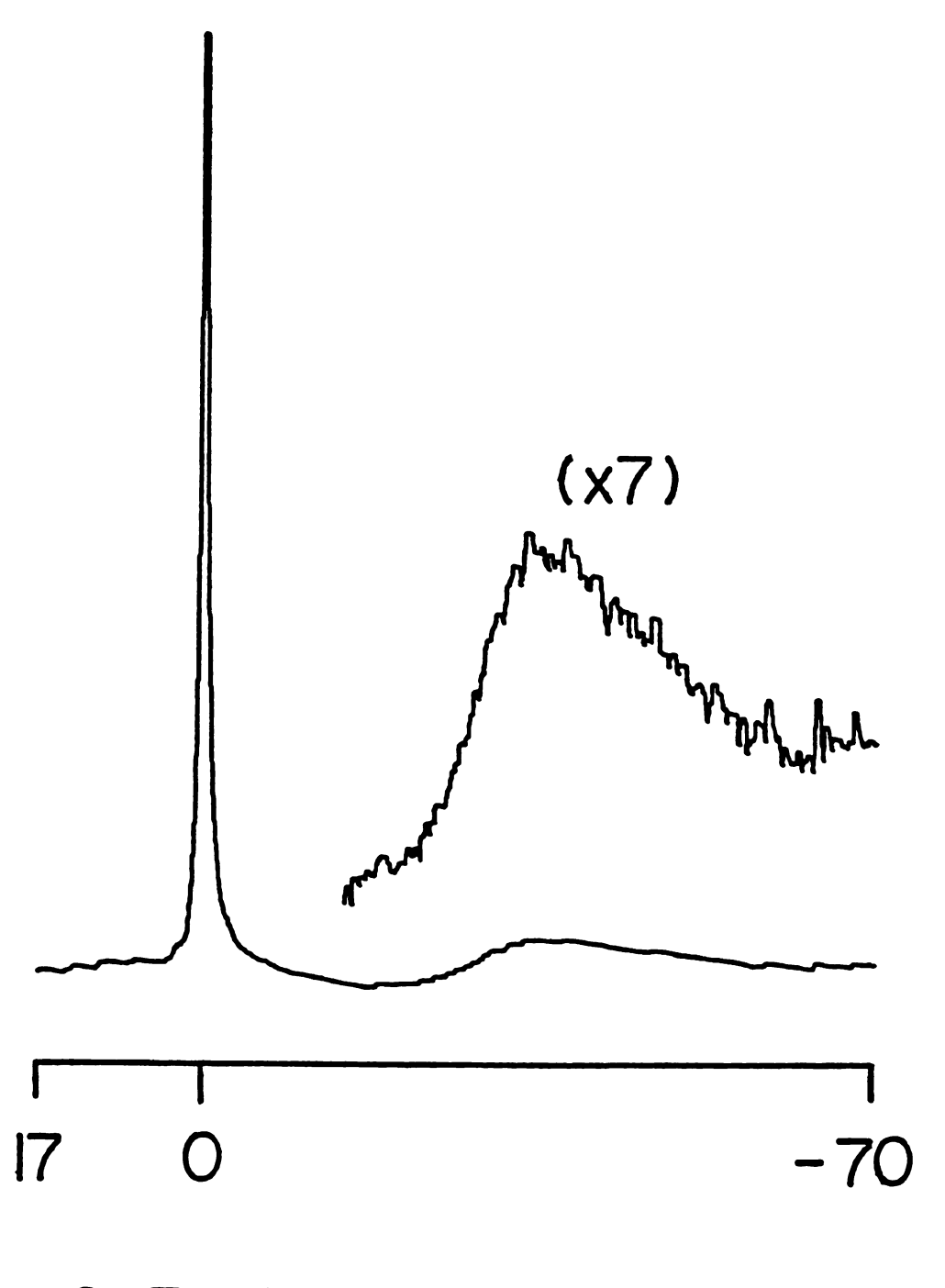
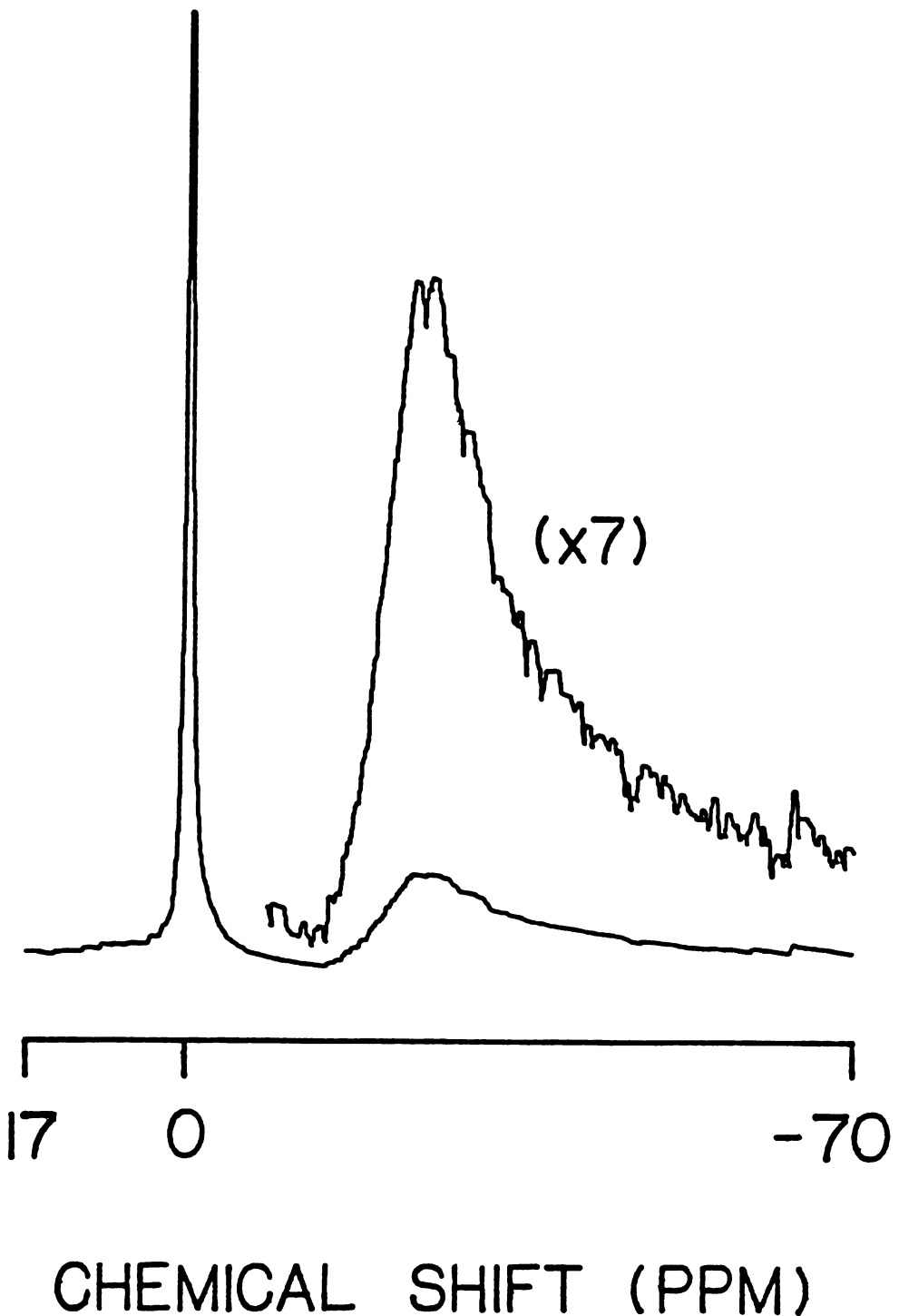


Figure 20 Sodium-23 NMR spectrum of Me₅CpNa (0.050 \underline{M}) and 18C6 (0.026 \underline{M}) in THF with NaCl (0.1 \underline{M}) in D₂O as external reference. T = 23.6°C



Sodium-23 NMR spectrum of Me₅CpNa (0.050 \underline{M}) and DA18C6 (0.025 \underline{M}) in THF with NaCl (0.1 \underline{M}) in D₂O as external reference. T = 23.6°C Figure 21

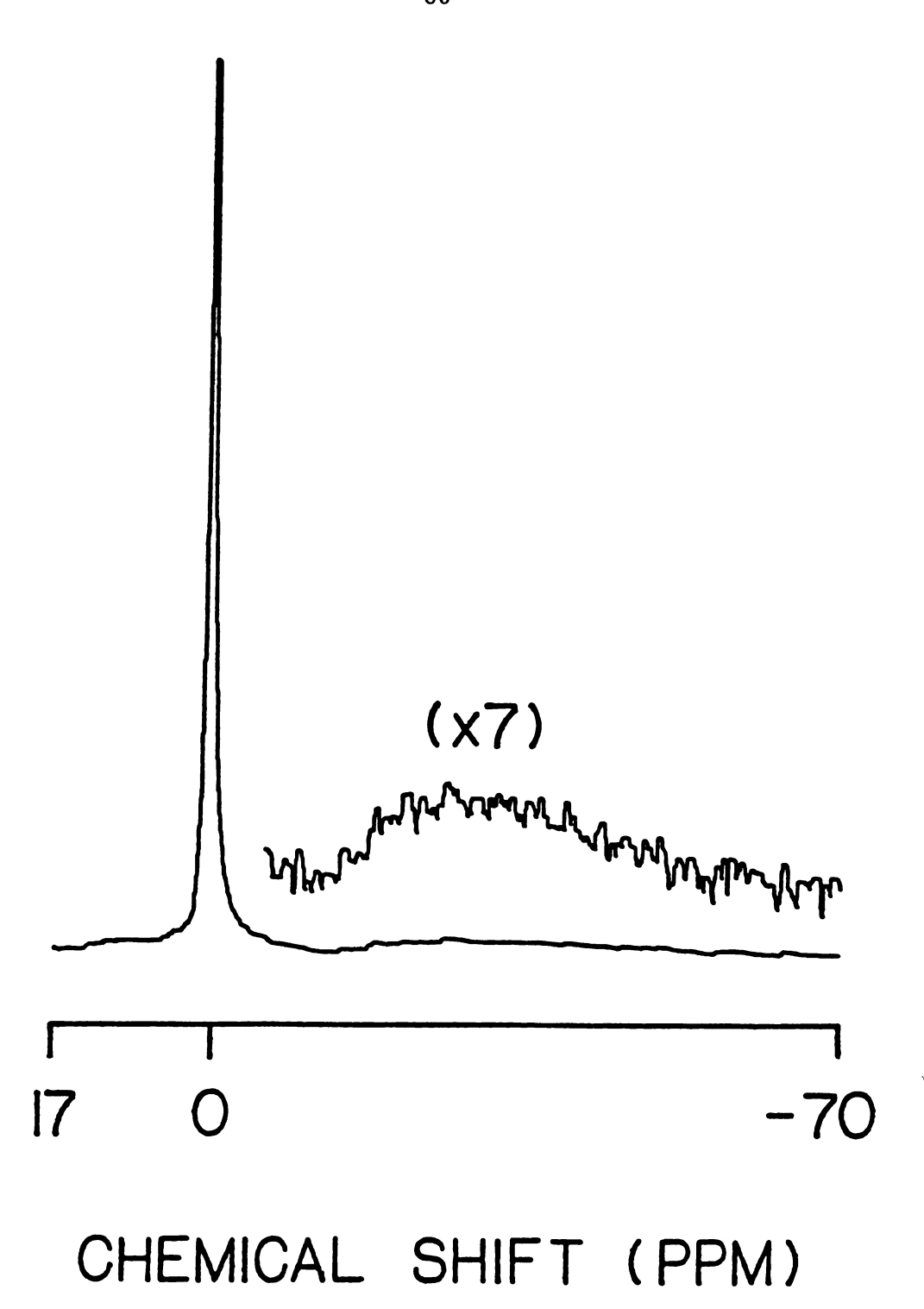


Figure 22 Sodium-23 NMR spectrum of Me₅CpNa (0.050 <u>M</u>) and DB18C6 (0.024 <u>M</u>) in THF with NaCl (0.1 <u>M</u>) in D₂O as external reference. T = 23.6°C

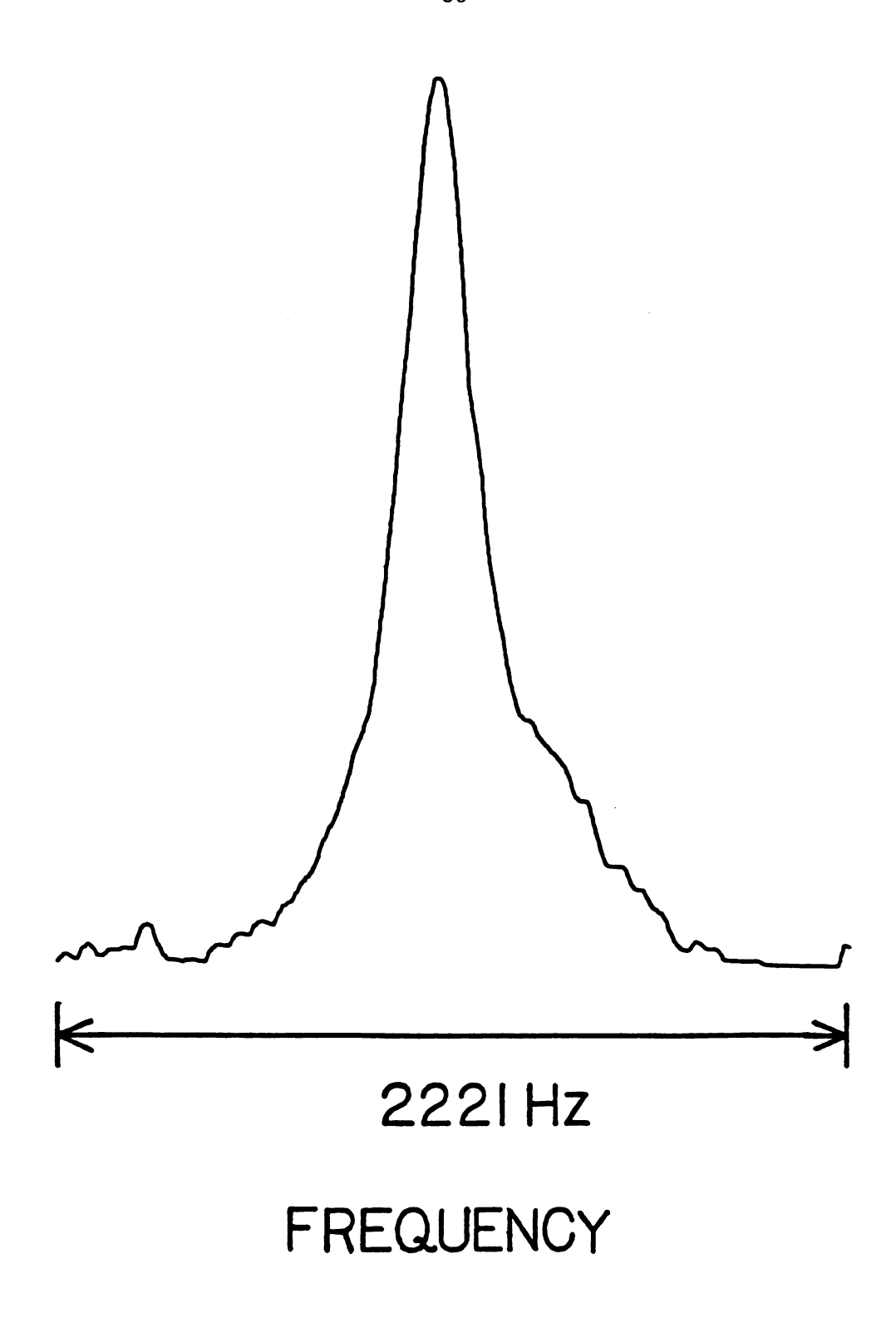


Figure 23 Sodium-23 NMR spectrum of NaI (0.0051 \underline{M}) and N,N'-diethanol-DA18C6 (0.0027 \underline{M}) in THF. T = 23.8°C

a quadrupolar nucleus, e.g., ²³Na, is placed in an environment which does not have cubic symmetry, the line width of the NMR signal increases due to the asymmetry of the electric field at the nucleus²². In general, the lines are broader for the crown complexes than for the solvated species indicating that the electric field produced by the planar structure of the former is less symmetrical than that created by the solvation spheres of the solvent molecules. Both, the number and the position of the donor atoms of the crown ethers are essential in determining the alkali metal NMR line width. Another factor broadening the NMR signal is the charge-charge interaction between the alkali metal ion and the counter anion. In low dielectric solvents, such as THF, ions are very largely associated to form ion pairs and higher aggregates; as a result the asymmetry of the electric field around the metal ion is increased and the NMR signal is broadened.

On theoretical grounds, an increase of electron density around the nucleus is characterized by a paramagnetic or downfield shift, i.e., the chemical shift becomes more positive. It is usually viewed in terms of short-range repulsive overlap of the electron donor with the cation. This was found to be borne out by experiment in a number of cases such as the "inclusive" Cs⁺·C222 complex⁴⁴.

Let us first discuss the meaning of coalescence. The coalescence temperature is the temperature at which the two signals corresponding to the solvated and complexed sites of the nucleus merge into one, i.e., the "valley" between the two separate peaks disappears. The determination of coalescence temperature is, therefore, directly related to the resolution of the instrument which is a function of the magnetic field used and is of limited interest for the understanding of the dynamics of exchange. For a system under chemical exchange, i.e., at a ligand to salt mole ratio of about

- 0.5, there are three possible observable types of NMR spectrum.
- 1. Above coalescence temperature, if the exchange is fast on the NMR time scale, i.e., the relaxation time τ is short; one population averaged NMR signal is observed, that is characterized by the following chemical shift and line width.

$$W_{1/2obs} = p_A W_{1/2A} + p_B W_{1/2B}$$
 (3.1)

$$\delta_{\text{obs}} = p_{\text{A}} \delta_{\text{A}} + p_{\text{B}} \delta_{\text{B}} \tag{3.2}$$

2. Above coalescence temperature, if significant exchange broadening occurs, an NMR signal at a chemical shift described by equation (3.2) and with a line width at half-height broadened by chemical exchange will be observed. The linewidth at half-height is given by the equation below.

$$W_{1/2obs} = p_A W_{1/2A} + p_B W_{1/2B} + 4 \pi p_A p_B (v_A - v_B)^{2\tau}$$
 (3.3)

The exchange broadening factor being $4\pi\,p_A p_B (\ \nu_A - \nu_B)^2 \tau$.

3. Below coalescence temperature, the exchange is slow on the NMR time scale and two NMR signals, broadened by chemical exchange, are observed. The limiting chemical shifts and line widths of these two signals when τ is very long, are those of the solvated and complexed species.

Thus a comparison of the data from Table 12 is rather difficult since the case in which a particular spectrum falls above coalescence is not known. However, being given that the complex is stable and that the [ligand]/[Na⁺] ratio is constant and since the resonance frequency of a solvated sodium salt remains constant, the frequency of the population averaged NMR signal

is directly related to the frequency of the complexed species according to equation (3.2) and the comparison of the observed chemical shifts for a given sodium salt undergoing fast exchange can be made. The observed trend is shown below.

DT18C6 > DA18C6 > DC18C6 > 18C6

The diamagnetic shift observed upon complexation shows that the electron density around the sodium ion is greater in the solvated state than in the complexed state. This is in good agreement with the good solvation ability of THF which has a Gutmann donor number of 20.0 and also with the cavity size of the crowns which have been shown to be too large for the sodium ion¹² resulting in less short-range interactions of the donor atoms with the cation. Thus, the trend shown above can be seen in terms of stability of the complexes, the more stable the complex is, the less cation-solvent interactions occur. The more upfield shift observed upon complexation of the Na⁺ ion by 18C6 is probably also due to the great flexibility of this crown ether which can envelope the sodium ion better than the other crowns. It has been observed that this ligand has a D_{3d} symmetry in the complexed state with alternating oxygen atoms being in two parallel planes¹¹⁷.

Another interesting observation is that the chemical shifts obtained with the pentamethylcyclopentadienide anion are strongly shifted upfield.

A comparison of the observed line widths is certainly less straightforward since the spectra can be differently broadened by chemical exchange. However, knowing that considerable ion pairing occurs in THF, the resulting line widths of the solvated and complexed species should generally be broad (> 100 Hz) and one can reasonably assume that the exchange broadening will be small

enough to allow a qualitative comparison as done above with the chemical shifts. a given sodium salt, the linewidth data show DC18C6(cis-syn-cis) generally gives a broader signal indicating a very asymmetric electric field for the sodium complex due to the two cyclohexyl rings being both on the same side of the average plane of the crown. A noticable exception to this trend is obtained with NaAsF₆ and 18C6; at room temperature, this system is very probably close to coalescence and the signal is largely broadened by chemical exchange. On the other hand, the lines obtained with DT18C6 are fairly narrow for sodium-23 NMR probably indicating a conformational rearrangement of this ligand upon complexation resulting in a better symmetry around the sodium ion. As previously noted, the pentamethylcyclopentadienide has a very different behaviour and gives a broader signal than the other anions.

With regards to the exchange rate alone (fast or slow on the NMR time scale), it is slow with 18C6, the two DC18C6 and DB18C6 when the anion is the tetraphenylborate and becomes fast with the thiocyanate, the iodide, the perchlorate, the hexafluoroarsenate and the pentamethylcyclopentadienide. The latter was selected to show whether the organic character and the bulkiness of the counter anion plays a significant role or not. The results are quite clear and indicate that the ionic association undoubtedly governs the exchange rate since the anion is the only parameter which is varied in all these systems.

Trying to derive a rational explanation on why fast exchange occurs with NaBPh₄ when the crown ether is the DA18C6 or the DT18C6 is more difficult because the observation of coalescence is directly related to the chemical shift range between solvated and complexed species according to the following equation.

$$k_{c} = \sqrt{\frac{\pi}{2}} \left(v_{A} - v_{B} \right) \tag{3.4}$$

where k_{C} is the rate of decomplexation at coalescence, the other symbols have their usual meaning. The observation of coalescence is also related to the linewidths of the two sites. For a given nucleus and frequency range ($\nu_{A} - \nu_{B}$), the coalescence temperature of a system with relatively narrow lines for the two non-exchanging sites will be higher than that of a system with broad lines for the solvated and complexed sites. For the reasons given above, the phenomena observed with NaBPh₄ and all the studied crowns cannot be explained at this time since it is shown above that the crown ethers behave quite differently with a given sodium salt regarding line widths and chemical shifts.

Another interesting result is the slow exchange observed with the "lariat" ether N,N'-diethanol-DA18C6 and sodium iodide (see Figure 23) while this sodium salt gives a fast exchange with all the other crowns. This confirms the results already observed^{78-83,85} and discussed before (see Section 1.3) which show that the two donor atom containing side arms participate in the complexation and give to this ligand a complexing ability intermediate between crowns and cryptands. As a result the complex is more stable which lowers the rate of decomplexation and gives slow exchange at room temperature.

3.3. Conclusion

This study clearly shows the dependency that the exchange kinetics of the sodium ion with 18C6 and its substituted analogs in low dielectric solvents have on the anion. These results confirm those previously obtained by J.D. Lin^{19,109}. Although the quite different behaviour of the different crowns toward NaBPh₄ cannot be explained from these results only, it is still surprising

to note such different results with ligands which are so structurally similar. A more elaborate and complete study of this crown influence should lead to results as profitable as those concerning the anion influence in order to fully understand the exchange kinetics of the sodium ion with 18 member ring crown ethers in THF solutions.

CHAPTER IV

CONDUCTANCE STUDY OF THE IONIC ASSOCIATION BETWEEN
THE SOLVATED AND COMPLEXED SODIUM ION AND SOME ANIONS IN THF

4.1. Introduction

The exchange kinetics of the Na⁺ ion between the "free" and complexed sites in THF have been investigated by ²³Na NMR spectroscopy. In particular we wished to study what influence the anion and substituent groups on 18C6 have on this exchange. It was shown that the nature of the counter anion drastically influences the rate of exchange in THF solutions 109. These results suggest that anion-cation interactions strongly affect the complexation kinetics. It was, therefore, of interest for us to get a qualitative measure which would allow a comparison of the ionic association of the sodium salts in our solutions. Electrical conductivity was the chosen physicochemical technique for this study. Since a strong ionic association can be changed to a great extent after complexation by a crown because of the charge-dipole repulsion between the donor atoms of the crown and the counter anion, an investigation of the ionic association between the complexed sodium ion and the anions previously studied is also reported. 18C6 was the selected crown mainly because it is the crown which shows the strongest anion dependence on the exchange rate. A few measurements involving DA18C6 complexes are also reported in order to illustrate the difference in the behaviour of the two crowns towards NaBPh₄.

4.2. Results and Discussion

The resistance of the sodium salts solvated and complexed by 18C6 and DA18C6 (for NaBPh₄ and NaSCN) were measured at a total salt concentration of 0.010 M and at 25.00°C. Measurements were made at 398 Hz, 629 Hz, 971 Hz, 1942 Hz and 3876 Hz. The cell was always connected in parallel with a capacitor and when the cell resistance was greater than 90,000 ohms, the cell was shunted in parallel with a 90,000 ohms standard precision resistor.

In this case, the resistance of the solution at each frequency was computed from the parallel resistance according to the following equation

$$\frac{1}{R_{sol}} = \frac{1}{R_{sol} + sR} - \frac{1}{R_{sR}}$$
 (4.1)

where R_{SOl} , R_{SR} and R_{SOl} + SR are the resistances of the solution, the standard resistor and the solution shunted by the standard resistor respectively. The conductivity of each solution was then calculated from the following equation.

$$\gamma \left(\Omega^{-1}.cm^{-1}\right) = K(cm^{-1})/R_{sol}(\Omega) \tag{4.2}$$

where and K are the conductivity of the solution and the cell constant (see section 2.5.2.) respectively. Finally, the equivalent conductances were obtained from the following equation.

$$\Lambda(eq^{-1}.cm^{2}.\Omega^{-1}) = \frac{1000 \,\Upsilon}{C(eq. \, l^{-1})} = \frac{1000 \,K}{R_{sol}C}$$
 (4.3)

where Λ and C are the equivalent conductance and the concentration in eq. l^{-1} respectively. The conductivity of THF (3 x 10^{-1} Ω^{-1} .cm⁻¹ at 25°C) is lower than the experimental error on the other solutions conductivities. Therefore no correction to the observed conductivities is necessary. The results are presented in Table 13.

Let us first consider the results obtained with only the sodium salts in solution. The equivalent conductance drops from an averaged value of 20.8 with NaBPh₄ down to averaged values of 1.40 with NaAsF₆, 0.258 with NaClO₄, 0.210 with NaI and 0.128 with NaSCN while no significant electrical

Table 13. Equivalent Conductances of Some Sodium Salts Solvated and Complexed by 18C6 and DA18C6 At a Concentration of 0.010 \underline{M} and at 25.00 \pm 0.05°C in THF(a)

Sample (cell)	Frequency(b)	Rsolution	γ (cm ⁻¹ . α ⁻¹)	(eq $^{-1}$.cm 2 . Ω^{-1})
NaBPh4 (30 ml)	1 2 8 4 4 5 5	7027 ± 1 7023 ± 1 7020 ± 1 7016 ± 1 7008 ± 1	2.12 x 10^{-4} ± 5 x 10^{-6} 2.10 x 10^{-4} ± 5 x 10^{-6} 2.08 x 10^{-4} ± 5 x 10^{-6} 2.07 x 10^{-4} ± 5 x 10^{-6} 2.05 x 10^{-4} ± 5 x 10^{-6}	21.2 ± 0.5 21.0 ± 0.5 20.8 ± 0.5 20.7 ± 0.5 20.5 ± 0.5
NaBPh ₄ ·18C6 (30 ml)	1 8 8 9 2	8844 ± 1 8839 ± 1 8834 ± 1 8827 ± 1 8815 ± 1	1.68 x 10 ⁻⁴ ± 4 x 10 ⁻⁶ 1.67 x 10 ⁻⁴ ± 4 x 10 ⁻⁶ 1.66 x 10 ⁻⁴ ± 4 x 10 ⁻⁶ 1.64 x 10 ⁻⁴ ± 4 x 10 ⁻⁶ 1.63 x 10 ⁻⁴ ± 4 x 10 ⁻⁶	16.8 ± 0.5 16.7 ± 0.5 16.6 ± 0.5 16.4 ± 0.5 16.3 ± 0.5
NaSCN (25 ml)	 8 8 9 11	1.866 x 106 ± 1.5 x 103 1.863 x 106 ± 1.5 x 103 1.862 x 106 ± 1.5 x 103 1.860 x 106 ± 1.5 x 103 1.867 x 106 ± 1.5 x 103	1.24 x 10^{-6} ± 3 x 10^{-8} 1.30 x 10^{-6} ± 3 x 10^{-8} 1.30 x 10^{-6} ± 3 x 10^{-8} 1.29 x 10^{-6} ± 3 x 10^{-8} 1.27 x 10^{-6} ± 3 x 10^{-8}	0.124 ± 0.004 0.130 ± 0.004 0.130 ± 0.004 0.129 ± 0.004 0.127 ± 0.004
NaSCN·18C6 (25 ml)	1 2 8 4 2	1.396 x $10^5 \pm 2 \times 10^2$ 1.396 x $10^5 \pm 2 \times 10^2$	1.66 x 10^{-5} ± 3 x 10^{-7} 1.74 x 10^{-5} ± 3 x 10^{-7} 1.73 x 10^{-5} ± 3 x 10^{-7} 1.72 x 10^{-5} ± 3 x 10^{-7} 1.70 x 10^{-5} ± 3 x 10^{-7}	1.66 ± 0.03 1.74 ± 0.03 1.73 ± 0.03 1.72 ± 0.03 1.70 ± 0.03

Table 13 - cont.

Sample (cell)	Frequency(b)	Rsolution	τ (cm ⁻¹ , α ⁻¹)	(eq ⁻¹ .cm 2 . α ⁻¹)
NaBPh ₄ ·DA18C6 (30 ml)	1 2 8 4 3 5	8954 ± 1 8946 ± 1 8940 ± 1 8930 ± 1 8917 ± 1	1.66 x 10 ⁻⁴ ± 5 x 10 ⁻⁶ 1.65 x 10 ⁻⁴ ± 5 x 10 ⁻⁶ 1.64 x 10 ⁻⁴ ± 5 x 10 ⁻⁶ 1.62 x 10 ⁻⁴ ± 5 x 10 ⁻⁶ 1.61 x 10 ⁻⁴ ± 5 x 10 ⁻⁶	16.6 ± 0.5 16.5 ± 0.5 16.4 ± 0.5 16.2 ± 0.5 16.1 ± 0.5
NaSCN·DA18C6 (25 ml)	1 2 8 7 2 2	7.323 x 10^5 ± 4 x 10^2 7.346 x 10^5 ± 4 x 10^2 7.333 x 10^5 ± 4 x 10^2 7.339 x 10^5 ± 4 x 10^2 7.349 x 10^5 ± 4 x 10^2	3.17 x 10 ⁻⁶ ± 5 x 10 ⁻⁸ 3.31 x 10 ⁻⁶ ± 5 x 10 ⁻⁸ 3.29 x 10 ⁻⁶ ± 5 x 10 ⁻⁸ 3.28 x 10 ⁻⁶ ± 5 x 10 ⁻⁸ 3.23 x 10 ⁻⁶ ± 5 x 10 ⁻⁸	$\begin{array}{c} 0.317 \pm 0.005 \\ 0.331 \pm 0.005 \\ 0.329 \pm 0.005 \\ 0.328 \pm 0.005 \\ 0.323 \pm 0.005 \end{array}$
Nai (30 ml)	L 2 & 4 &	6.987 x $10^5 \pm 6$ x 10^2 6.964 x $10^5 \pm 6$ x 10^2 6.978 x $10^5 \pm 6$ x 10^2 6.983 x $10^5 \pm 6$ x 10^2 6.974 x $10^5 \pm 6$ x 10^2	2.13 x 10-6 ± 5 x 10-8 2.12 x 10-6 ± 5 x 10-8 2.10 x 10-6 ± 5 x 10-8 2.08 x 10-6 ± 5 x 10-8 2.06 x 10-6 ± 5 x 10-8	$\begin{array}{c} 0.213 \pm 0.005 \\ 0.212 \pm 0.005 \\ 0.210 \pm 0.005 \\ 0.208 \pm 0.005 \\ 0.206 \pm 0.005 \end{array}$
Nal·18C6 (25 ml)	L 2 & 4 G	5.059 x 104 ± 70 5.057 x 104 ± 70 5.055 x 104 ± 70 5.054 x 104 ± 70 5.055 x 104 ± 70	2.94 x 10^{-5} ± 5 x 10^{-7} 2.92 x 10^{-5} ± 5 x 10^{-7} 2.90 x 10^{-5} ± 5 x 10^{-7} 2.89 x 10^{-5} ± 5 x 10^{-7} 2.87 x 10^{-5} ± 5 x 10^{-7}	2.94 ± 0.05 2.92 ± 0.05 2.90 ± 0.05 2.89 ± 0.05 2.87 ± 0.05

Table 13 - cont.

Sample (cell)	Frequency(b)	Rsolution	γ (cm ⁻¹ . a ⁻¹)	(eq ⁻¹ .cm ² . α ⁻¹)
NaC104 (30 ml)	L 0 6 4 G	5.683 x $10^5 \pm 5$ x 10^2 5.678 x $10^5 \pm 5$ x 10^2 5.677 x $10^5 \pm 5$ x 10^2 5.677 x $10^5 \pm 5$ x 10^2 5.679 x $10^5 \pm 5$ x 10^2	2.62 x 10 ⁻⁶ ± 6 x 10 ⁻⁸ 2.60 x 10 ⁻⁶ ± 6 x 10 ⁻⁸ 2.58 x 10 ⁻⁶ ± 6 x 10 ⁻⁸ 2.56 x 10 ⁻⁶ ± 6 x 10 ⁻⁸ 2.52 x 10 ⁻⁶ ± 6 x 10 ⁻⁸	0.262 ± 0.006 0.260 ± 0.006 0.258 ± 0.006 0.256 ± 0.006 0.252 ± 0.006
NaClO ₄ ·18C6 (25 ml)	1 2 8 4 5	4.075 x 10^4 ± 90 4.074 x 10^4 ± 90 4.074 x 10^4 ± 90 4.074 x 10^4 ± 90 4.074 x 10^4 ± 90	5.70 x $10^{-5} \pm 8$ x 10^{-7} 5.97 x $10^{-5} \pm 8$ x 10^{-7} 5.93 x $10^{-5} \pm 8$ x 10^{-7} 5.91 x $10^{-5} \pm 8$ x 10^{-7} 5.83 x $10^{-5} \pm 8$ x 10^{-7}	5.70 ± 0.08 5.97 ± 0.08 5.91 ± 0.08 5.91 ± 0.08 5.83 ± 0.08
NaAsF ₆ (30 ml)	1 2 2 4 3 5	1.0472 x $10^5 \pm 1.5$ x 10^2 1.0470 x $10^5 \pm 1.5$ x 10^2 1.0469 x $10^5 \pm 1.5$ x 10^2 1.0470 x $10^5 \pm 1.5$ x 10^2 1.0469 x $10^5 \pm 1.5$ x 10^2	1.42 x 10^{-5} ± 3 x 10^{-7} 1.41 x 10^{-5} ± 3 x 10^{-7} 1.40 x 10^{-5} ± 3 x 10^{-7} 1.38 x 10^{-5} ± 3 x 10^{-7} 1.37 x 10^{-5} ± 3 x 10^{-7}	1.42 ± 0.05 1.41 ± 0.05 1.40 ± 0.05 1.38 ± 0.05 1.37 ± 0.05
NaAsF ₆ ·18C ₆ (c) THF (20 ml)	4 v	1.6488 x $10^7 \pm 1.5 \times 10^4$ 1.7163 x $10^7 \pm 1.5 \times 10^4$	3.1 x $10^{-8} \pm 2 \times 10^{-9}$ 2.9 x $10^{-8} \pm 2 \times 10^{-9}$	1 1

Table 13 - cont.

Sample	Frequency(b)	Rsolution	-	V
(cell)		(a)	(cm ⁻¹ . a ⁻¹)	$(eq^{-1}.cm^2. a^{-1})$
NaCp(CH ₃) ₅ (d)				
NaCp(CH ₃) ₅ •18C6	T 2 & 4 &	8.806 x $10^5 \pm 6 \times 10^2$ 8.852 x $10^5 \pm 6 \times 10^2$ 8.855 x $10^5 \pm 6 \times 10^2$ 8.857 x $10^5 \pm 6 \times 10^2$ 8.857 x $10^5 \pm 6 \times 10^2$ 8.865 x $10^5 \pm 6 \times 10^2$	1.69 x 10-6 ± 5 x 10-8 1.67 x 10-6 ± 5 x 10-8 1.65 x 10-6 ± 5 x 10-8 1.64 x 10-6 ± 5 x 10-8 1.62 x 10-6 ± 5 x 10-8	0.169 ± 0.006 0.167 ± 0.006 0.165 ± 0.006 0.164 ± 0.006 0.162 ± 0.006

(a) The uncertainties on $R_{Solution}$ were determined from the experiment. An uncertainity of 0.03 on the cell constants was used to calculate the errors on the conductivity γ and the equivalent conductance Λ (see Appendix VI); (b) 1,2,3,4, and 5 correspond to 398 \pm 2, 629 \pm 2, 971 \pm 6, 1942 \pm 11 and 3876 \pm 18 Hz respectively; (c) The complex is insoluble at this concentration; (d) The resistance of the solution is in the same order of magnitude than that of the solvent THF.

conductance is observed for NaCp(CH₃)₅. These data are in excellent agreement with studies reported on the ionic association of NaBPh4 and of NaSCN in THF solutions; Swarc et al. 113,118 carried out an extensive study on ionic association in THF and DME solutions. By measuring the conductivity of alkali tetraphenylborides and of butyltriisoamylammonium tetraphenylboride in these solvents, the authors determined the Stokes radii of the ions, the ion pairs dissociation constants K_d's and their related thermodynamic quantities ΔH°d and ΔS°d. Their most interesting conclusion which relates to our work is that sodium tetraphenylboride forms solvent-separated ion pairs in both solvents. They described these ion pairs as a sodium ion coordinated (specifically solvated) with the solvent, the first solvation shell of the cation being in contact with a non-coordinated BPh₄ anion. Very recently, Chabanel and Wang 119 used vibrational spectroscopy to study several thiocyanates, including sodium thiocyanate, in THF solutions. They observed that in this solvent NaSCN exists primarily as contact ion pairs NaSCN and quadrupoles (NaSCN)₂ with a small amount of triple ions NaSCNNa⁺ and Na(NCS)₂⁻; no measurable quantities of free ions were detected. Therefore, by comparing the data in Table 13 and knowing the two results mentioned above, it seems reasonable to conclude that NaBPh₄ is mainly present as solvent-separated ion pairs and that the other sodium salts are strongly associated in solution and form contact ion pairs or higher aggregates. Furthermore, these observations are confirmed in an interesting review article by ${\sf Garst}^{120}$ who concludes that sodium tetraphenylborate ion pairs are probably of the loosest variety in THF solutions. Equivalent conductances at infinite dilution Λ_{0} of 86.2 at 25°C 113 , 82.3 at 20°C 121 , 88.5 at 25°C 118 , and 87.7 at 25°C 107 have already been reported for NaBPh4 in THF. It is also interesting to note that the trend observed for the equivalent conductance of our sodium salts follows relatively well that observed by Wong and Popov¹²² who studied a large variety of alkali metal salts in THF by vapor phase osmometric technique and who derived the ratio of an apparent molar weight to real molar weight of 1.10, 1.17, 1.24 and 1.41 for NaBPh₄, NaI, NaClO₄ and NaSCN respectively. The above conclusions about the type of ionic association for the sodium salts in THF solutions do not necessarily apply to NaAsF₆ whose averaged equivalent conductance of 1.40 is greater than that of NaSCN, NaI, NaClO₄ and NaCP(CH₃)₅ by about one order of magnitude.

In order to interpret the change in equivalent conductance observed after complexation by 18C6, it is necessary to briefly review some of the previous studies in this field. Boileau and co-workers 123 studied the conductance of sodium tetraphenylborate complexed by the cryptand C221 in THF solutions while Schori \underline{et} \underline{al} . 124 studied the same salt complexed by DB18C6 in DME solutions. As it was discussed previously, solvent-separated ion pairs of this salt exist in both solvents. A drop in the conductance was observed upon complexation giving $\Lambda_{\rm O}$ = 76.6 at 20°C in the former case and Λ_{O} = 83.6 at 20°C in the latter ($\Lambda_{O}(NaBPh_{4})$ = 101.2 at 20°C in DME). Smid et al.125 studied the loose ion pair flurorenylsodium complexed by 4,4'-dimethyl-DB18C6 in THF and observed a drop from $\Lambda_{\rm O}$ = 95 down to $\Lambda_{\rm O}$ = 88 upon complexation. Other authors observed the same phenomenon when studying the conductance of alkali metal salts solvated and complexed by crown ethers in acetonitrile 126,127, ethanol 128 and methanol 127. It should be noted that in all these studies, only a weak or a negligible amount of contact ion pairing was observed. In every case the drop in equivalent conductance was interpreted as an increase in the intrinsic radius of the cation which decreases the conductance according to the primitive model of ${
m Stokes}^{129}$ described by the equation below.

$$\lambda^{\circ}_{+} = A/(\eta R_{+}) \tag{4.4}$$

where λ^{0} is the equivalent conductance of the cation at infinite dilution, R+ is the radius of the cation, A is a constant that depends on the charge of the ion and n the viscosity of the solvent. In other words, the change in Λ_{0} reflects the decreased mobilities of the complexes. This corresponds to what we observe for NaBPh₄ complexed with 18C6. The conductance of this salt drops from 20.8 down to 16.6 upon complexation. It can reasonably be attributed to a change in mobility and the complex is probably still a solvent-separated ion pair in THF. However, an increase of the equivalent conductance by one order of magnitude or more is observed when NaSCN, Nal, NaClO₄ and NaCp(CH₃)₅ are complexed by the 18C6. This does not fit the model proposed above and it can be rationalized again in terms of the ionic association of the solvated sodium salts in THF. As discussed above, the ionic association of NaSCN in THF solutions is already known therefore it is the example considered for the following discussion, the reasoning being then extented to NaI, NaClO₄ and NaCp(CH₃)₅ which show quite similar results. For NaSCN, the quadrupole formation from the ion pairs is described by the equation below.

2 NaNCS
$$\frac{K_{app}}{}$$
 (NaNCS)₂ (4.5)

$$K_{ADD} = [(NaNCS)_2] / [NaNCS]^2$$
 (4.6)

where K_{app} is the apparent dimerization constant and is equal to 40 \underline{M}^{-1} at 0.01 \underline{M} and 25°C¹¹⁹. Our data indicate that, except NaAsF₆, the other

salts should behave quite similarly. Since these sodium salts are quantitatively complexed by 18C6 in THF to form a stable 1:1 complex, we can interpret the increase in Λ by considering the following equilibria.

$$(NaX)_2 + 2C \rightleftharpoons 2NaX + 2C \rightleftharpoons 2Na \cdot C^+X^-$$
 (4.7)

$$2Na \cdot C^{+}X \Longrightarrow 2NaC^{+} + 2X^{-} \tag{4.8}$$

After complexation, which most presumably occurs between contact ion pair and ligand, the crown ether encapsulates the sodium ion forming an organic layer around the cation and probably weakening the stability of the contact ion pairs. As a result, the number of dissociated and conducting species is increased and a larger conductance is observed.

The proposed models for either the increase or the decrease in conductivity are in fairly good agreement with the results obtained for DA18C6. The equivalent conductances obtained for NaBPh₄ with both crown are not significantly different since no significant anion-crown repulsion occurs due to the solvent-separated ion pairs of the salt and of the complex in THF solutions. Since 18C6 and DA18C6 cavities have approximately the same size, the primitive model of the Stokes described by equation (4.4) still holds and the same conductances are observed for both complexes. On the other hand, the stronger ionic association of NaSCN as well as the weaker stability of its DA18C6 complex compared with that of the 18C6 make the equilibrium (4.8) less shifted to the right. As a direct result, the increase in equivalent conductance is smaller with NaSCN·DA18C6 than with NaSCN·18C6.

Regarding a plausible explanation on why slow exchange is observed on the NMR time scale at room temperature with NaBPh₄ and 18C6, DC18C6

and DB18C6 while it is fast with the other sodium salts as already discussed in Chapter III, it seems that the ionic association in solution is probably the cause of the observed phenomena which can be analyzed in terms of dissociation rates of the complex since it is shown in Chapter I that the crown complexation rates are all approximately equal and diffusion controlled. With NaBPh4, because of the solvent-separated ion pairs for the solvated and complexed species, once the cation desolvation-complexation step is achieved, the final sodium complex is less destabilized by the BPh₄- anion than by the other anions. In this case, the complexation can be seen as a charge-dipole attraction. With the other sodium salts, the situation is quite different and a dipole-dipole attraction between contact ion pairs and ligand is a more suitable model for explaining the complexation step. In these final complexes, which are presumably contact ion pairs, the anions upset the crown-cation interactions and compete directly with the crown for the cation. This results in a faster decomplexation rate giving fast exchange on the NMR spectrum. Also the large localized electron density of SCN-, I-, ClO_4 -, AsF_6 - and Cp(CH₃)₅ compared with that of the bulky soft BPh₄ anion is in favor of the interpretation proposed above.

On the contrary, ionic association is not the reason why either slow exchange occurs with NaBPh₄ and 18C6, DC18C6 and DB18C6 or fast exchange occurs with the same salt and DA18C6 and DT18C6. The conductance study involving one crown of each category, <u>i.e.</u>, 18C6 and DA18C6, shows that the ionic association of the NaBPh₄ complex is the same with both of them. The possible explanation for the different NMR spectra obtained with these two crowns and NaBPh₄ (see Chapter III) is probably related to the stability of the sodium complex by itself. It has already been shown that the sodium and potassium complexes with 18C6 are more stable than with DA18C6 in

methanol solutions 130,131 therefore it seems reasonable to assume the same behaviour in our solutions. Since no significant anion-crown repulsion occurs with the BPh₄⁻ anion, the rate of decomplexation is directly related to the stability of the complex and is probably faster with DA18C6. Also as it is discussed in Chapter III, a DA18C6 complex results is a smaller diamagnetic shift of the 23 Na NMR signal than an 18C6 complex leading to a smaller chemical shift range ($\nu_A - \nu_B$) between solvated and complexed species and favoring the observation of fast exchange. The two explanations proposed above show fairly well why room temperature is above coalescence with the DA18C6·NaBPh₄ system while it is below coalescence with the 18C6-NaBPh₄ system.

4.3. Conclusion

We have qualitatively investigated the ionic association of a variety of sodium salts solvated and complexed by 18C6 and DA18C6 in THF. It shows a good correlation with the room temperature sodium-23 NMR spectra presented in Chapter III. A strong ionic association of these salts in solution results in a fast exchange of the sodium ion while the solvent-separated ion pair in THF solutions, i.e., NaBPh₄, promotes slow exchange with 18C6 and its derivatives. The change in stability of Na⁺ complexed with different crowns also has a great influence on the observed ²³Na NMR spectra.

CHAPTER V

KINETICS OF COMPLEXATION OF SODIUM THIOCYANATE WITH

DA18C6 AND WITH THE CIS-ANTI-CIS AND CIS-SYN-CIS ISOMERS

OF DC18C6 IN THF BY SODIUM-23 NMR SPECTROSCOPY

5.1. Introduction

We have seen that for complexation reactions between the sodium ion and crown ethers in low dielectric solvents such as THF, the nature of the anion and consequently the anion-cation association as well as the nature of the crown govern the kinetics of exchange. Several authors²⁰⁻²², ²⁴⁻²⁵, ⁴³⁻⁴⁵, ⁶⁷⁻⁶⁹ used alkali metal NMR spectroscopy to study the complexation kinetics of alkali metal ions with crowns and cryptands in several nonaqueous solvents. Among these authors, Schmidt and Popov⁶⁷ reported the first bimolecular exchange mechanism ever seen with crown ethers when they studied the complexation kinetics of K⁺·18C6 in 1,3-dioxolane using ³⁹K NMR. From these results it is clear that the same technique could be used to study the complexation kinetics of the Na⁺ ion with crown ethers.

The goal of the work presented in this chapter was to determine if the activation parameters for the release of the sodium ion from substituted analogs of 18C6 as well as the corresponding exchange mechanism depend on the nature of the substituent groups. Consequently, we decided to use 23 Na line shape analysis to study the complexation kinetics of sodium thiocyanate with DA18C6 and the two isomers of DC18C6 in THF.

5.2. Results and Discussion

As pointed out in Chapter I, several alkali metal NMR methods can be used to derive the activation parameters of decomplexation. Some of these methods are based on approximations which do not apply in our case as it will be discussed later, therefore the complete lineshape analysis described by Ceraso et al.^{20,69} was used to analyze the data. In this method, the treatment of kinetic data depends on the chemical shifts and line widths of the solvated sodium ion and of the complexed sodium ion, in the absence

of chemical exchange as well as on the population of solvated and complexed species undergoing chemical exchange at equilibrium. Therefore it is necessary to characterize the two sites before discussing the kinetic results. In the following discussion site A refers to the solvated site and site B refers to the complexed site.

5.2.1. Sodium-23 NMR of the Solvated and Complexed Sodium in the Absence of Chemical Exchange

To obtain the transverse relaxation times, T_{2A} and T_{2B} , and the chemical shifts, δ_A and δ_B , in the absence of exchange, solutions containing sodium thiocyanate only and sodium thiocyanate with an excess of ligand were prepared. Since the sodium complex with DC18C6 is quite stable, i.e., $\log K_f = 3.68$ and 4.08 in MeOH at 25°C for the cis-anti-cis and cis-syn-cis isomer respectively¹³², only a slight excess of this ligand was sufficient to complex all of the cation. On the other hand, since the stability of the sodium complex with DA18C6 is not known, a larger excess of ligand was used in this case. In all solutions, chemical exchange between the solvated and complexed sodium is absent but, because of the ionic association of NaSCN in THF, exchange between "free" ions, contact ion pairs and quadrupoles is probably present to a significant extent.

The temperature dependence of $1/T_{2A}$, $1/T_{2B}$, ω_A and ω_B is given in Table 14. The angular frequencies were obtained with the method described earlier in Section 2.4.2.4. The reciprocal transverse relaxation times were obtained by fitting the observed spectra to the theoretical Lorentzian function corrected for delay time, line broadening and zero-order dephasing and derived in Appendix VII. These fits were performed by using the KINFIT program¹⁰³ with the subroutine EQN. given in Appendix III. A typical fit is shown on

Table 14. Transverse Relaxation Times and Sodium-23 NMR Frequencies
for NaSCN Solvated or Complexed in THF Solutions
At Various Temperatures

Solute	T(a)	$10^3/{ m T}^{(b)}$	10 ³ T ₂ (c)	$ln(1/T_2)$ (d) (rad/s)	ω (e) (rad/s)
	···				
NaSCN(f)	22.3	3.384	3.63	5.62	- 798 ± 30
	11.7	3.510	3.39	5.69	- 843 ± 30
	1.1	3.646	3.21	5.74	- 813 ± 30
	-10.0	3.799	2.88	5.85	- 844 ± 30
	-20.8	3.962	2.45	6.01	- 874 ± 30
	-31.4	4.136	2.04	6.20	- 874 ± 30
	-41.2	4.310	1.69	6.38	- 936 ± 30
	-52.2	4.525	1.36	6.60	- 936 ± 30
NaSCN/	24.0	3.365	3.01	5.81	-1877 ± 60
DA18C6(f)	11.0	3.519	2.62	5.95	-1897 ± 60
	0.3	3.657	2.29	6.08	-1917 ± 60
	- 9.7	3.796	1.98	6.23	-1917 ± 60
	-20.4	3.956	1.64	6.41	-1917 ± 60
	-30.5	4.121	1.36	6.60	-1957 ± 60
	-41.3	4.313	1.08	6.83	-1957 ± 60

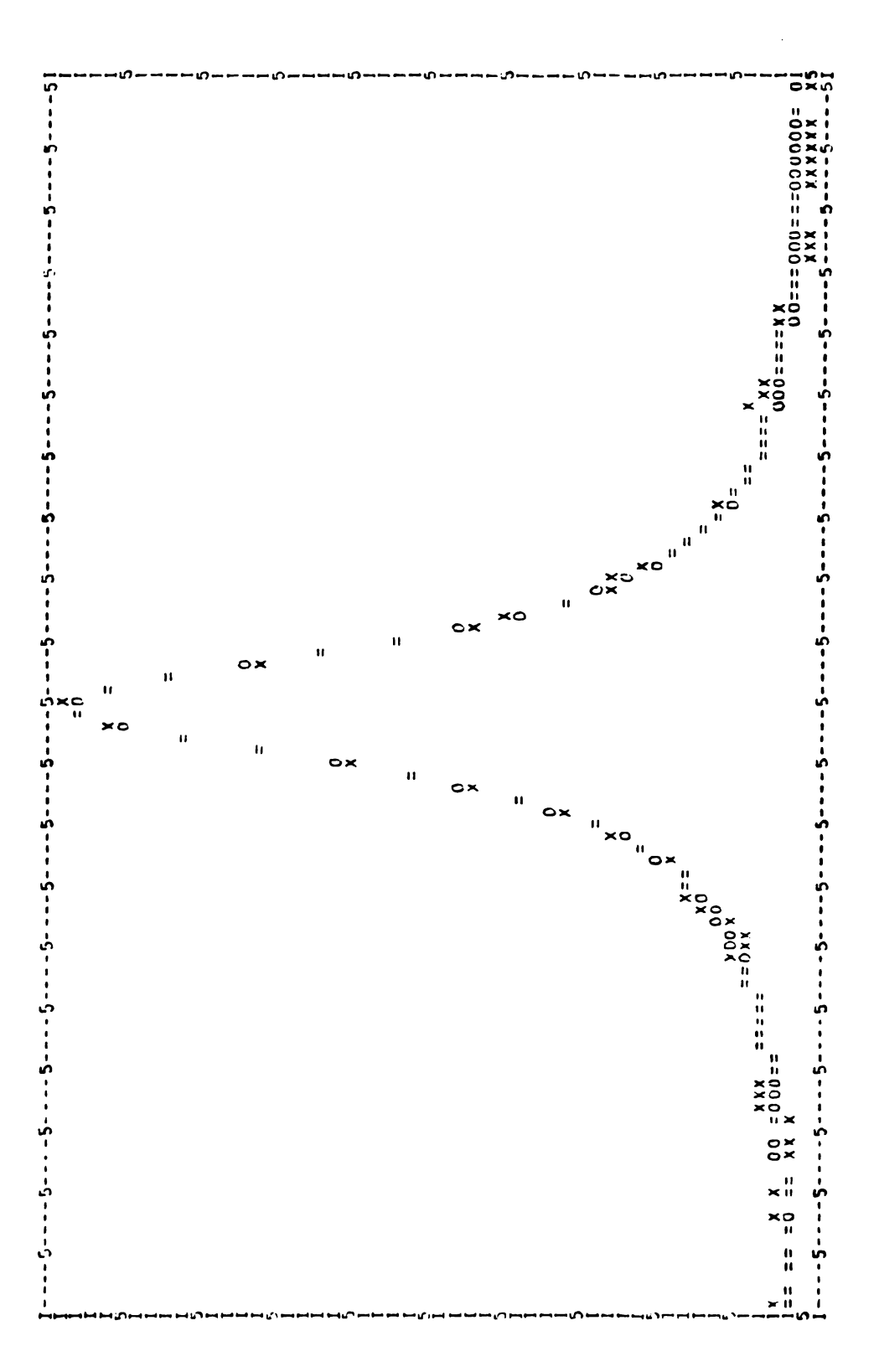
Table 14 - cont.

Solute	(°C)	10 ³ /T(b)	10 ³ T ₂ (c)	ln(1/T ₂)(d) (rad/s)	ω (e) (rad/s)
NaSCN/	22.0	3.388	1.18	6.74	-2632 ± 90
DC18C6	10.0	3.532	0.907	7.01	-2510 ± 90
(cis-anti-cis)(f)	0.1	3.660	0.685	7.29	-2632 ± 90
	- 9.8	3.797	0.535	7.53	-2541 ± 90
	-20.4	3.956	0.424	7.77	-2632 ± 90
	-30.6	4.123	0.339	7.99	-2755 ± 90
NaSCN/	47.0	3.124	1.91	6.26	-2959 ± 90
DC18C6	35.7	3.238	1.49	6.51	-2965 ± 90
(cis-syn-cis)(f)	23.5	3.371	1.18	6.74	-2978 ± 90
	15.5	3.464	0.949	6.96	-2978 ± 90
	6.1	3.581	0.793	7.14	-2984 ± 90
	- 4.1	3.717	0.599	7.42	-2990 ± 90
	-14.2	3.862	0.457	7.69	-2997 ± 90

⁽a) \pm 0.1°C; (b) \pm 10⁻⁶K⁻¹; (c) \pm 10%; (d) \pm 0.01 rad/s; (e) ω = 2 $\pi\nu$ where ν is the resonance frequency in Hertz. The angular frequencies are given vs. NaCl (0.1 M) in D₂O. An error of \pm 30 rad/s corresponds to \pm 0.1 ppm; (f) [NaSCN] = 0.01 $\overline{00}$ M \pm 0.0003 M with a ligand to salt mole ratio of 1.93, 1.09 and 1.22 for DA18C6, DC18C6 (cis-anti-cis) and DC18C6 (cis-syn-cis) respectively.

Figure 24. This corrected equation is of limited interest to us since, application of delay time and line broadening does not change the original exponential decaying factor of the FID, i.e., $-1/T_2$. Thus, the same value of T₂ would be obtained whether the Lorentzian shape of the spectrum is corrected or not. However, the corrected equation presents other advantages and it is interesting to discuss on their usefulness. Equation (VII.17) of Appendix VII contains some new terms as compared to a typical Lorentzian profile $T_2/[1 + T_2^2(\omega - \omega_A)^2]$. Firstly, the new term exp(-DE/T) shows that the intensity of the NMR signal is affected by the applied delay time. Consequently, the integrated area of the signal depends on the delay time to an extent which is related to the linewidth of the peak. For example, let's consider an NMR signal with $W_{1/2} = 150$ Hz obtained with or without line broadening. 95.4% of the real intensity is actually seen with a delay time DE = 100 μ sec while only 68.6% is seen with DE = 800 μ sec. These percentages respectively drop down to 91.0% and 47.0% when $W_{1/2}$ = 300 These results show that FT-NMR results concerning intensities or integrated areas can no longer be done without correcting for delay time. Secondly, the phase correction, earlier described by Ceraso⁶⁹ as [cos(θ $_{\text{O}}$ + θ') - $T_2(\omega - \omega_A)\sin(\theta_0 + \theta')$] where θ_0 and θ' are the zero-order and first-order phase correction respectively, allows us to know the expression of the first-order phase correction, i.e., $\theta' = (\omega - \omega_A)DE$. We see that this correction varies over the frequency range and is directly related to the delay DE in the start of data acquisition. Very significant phase distortion of the calculated spectrum can occur when a large delay time is used. This inconvenience can be overcome since the algebraic expression is known and can be substracted from the theoretical lineshape.

Figure 25 shows plots of the logarithm of the observed relaxation rates



Computer analysis of the 23 Na Lorentzian lineshape of a solution containing NaSCN 0.0099 \underline{M} and DA18C6 0.0191 \underline{M} in THF at -41.3° C Figure 24

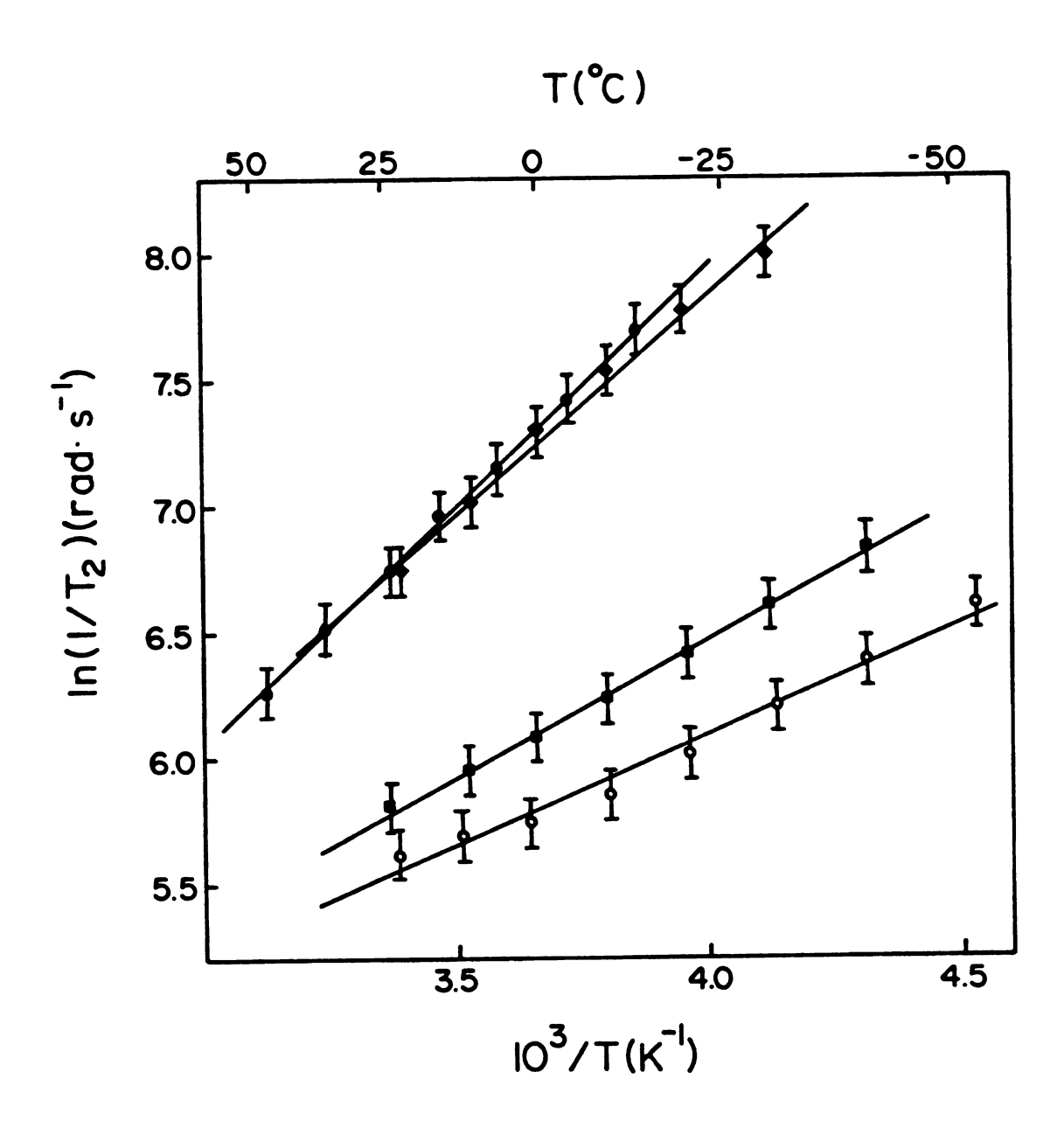


Figure 25 Semilog plots of sodium-23 transverse relaxation rates vs. 1/T for NaSCN (O), NaSCN·DA18C6 (■), NaSCN·DC18C6 (cis-anti-cis) (◆) and NaSCN·DC18C6 (cis-syn-cis) (◆) at 0.0100 M in THF

vs. reciprocal absolute temperature for all the species studied. Figure 26 shows the temperature dependence of the chemical shifts of all the species studied.

The quadrupolar reciprocal relaxation times, T_1 and T_2 , for 23 Na in dilute solutions and in the absence of chemical exchange is given by the equation 133 :

$$\frac{1}{T_1} = \frac{1}{T_2} = \frac{3}{40} \cdot \frac{2I+3}{I^2(2I-1)} \left(1 + \frac{v^2}{3}\right) \left(\frac{eQ}{h} \cdot \frac{\partial^2 V}{\partial Z^2}\right)^2 \tau_C$$
 (5.1)

where I is the spin of the nucleus, v is the asymmetry parameter (v = 0 for a symmetric field gradient at the nucleus, $0 \le v \le 1$), Q is the quadrupole moment of the nucleus, $\frac{\partial^2 V}{\partial Z^2}$ is the z component of the electric field gradient at the nucleus produced by solvent fluctuations and τ_C is the correlation time which characterizes these fluctuations. For a simple reorientation process, τ_C may be expressed by the equation 134:

$$\tau_{C} = A' \exp(-E_{r}/RT)$$
 (5.2)

where E_r is an activation energy for solvent reorganization. We prefer to use this general expression rather than Debye's formula $\tau_C = 4\pi\eta \ a^3/3kT$ ($\eta = viscosity$) which has been found to give too large τ_C values for solvated species 135 as well as for complexes 136 . Also, the macroscopic viscosity does not adequately describe the frictional forces acting on a solute molecule 137 . If the nuclear quadrupole coupling constant (NQCC) eQ/h x $\frac{\partial^2 V}{\partial Z^2}$ is assumed not to change with temperature, then the reciprocal transverse relaxation times will vary exponentially as a function of

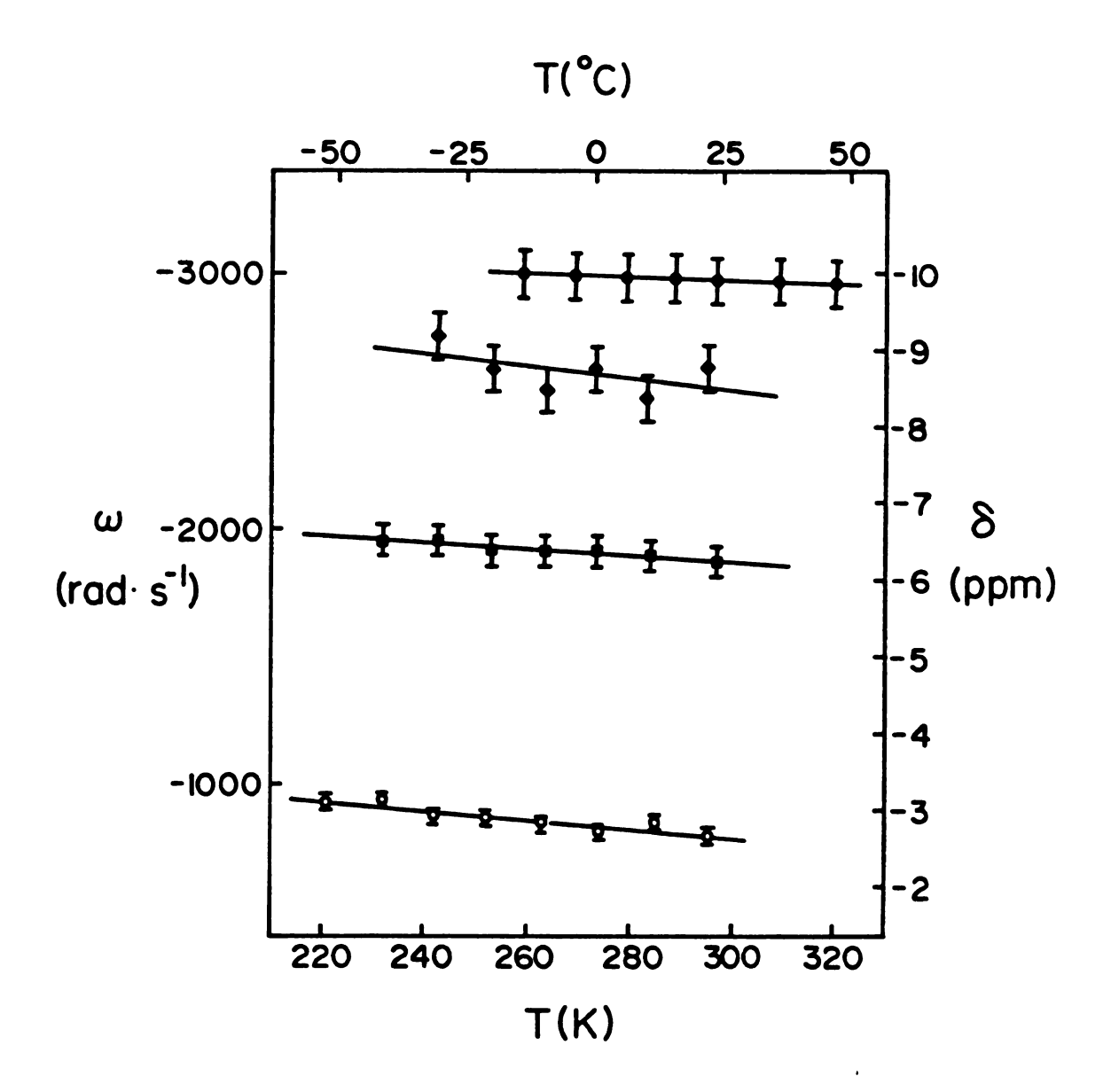


Figure 26 Temperature dependence of the sodium-23 angular frequencies and chemical shifts vs. NaCl 0.10 \underline{M} in D₂O at 22.3°C for NaSCN (\bigcirc), NaSCN·DA18C6 (\underline{C}), NaSCN·DC18C6 (cis-anti-cis) (\bigoplus) and NaSCN·DC18C6 (cis-syn-cis) (\bigoplus) at 0.0100 \underline{M} in THF

temperature. Figure 25 shows that this behaviour is observed within experimental error for all the species studied. The two major isomers of DC18C6 give approximately the same relaxation times with the same temperature dependence although the cis-syn-cis isomer tends to have a smaller T₂ at low temperatures. Some deviation from linearity is observed in the case of NaSCN solutions. This behavior is probably related to a temperature dependence of chemical exchange between various species such as contact ion pairs of quadrupoles. The relaxation rates of the complexed sites are much larger than those of the solvated site. This is caused by the asymmetry of the electric field gradient at the sodium nucleus due to the planar structure of the crowns and is more pronounced for DC18C6 because of the two cyclohexyl rings. Equations (5.1) and (5.2) were combined to derive the following expression.

$$(1/T_2)_T = (1/T_2)_{298.15} \exp[E_r/R(1/T-1/298.15)]$$
 (5.3)

The experimental results were fitted to equation (5.3) and the results obtained are presented in Table 15.

The change in chemical shifts observed on Figure 26 confirms the trends already proposed and discussed in Chapter III. From the results presented above, we see that none of the approximations described in Chapter I and represented by equations (1.2), (1.3) and (1.14) can be made. Schmidt²⁵ proposed that Schori's method is applicable when the product $(\nu_A - \nu_B)T_{2B}$ does not exceed 0.1. At 25°C, this product is 0.94, 0.48 and 0.57 for NaSCN·DA18C6, NaSCN·DC18C6 (cis-anti-cis) and NaSCN·DC18C6 (cis-syn-cis) respectively. Thus, it is clear that no approximations can be made in solving the Bloch-McConnell equations for the systems we are

Table 15. Activation Energy, E_r , for Solvent Reorganization and Transverse Relaxation Time T_2 at 25°C for NaSCN 0.0100 \underline{M} Solvated and Complexed in THF

Species(a)	(T ₂) _{298.15} K	$\mathbf{E}_{\mathbf{r}}$
	(rad/s)	(cal/mole)
NaSCN	$3.98 \times 10^{-3} \pm 1.4 \times 10^{-4}$	1729 ± 102
NaSCN DA18C6	$3.14 \times 10^{-3} \pm 4 \times 10^{-5}$	2171 ± 47
NaSCN DC18C6 cis-anti-cis	$1.21 \times 10^{-3} \pm 4 \times 10^{-5}$	3428 ± 153
NaSCN DC18C6 cis-syn-cis	$1.209 \times 10^{-3} \pm 7 \times 10^{-6}$	3775 ± 76

⁽a) The ligand to salt mole ratio are the same as those reported in Table 14.

interested in, therefore a complete line shape analysis has to be done for the derivation of the kinetic results.

5.2.2. Kinetics and Mechanism for the Exchange Between NaSCN Solvated and Complexed by DA18C6 in THF.

Preliminary studies on this system show a strong curvature on the $\ln(1/\tau)$ vs. 1/T plot. As it will be discussed later, this plot should be a straight line with a slope proportional to the Arrhenius activation energy E_a . The above results were obtained by assuming a large formation constant K_F of the complex, therefore assuming that the population of complexed sodium at chemical equilibrium is equal to the analytical amount of ligand in solution. Since the treatment of the kinetic data depends on the population of solvated and complexed sodium, our first guess for explaining that strong curvature was that the formation constant was smaller than expected and that its temperature dependence was strongly influencing the relative populations at equilibrium and therefore the kinetic results. Thus, we decided to study the thermodynamic stability of the DA18C6 complex of NaSCN in THF as a function of temperature with 23 Na NMR spectroscopy.

5.2.2.1. Sodium-23 NMR Study of the Stability of the DA18C6 Complex of NaSCN in THF at Various Temperatures.

The 23 Na chemical shifts were measured as a function of the DA18C6/NaSCN mole ratio. The concentration of the salt was held constant at 0.0100 M since it is the concentration at which the kinetic study was done. The exchange rate of the sodium between the solvated and the complexed site is fast on the 23 Na NMR time scale so that only one population averaged line was observed. If only a 1:1 complex is present, the observed chemical shift, $\delta_{\rm obs}$, is given by:

$$\delta_{\text{obs}} = X_{\text{M}} \delta_{\text{M}} + X_{\text{ML}} \delta_{\text{ML}}$$
 (5.4)

where δ_M and δ_{ML} are the averaged chemical shifts of the solvated (or free) and complexed species, respectively. X_M and X_{ML} are the respective mole fractions of the "two" species. The apparent concentration equilibrium constant for the formation of the complexed is,

$$K_{F} = \frac{[ML^{+}]}{[M^{+}][L]}$$
 (5.5)

where [ML⁺], [M⁺] and [L] denote the equilibrium molar concentrations of the complex, the cation and the ligand, respectively.

By combining equations (5.4) and (5.5) with the mass balance equations it can be shown that

$$\delta_{\text{obs}} = [K_{\text{F}}C_{\text{M}}^{\text{T}} - K_{\text{F}}C_{\text{L}}^{\text{T}} - 1 + ((K_{\text{F}}C_{\text{L}}^{\text{T}} - K_{\text{F}}C_{\text{M}}^{\text{T}} + 1)^{2} + 4K_{\text{F}}C_{\text{M}}^{\text{T}})^{1/2}] \times \frac{\delta_{\text{M}}^{-\delta}ML}{2K_{\text{F}}C_{\text{M}}^{\text{T}}} + \delta_{\text{ML}}$$
(5.6)

In equation (5.6) the total concentration of the cation and of the ligand (C_M^T and C_L^T respectively) are known and δ_M is determined by measuring the cation chemical shift in the absence of the ligand. The two unknown quantities, K_F and δ_{ML} can be evaluated by a non-linear least-squares procedure starting with reasonable estimates of K_F and δ_{ML} . The program KINFIT¹⁰³ was used to perform the iterations and to obtain statistical information regarding the unknowns. Details about the use of this program for this purpose can be found in Appendix V.

The chemical shifts as a function of the DA18C6/NaSCN mole ratio at different temperatures are given in Table 16 and plotted in figure 27 where, for more clarity, the chemical shifts are given on a relative scale. As pointed out in the experimental part, the reference solution concentration was not known for this experiment and only chemical shifts relative to the signal at zero mole ratio could be obtained. However, since the temperature dependence of the ²³Na NMR chemical shift for a NaSCN solution 0.0100 M in THF is known, the data reported in Table 16 were calculated according to this temperature dependence extrapolated to the desired temperatures, i.e., 22.5, 43.0 and 56.5°C.

A data analysis using KINFIT yielded to the values shown below:

T(K)	log K _F (M ⁻¹)	δ _{ML} lim (ppm)
295.65 ± 0.1	3.87 ± 0.22	-6.36 ± 0.70
316.15 ± 0.1	3.77 ± 0.20	-6.24 ± 0.70
329.65 ± 0.1	3.44 ± 0.17	-6.15 ± 0.90

where δ_{ML}^{lim} is the calculated limiting chemical shift of the complex. These values are in good agreement with those already reported in Section 5.2.1 and shown in Figure 26. The errors on log K_F were calculated with the following equation:

$$\delta(\log K_F) = \frac{\delta(\ln K_F)}{\ln 10} = \frac{\delta K_F}{K_F \ln 10}$$
 (5.7)

It has been shown repeatedly that this NMR technique cannot be used to measure large values of K_F and usually has an upper limit of 10^4 - 10^5 depending on the investigated nucleus. It is therefore of interest to derive a theoretical upper limit of K_F in order to check the reliability of our results.

Table 16 Sodium-23 Chemical Shifts of Solutions Containing NaSCN^(a) and DA18C6 at Various Mole Ratios and Temperatures in THF

[DA18C6] [NaSCN]	T = 22.5°C	Chemical Shifts (ppm) ^(b) T = 43.0°C	T = 56.5°C
0.00	-2.66	-2.54	-2.45
0.49 ± 0.02	-4.30	-4.18	-4.01
0.72 ± 0.03	-5.32	-5.11	-5.09
0.81 ± 0.03	-5.33	-5.26	-5.09
0.90 ± 0.03	-5.43	(c)	(c)
1.02 ± 0.03	-6.04	-5.88	-5.50
1.17 ± 0.04	-6.20	-6.08	-5.66
1.20 ± 0.04	-6.12	-5.93	-5.71
1.35 ± 0.04	-6.25	-6.08	-5.86
1.55 ± 0.05	-6.33	-6.26	-5.91
1.98 ± 0.06	-6.35	-6.21	-5.97
2.89 ± 0.09	-6.30	-6.18	-6.09

⁽a) [NaSCN] = $0.0100 \ \underline{M} \pm 0.0003 \ \underline{M}$; (b) The chemical shifts are \underline{vs} . NaCl $0.10 \ \underline{M}$ in D_2O at $22.3^{\circ}C$ and are given ± 0.10 ppm; (c) The sample has been contaminated by moisture.

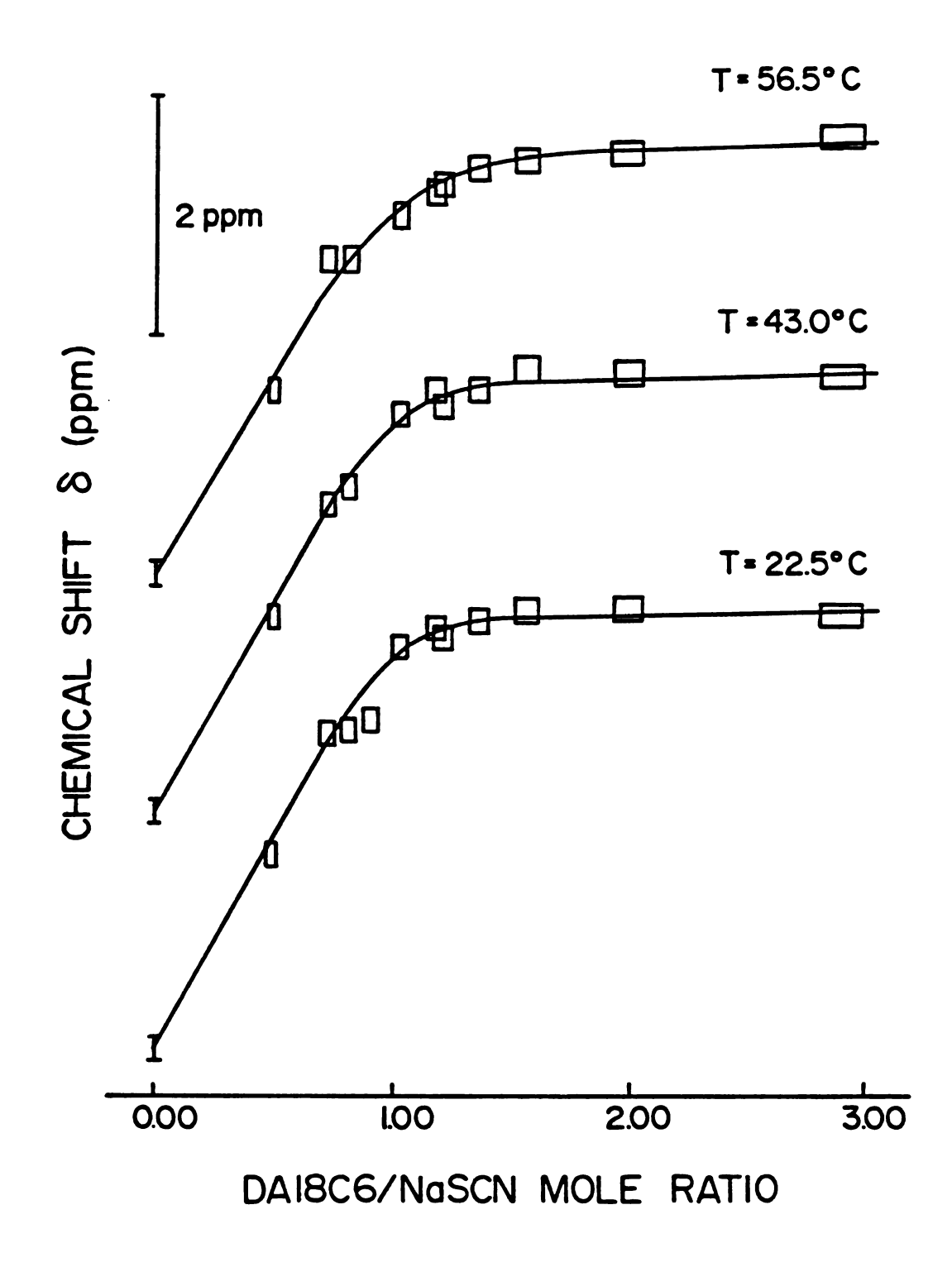


Figure 27 Sodium-23 chemical shifts vs. DA18C6/NaSCN mole ratio in THF

This can be done by considering the uncertainty on the chemical shifts and reasoning at a mole ratio of 1.00. By checking Figure 27, we can see that if the complex is "infinitely stable", at a mole ratio MR = 1.00, essentially all of the metal ion is complexed and the observed chemical shift is that of the complex. In this case, we observe two straight lines intercepting at MR = 1.00. We immediately see that the applicability of this method depends on an observable difference between the observed chemical shift $\delta_{\rm obs}$ at MR = 1.00 and $\delta_{\rm ML}$. In other words, the error range on $\delta_{\rm obs}$ must not overlap the error range on $\delta_{\rm ML}$ at MR = 1.00. This can be represented by the following equation.

At MR = 1.00,
$$\delta_{\text{obs}} = X_{\text{M}} \delta_{\text{M}} + X_{\text{ML}} \delta_{\text{ML}} < \delta_{\text{ML}} - \Delta \delta_{\text{obs}} - \Delta \delta_{\text{ML}}$$
 (5.8)

where $\Delta \delta_{\text{obs}}$ and $\Delta \delta_{\text{ML}}$ are the estimated errors on δ_{obs} and δ_{ML} respectively. Defining the chemical shift range between solvated and complexed species as $\delta_{\text{R}} = \delta_{\text{ML}} - \delta_{\text{M}}$ and considering the relationship $X_{\text{M}} + X_{\text{ML}} = 1$ both combined in equation (5.8) lead to the following equation.

$$X_{M} > \frac{\Delta \delta_{ML} + \Delta \delta_{Obs}}{\delta_{R}}$$
 (5.9)

Rearranging equation (5.5) in terms of mole fractions and combining it with equation (5.9) gives,

$$K_{F} < \frac{\delta_{R}(\delta_{R} - \Delta \delta_{Obs} - \Delta \delta_{ML})}{(\Delta \delta_{Obs} + \Delta \delta_{ML})^{2} C_{M}^{T}}$$
(5.10)

For this study, the upper limit of K_F obtained with equation (5.10) is 32,375 \underline{M}^{-1} proving our results to be reliable.

By considering the following equation,

$$K_{F} = \exp(-\Delta G^{\circ}/RT) \qquad (5.11)$$

where ΔG° is the free energy for the complexation reaction, one sees that K_F should vary exponentially as a function of temperature. This is true within experimental error as shown in Figure 28. However, the enthalpy ΔH° and the entropy ΔS° for the complexation reaction which can be derived from the slope and the intercept of the Van't Hoff plot will not be calculated since the three data points obtained are too few and too scattered to get reasonable estimates of ΔH° and ΔS° but the positive slope indicates that the complex is enthalpy stabilized which is a characteristic feature of crown complexation reactions 12.

5.2.2.2 The Kinetic Results

The relaxation times which characterize the complexation reaction were obtained by fitting the NMR spectra of species undergoing chemical exchange to the theoretical equation describing the NMR spectrum of an uncoupled spin system undergoing chemical exchange between two nonequivalent sites. This equation, first derived for FT NMR spectroscopy by Gupta et al. 138 was recently modified for delay time (DE) and line broadening (LB) corrections by Strasser and Hallenga 139 to give the following expression,

$$S(\omega) = -C_1 \exp[(\Lambda_1 - LB)DE]/(\Lambda_1 - LB) - C_2 \exp[(\Lambda_2 - LB)DE]/(\Lambda_2 - LB)$$
 (5.12)

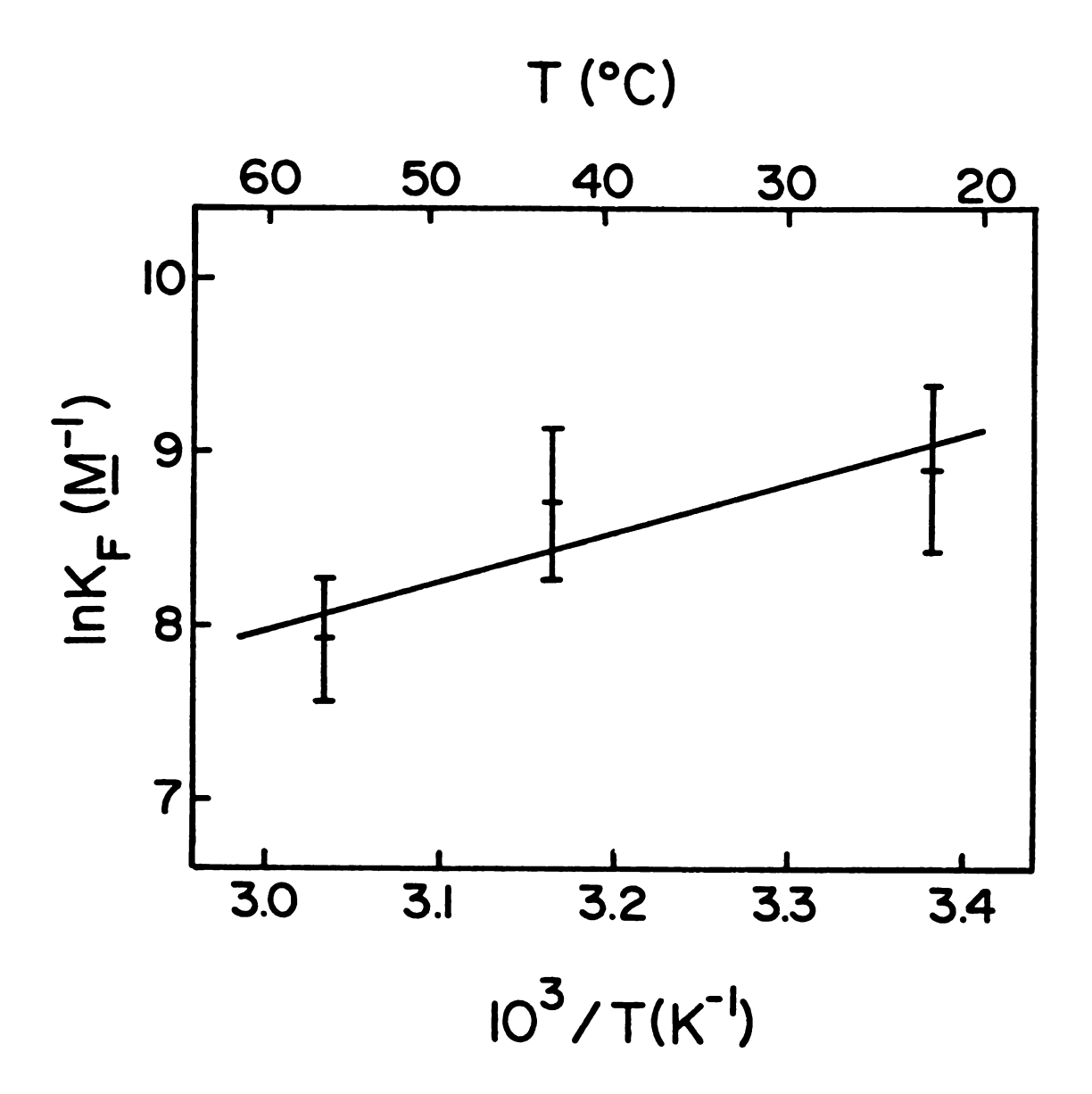


Figure 28 Van't Hoff plot for the complexation of NaSCN 0.0100 M by DA18C6 in THF

with

$$\Lambda_1, \Lambda_2 = -(\alpha_A + \alpha_B + \tau^{-1}) \pm [(\alpha_A - \alpha_B + \tau_{B}^{-1} - \tau_{B}^{-1})^2]$$

$$+4 \tau^2 p_A^{-1} p_B^{-1}]^{1/2} /2$$
 (5.13)

$$\alpha_{\mathbf{A}} = \mathbf{T}_{2\mathbf{A}}^{-1} + \mathbf{i}(\omega_{\mathbf{A}} - \omega) \tag{5.14}$$

$$\alpha_{\rm B} = T_{\rm 2B}^{-1} + i(\omega_{\rm B} - \omega)$$
 (5.14)

$$C_1 = -iM_0(\Lambda_2 + p_A \alpha_A + p_B \alpha_B)/(\Lambda_1 - \Lambda_2)$$
 (5.16)

$$C_2 = iM_0(\Lambda_1 + p_A\alpha_A + p_B\alpha_B)/(\Lambda_1 - \Lambda_2)$$
 (5.17)

As it was previously discussed in this chapter, corrections for delay time in a single Lorentzian profile can lead to very useful information concerning the intensity of the NMR lines but can also drastically change the phasing of the calculated spectrum and therefore give very poor fit and consequently large uncertainties in the sought unknowns. Experience showed us that the same phase distortion occurs in the calculated spectrum described by equation (5.12). It was therefore of interest for us to derive the expression of the phase correction in the expression describing the NMR signal of an uncoupled spin system undergoing chemical exchange between two nonequivalent sites in order to get rid of an unwanted phase distortion and keep the corrected intensities. Unfortunately, we found out that the real and imaginary parts of the theoretical spectrum could not be separated and therefore the expression of the phase correction could not be algebraically derived. Thus, we must know at this point whether or not it is worth keeping

the delay time correction in the calculated equation. If we recall the shape of an NMR spectrum of species undergoing chemical exchange between the two sites, we know that below coalescence two NMR signals broadened by chemical exchange are observed. Usually, for complexation reactions involving synthetic crown ethers, the signal corresponding to complexed species is broader and therefore less intense than that of solvated species. This broader signal, whose shape is essential for determining the relaxation time τ , is the most affected by the lack of information at low intensities when no delay time correction is done. In this case, the computer generated spectrum always lies above the experimental spectrum as, for example, it can be seen in the work done by Ceraso⁶⁹. Consequently, a delay time correction must be done in order to improve the fit and the resulting phase distortion can be controlled by choosing a very small delay time (< 50 μ sec) when acquiring the FID and by introducing it in the theoretical equation when fitting the spectrum.

On the other hand, one signal averaged resonance signal is observed above coalescence and the use of the delay time correction can be left to the user's decision depending on the quality of the fits. We have seen that the corrected equation (5.12) is not absolute and in order to optimize the fits, the users of this method must be able to recognize when it is more important to correct for the lack of information at low frequencies despite the resulting phase distortion and vice versa.

We already know that an aqueous solution of sodium halide like NaCl gives the narrowest ²³Na NMR signal and is therefore very convenient as a reference since its position can be known with an excellent accuracy. However, since such solution cannot be used below 0°C, we decided to obtain the NMR spectra without any reference. Therefore, the absolute frequencies

could not be known and we had to introduce a frequency shift parameters in equation (5.12). This is done by replacing equations (5.14) and (5.15) with the following ones.

$$\alpha_{\mathbf{A}} = \mathbf{T}_{2\mathbf{A}}^{-1} + \mathbf{i}(\omega_{\mathbf{A}} + \Delta\omega - \omega)$$
 (5.18)

$$\alpha_{\rm B} = T_{\rm 2B}^{-1} + i(\omega_{\rm B} + \Delta\omega - \omega) \tag{5.19}$$

This frequency shift parameter allows the absolute frequency in equation (5.12) to shift without changing the shape of the function. The <u>relative</u> chemical shifts at the two sites without chemical exchange were not adjusted. Also, a zero-order phase correction θ_0 was introduced in equation (5.12) by numerically extracting the real and imaginary parts of the calculated spectrum $S(\omega)$ with the FORTRAN functions REAL and AIMAG respectively and by using the following equation.

$$S'(\omega) = AIMAG[S(\omega)]\cos\theta_{O} - REAL[S(\omega)]\sin\theta_{O}$$
 (5.20)

where $S'(\omega)$ is the calculated spectrum corrected for zero-order dephasing. Finally, a baseline intensity correction similar to the one described in Appendix VII was added.

The complete KINFIT program used for this lineshape analysis is shown in Appendix IV. The final equation has 8 constants which are the population, the frequency and the transverse relaxation time of the two sites, the delay time and the line broadening. The 5 unknowns are an intensity factor, the intensity of the baseline, the zero-order phase correction, the frequency shift parameter and the relaxation time of the exchange process. If no delay

time correction is desired, the corresponding constant is set at zero.

Two solutions containing DA18C6 and NaSCN at crown to salt mole ratios of 0.53 and 0.72 were studied over a wide range of temperature (42.3°C to -49.1°C). A delay time of 153 µsec and a sweep width of 6536 Hz were used. Since no coalescence was observed for both solutions, the delay time correction and therefore the first-order phase correction was kept in the theoretical equation. For each spectrum analyzed, 80 to 99 points were found to be more than sufficient to determine τ . The program KINFIT gave complete statistical information about the fit of the data including standard deviation estimates for each of the parameters and the multiple correlation coefficient, which gives a measure of the coupling of each parameter to all of the others. Coupling between τ and the other four parameters was always next to the lowest which was found between baseline intensity and the other four parameters. A typical value of the τ coupling of about 0.6 $(0 \leqslant \text{coupling} \leqslant 1)$ gives a good reliability to our results. The transverse relaxation times and the frequencies of the two sites were respectively obtained from the computer fits and the linear regressions which are shown on Figures 25-26. The population of solvated and complexed species at equilibrium were calculated from the temperature dependence of the formation constant KF obtained from computer fit and shown in Figure 28.

The computer generated values of τ for both solutions are collected in Table 17. The corresponding Arrhenius plot $\ln(1/\tau)$ vs. 1/T is shown in Figure 29. As it will be seen later, the reciprocal relaxation time is directly proportional to the decomplexation rate k_d of whatever exchange mechanism involved, this rate being related to the reciprocal temperature according to the Arrhenius equation shown below.

Table 17. Temperature Dependence of the Relaxation Time of the Exchange Between

NaSCN Solvated and Complexed by DA18C6 in THF

[ligand] [salt]	T(°C)(a)	τ (msec)(b)
0.53(c)	42.3	0.1941 ± 0.0109(d)
	31.5	0.2094 ± 0.0108
	21.1	0.1943 ± 0.0093
	11.3	0.2300 ± 0.0095
	1.0	0.2366 ± 0.0116
	- 9.8	0.3266 ± 0.0162
	-19.3	0.3699 ± 0.0144
	-29.6	0.5094 ± 0.0198
	-39.2	0.9225 ± 0.0405
	-49.1	2.353 ± 0.412
0.72(e)	6.2	0.1545 ± 0.0124
	- 7.7	0.1874 ± 0.0149
	-21.0	0.2443 ± 0.0305
	-34.9	0.7306 ± 0.0850
	-45.6	1.496 ± 0.209

⁽a) \pm 0.1°C; (b) The values corresponding to a mole ratio fo 0.53 are the weighed averages of two different computer generated values obtained from the same spectra; (c) 0.01024 M NaSCN; (d) Represents one standard deviation; (e) 0.01011 M NaSCN - Another spectrum at 25°C gave a very poor fit and the corresponding τ value is not reported.

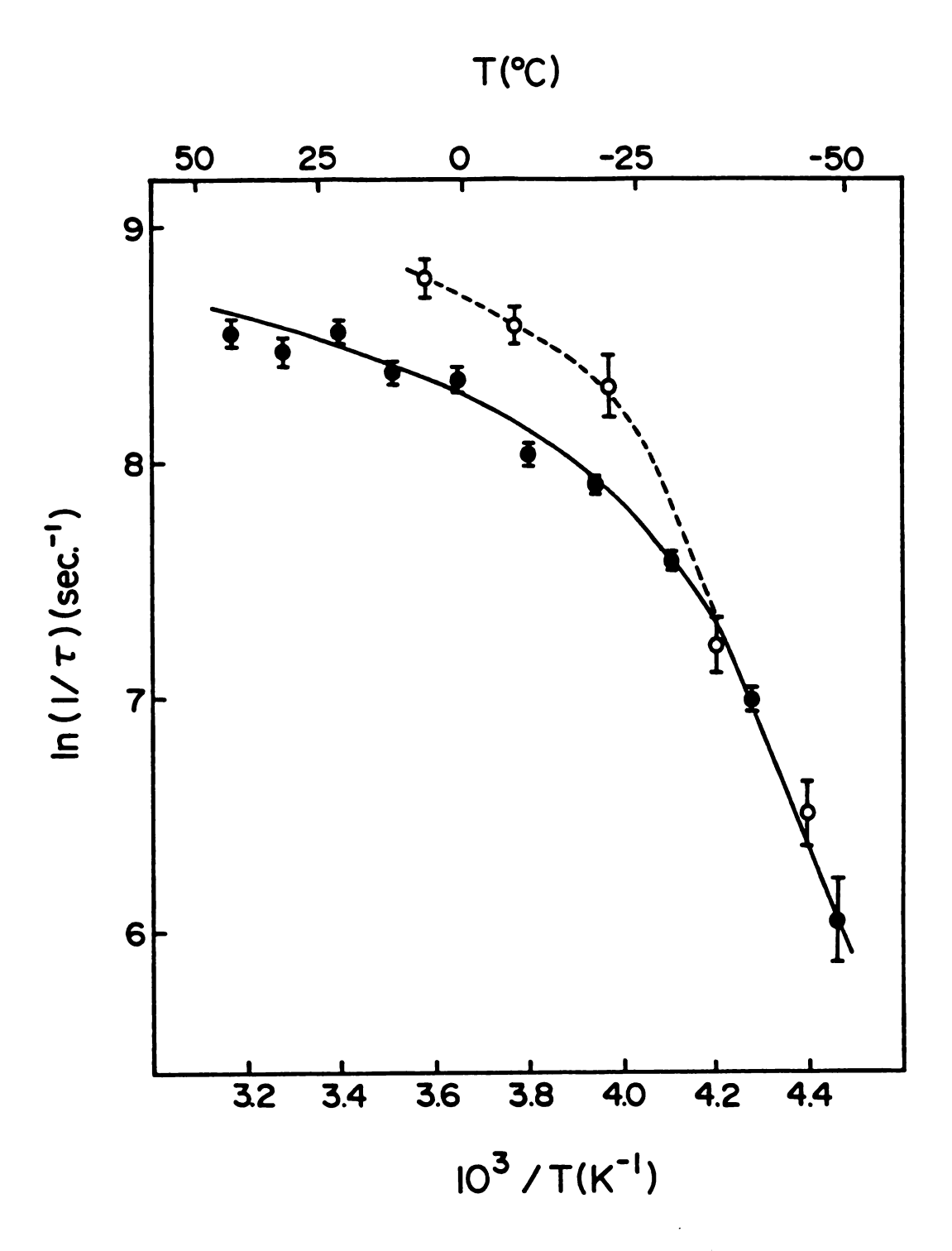


Figure 29 Arrhenius plot of $ln(1/\tau)$ vs. (1/T) for DA18C6/NaSCN in THF - (0) DA18C6/Na⁺ = 0.72 - (\bullet) DA18C6/Na⁺ = 0.53

$$k_{d} = A \exp(-E_{a}/RT)$$
 (5.21)

Therefore the Arrhenius plot should lead to a straight line with a slope equal to $-E_{\rm a}/R$. The curvature observed in Figure 29 at two different mole ratio rules out the above observation. As already noted by Schmidt and Popov⁶⁷, this phenomenon is either due to two mechanisms having different Arrhenius activation energies with one of them being predominant at high temperatures while the other one is predominant at low temperatures or it can be due to only one mechanism whose activation energy varies with the temperature. In order to check which one of the above supposition is valid, we decided to determine the mechanism of exchange.

As already discussed in Chapter I, the exchange of the Na⁺ ion between the solvated site and complexed site may proceed via two mechanisms: the bimolecular exchange mechanism I and the associative-dissociative mechanism II.

$$*Na^{+} + NaC^{+} = \frac{k_{1}}{k_{1}} Na^{+} + *NaC^{+}$$
 (I)

$$Na^{+} + C = \frac{k_{2}}{k_{-2}} = NaC^{+}$$
 (II)

Since these two mechanisms may contribute to the overall sodium exchange, we have to derive an expression involving both of them. In general, the relaxation time is given by 140 :

$$\frac{1}{\tau_i} = \frac{\text{rate of removal of molecules from site i by exchange}}{\text{number of molecules in site i}}$$
 (5.22)

By considering mechanisms I and II we can derive:

$$1/\tau_{Na}^{+} = k_{-2}[NaC^{+}]/[Na^{+}] + 2k_{1}[NaC^{+}]$$
 (5.23)

$$1/\tau_{NaC}^{+} = 2k_1[Na^+] + k_{-2}$$
 (5.24)

$$1/\tau = 1/\tau_{Na} + 1/\tau_{Na}C + = k_{-2}C_{Na} + /[Na^{+}] + 2k_{1}C_{Na} +$$
 (5.25)

where C_{Na}^{+} is the total concentration of sodium ion in solution. k_{-2} and k_{1} are in \sec^{-1} and $\underline{M}^{-1}.\sec^{-1}$ respectively. Here, we see the proportionality between $1/\tau$ and the dissociation rate k_{d} , the proportionality factor being $2C_{Na}^{+}$ for mechanism I and $C_{Na}^{+}/[Na^{+}]$ for mechanism II. It should be noted at this point that equation (5.23) is the one used to derive the exchange mechanism when the NMR method described by Schori et al. 24 is used. The same authors showed the influence of the ionic strength on the rate constants and therefore on the mechanism plot. They recommended to keep the ionic strength constant. Since THF has a very low dielectric constant, ions are highly associated and the extent of the association is not known therefore we cannot calculate the ionic strength of our solutions. However, since the concentration of free ions must be very low in all of them (shown by electrical conductance measurements) it seems reasonable to assume that if the total concentration of sodium salt is kept constant then the total concentration of free ions will not vary very much in our solutions.

From equation (5.25), we see that a plot of $1/\tau \times C_{Na^+} \underline{vs}$. $1/[Na^+]$ should

lead to a straight line with a slope equal to k_{-2} and intercept equal to $2k_1$ at a constant temperature. This mechanism plot is shown in Figure 30 and the data in Table 18. The plot clearly shows that two exchange mechanisms are going on in solution. The bimolecular one is predominant at low temperatures (<-35°C) and since the associative-dissociative one is obviously predominant at higher temperatures (>-21°C), the straight lines corresponding to this mechanism have been forced through the intercept. Schmidt and $Popov^{67}$ have already observed a bimolecular exchange when they studied the K⁺·18C6 system in 1,3-dioxolane. As an explanation to this first bimolecular process ever seen with crown and cryptand complexation of alkali metal ions, the authors suggested that when the energy barrier to decomplexation becomes very large it may eventually reach a point where lower energy pathways become available. They concluded that, in general, the slower is the dissociation of the complex, the more likely is the contribution of mechanism I to the cation exchange. We derived the values of the dissociation rates at different temperature and as it can be seen in Table 19, the above conclusion about dissociation rates is not exactly true and is better explained in our case in terms of 1/ $\tau_{\mbox{NaC}}\text{+}$ which represents the number of species leaving the complexed site per unit time. On the other hand, speculations as to the reason why the exchange process changes with temperature are more difficult since the solution chemistry of this system is not fully understood. Changes in complex and ion pair stabilities may play a part in the observed phenomenon. Also, a change of conformation of the complex over the range of temperature studied may account for both mechanism since the nonequivalent donor atoms probably make the DA18C6 molecule less symmetrical than the 18C6. The symmetry of 18C6 compared with the cage like cavity of the cryptands was one of the reasons proposed

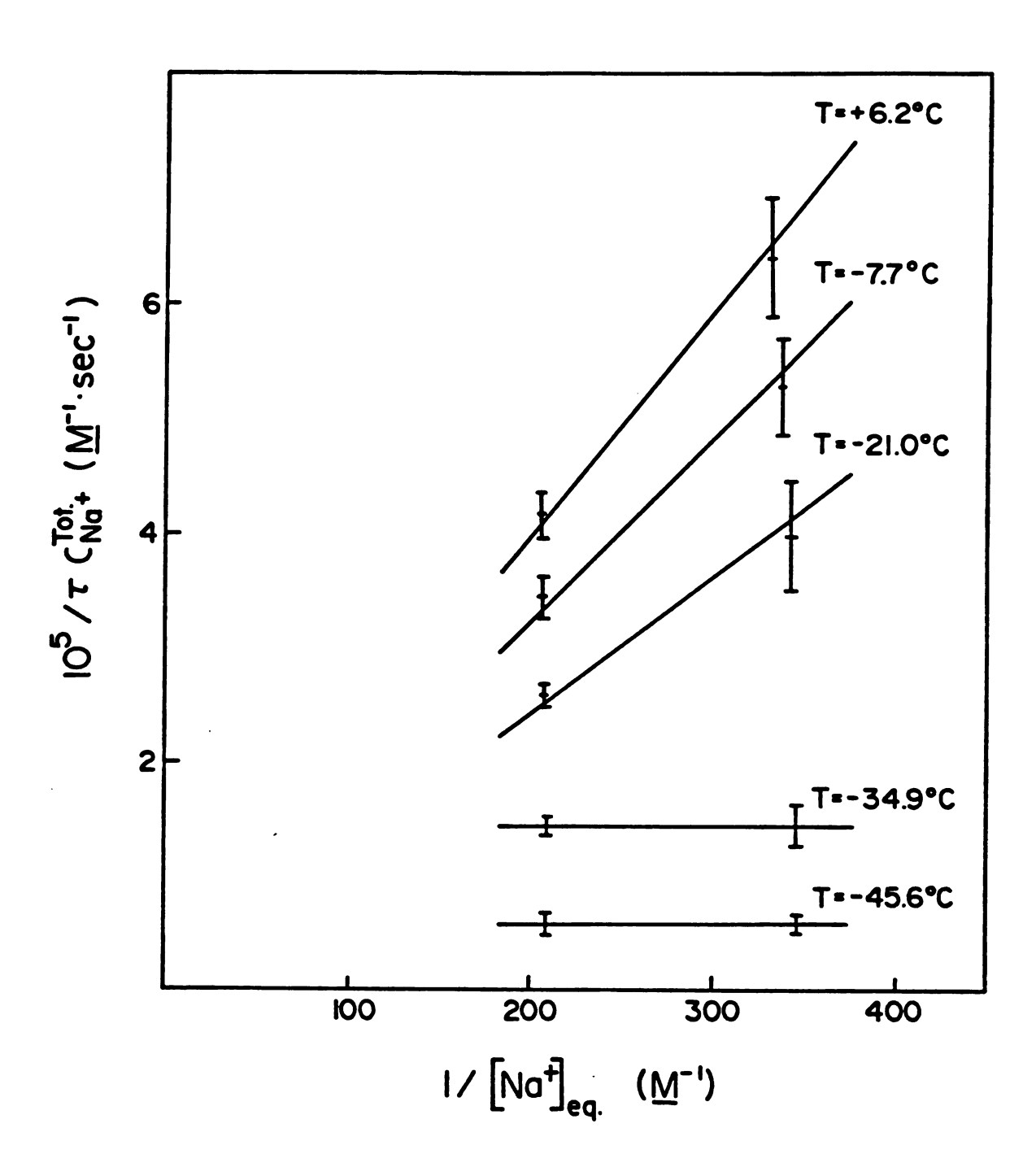


Figure 30 Plot of $1/\tau$ x C_{Na}^+ vs. $1/[Na^+]_{eq}$ for DA18C6/NaSCN systems in THF at various temperatures

Table 18. Values of 1/[Na⁺]_{eq}. and 1/(TXC_{Na}+) at Various Temperatures for NaSCN Solutions Containing DA18C6 at Two Different Concentrations in THF(a)

T(°C)	[ligand] [salt]	$1/(Na^{+}l_{eq}^{(b)}(M^{-1})$	ln(1/τ)(c)(sec ⁻¹)	$10^{5/_{\rm T}}{\rm x.C_{Ng^+}}({\rm M^{-1}.sec^{-1}})$
+ 6.2	0.53 0.72	206 330	8.36 ± 0.05 8.78 ± 0.08	$4.17 \pm 0.21 \\ 6.40 \pm 0.51$
- 7.7	0.53	207	8.17 ± 0.05 8.58 ± 0.08	3.45 ± 0.17 5.28 ± 0.42
-21.0	0.53	208 341	7.88 ± 0.04 8.30 ± 0.12	$\begin{array}{cccccccccccccccccccccccccccccccccccc$
-34.9	0.53 0.72	208 345	7.30 ± 0.05 7.30 ± 0.12	1.45 ± 0.07 1.45 ± 0.17
-45.6	0.53	209 346	6.38 ± 0.18 6.38 ± 0.14	$\begin{array}{c} 0.58 \pm 0.10 \\ 0.58 \pm 0.08 \end{array}$

(a) The total sodium concentration C_{Na}^+ is 0.01024 M and 0.01011 M at a mole ratio of 0.53 and 0.72 respectively; (b) Values obtained from the calculated temperature dependence of KF; (c) The values are estimated from the full and dashed curve in Figure 29.

Values of the Dissociation Rates and of $1/\tau_{NaC}$ + for a Table 19. THF Solution Containing NaSCN and DA18C6 at a Ligand/Na⁺ Mole Ratio of 0.53 and at Different Temperatures(a)

T(°C)	k ₋₂ (sec ⁻¹)	$k_{-1}(\underline{M}^{-1}.sec^{-1})$	$1/\tau \text{ NaC}^{+(b)} (\text{sec}^{-1})$
6.2	2010 ± 90	_	2010 ± 90
- 7.7	1640 ± 60	-	1640 ± 60
-21.0	1240 ± 50	-	1240 ± 50
-34.9	-	72500 ± 3500	700 ± 40
-45.6	-	29000 ± 4000	280 ± 40

⁽a) Values of k graphically obtained from Figure 30.(b) Values obtained from equation (5.24)

to explain the bimolecular exchange of K⁺·18C6 in 1,3-dioxolane⁶⁷. The symmetry of 18C6 gives identical probabilities of access of the cation from either side of the molecule while the cryptands must have an ion leaving their cavity before another one comes in. Two possible conformations for DA18C6 are the "chair" and the "boat" conformations. The symmetry of the former would probably favor mechanism I while, in the latter, the two nitrogen atoms are on the same side of the ligand and therefore give non identical probabilities of access of the cation from either side of the molecule consequently favoring mechanism II. Finally, a change of polarization of the two N-H bonds of DA18C6 upon complexation and therefore a change of ligand-solvent interaction may also account for the two different exchange processes. As we have seen, explaining why two mechanisms occur is not straightforward and the derivation of the activation parameters, which will be presented and discussed later along with those obtained with DC18C6, will probably give more insights about this very interesting phenomenon. To our knowledge, this is the first combination of two mechanisms ever observed with the same system.

5.2.3. Kinetics and Mechanism for the Exchange Between NaSCN Solvated and Complexed by DC18C6 in THF

The temperature dependence of the relaxation time, characterizing the complexation reaction between NaSCN and DC18C6 (cis-anti-cis or cis-syn-cis), was obtained with the method previously described in section 5.2.2.2. A delay time of 153 µsec and a sweep width of 6536 Hz were used. The delay time was kept in the theoretical equation (5.12). The computer generated values of τ for both isomers of DC18C6 are presented in Table 20 and the corresponding Arrhenius plots are shown in Figures 31-32. As

Table 20 - Temperature Dependence of the Relaxation Time of the Exchange Between NaSCN Solvated and Complexed by DC18C6 in THF

Ligand	T(°C)(a)	10 ⁴ τ (sec.)
DC18C6	36.7	2.114 ± 0.121(c)
cis-anti-cis(b)	31.5	2.196 ± 0.111
	26.1	2.436 ± 0.143
	20.7	2.533 ± 0.123
	15.2	2.942 ± 0.219
	10.8	3.148 ± 0.191
	5.8	3.715 ± 0.319
	1.3	3.661 ± 0.414
	-4.8	4.327 ± 0.537
	-9.2	3.986 ± 0.582
DC18C6	45.0	0.3291 ± 0.0310
cis-syn-cis(d)	39.6	0.3912 ± 0.0279
	34.1	0.3673 ± 0.0335
	28.6	0.4371 ± 0.0410
	22.7	0.4562 ± 0.0433
	18.8	0.5324 ± 0.0655
	12.2	0.4997 ± 0.0467
	6.1	0.5173 ± 0.0679
	0.5	0.7579 ± 0.0792

⁽a) \pm 0.1°C; (b) 0.01024 M NaSCN - [ligand]/[Na⁺] = 0.50; (c) Represents one standard deviation; (d) 0.01024 M NaSCN - [ligand]/[Na⁺] = 0.51.

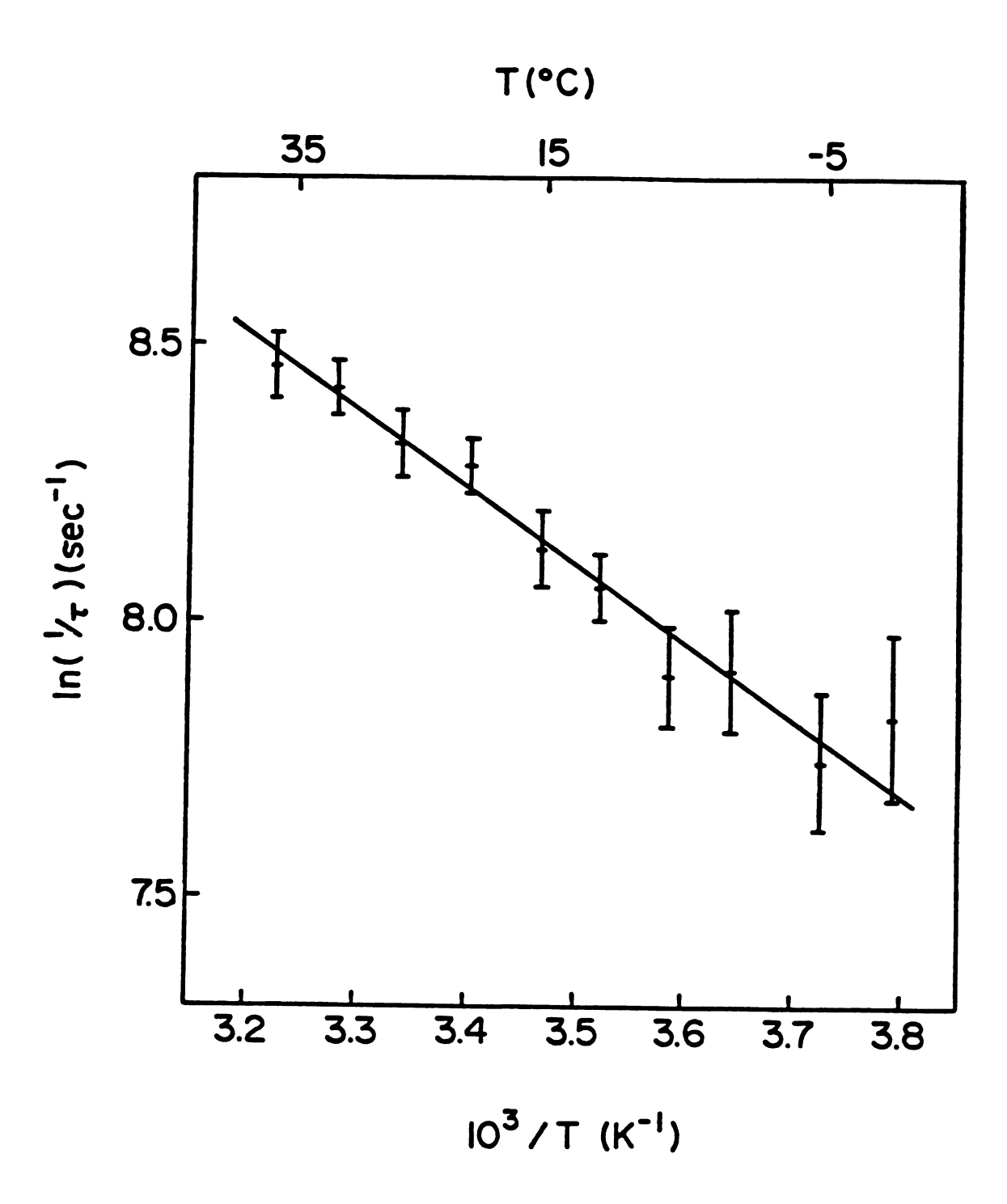


Figure 31 Arrhenius plot of $ln(1/\tau)$ vs. (1/T) for DC18C6 (cis-anti-cis)/NaSCN in THF - Ligand/Na⁺ = 0.50

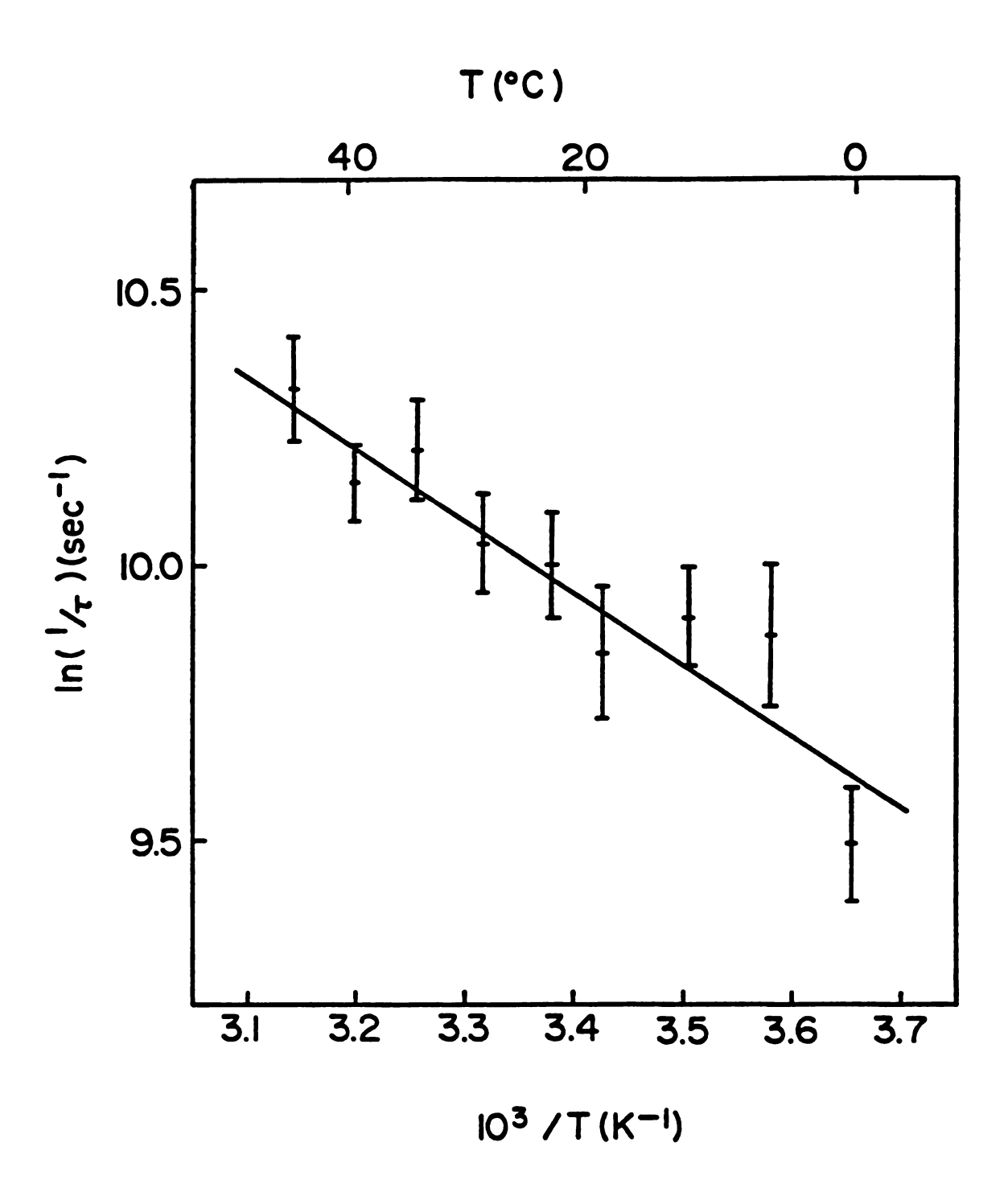


Figure 32 Arrhenius plot of $ln(1/\tau)$ vs. (1/T) for DC18C6 (cis-syn-cis)/NaSCN in THF - Ligand/Na⁺ = 0.51

expected, these plots show two straight lines indicating that only one exchange mechanism occurs for both systems in solution. Another direct observation is that small τ values obtained indicate a relatively fast exchange rate especially with the cis-syn-cis isomer. This results in a very small exchange broadening of the NMR signal and, as a direct result, the experimental errors are large and the data points are scattered.

In order to derive the exchange mechanism for both systems, several solutions at ligand/Na⁺ mole ratios ranging from 0.2 to 0.8 were studied at different temperatures but only solutions at a mole ratio MR close to 0.5 (0.45 < MR < 0.55) gave reproducible values of τ . The others gave extremely scattered data, in most cases with a relative error on τ greater than 100%. In order to explain this fact, we should first recall that, under fast exchange condition, the linewidth at half-height of an NMR line describing a system undergoing a two sites exchange is the population average of the linewidths of the two sites broadened by chemical exchange. This exchange broadening is given by $4\pi~p_A P_B (~\nu_A~-~\nu_B)^2 \tau~$ and has already been discussed in Chapter I in terms of relaxation times (see equation (1.13)). We know that the term $(v_A - v_B)$ in the exchange broadening expression, does not vary much (as previously shown on Figure 26). On the other hand the term pApB, which is a parabolic function of either population, does vary as we change the mole ratio. This term is at a maximum at MR = 0.5 and decreases drastically as the mole ratio is changed toward 0 or 1. Since τ is small in all cases, the computer analysis could only detect it at the maximum pape value. Because of the above observations, the mechanisms could not be derived since, at 0.45 < MR < 0.55, the values of $1/[M^+]_{eq}$ are too close to each other on the mechanism plot and the relative errors on τ are too large. Consequently, mechanisms I or II could not be unambiguously observed.

We can, however, deduce the mechanisms from the following observations: (1) As already discussed, the cis-syn-cis isomer is known to form more stable complexes with Na⁺ and K⁺ than the cis-anti-cis isomer 132 . Therefore, if the associative-dissociative mechanism was the predominant one, we would observe larger $1/\tau$ values with the cis-anti-cis isomer than with the cis-syn-cis isomer since $1/\tau$ is directly related to the decomplexation rate according to equation (5.25); (2) If the associative-dissociative mechanism was the predominant one, at MR < 0.5, the $1/\tau$ value would drop on the mechanism plot, or τ would increase. This effect should compensate for the decrease of the p_{APB} factor and the exchange broadening should still be experimentally observable at least down to MR = 0.3. This has been found not to be the case; (3) As it will be discussed in the next section, the activation parameters with both isomers are very similar to those found by Strasser et al. 141 for the NaSCN/18C6 system in THF. These authors found the bimolecular mechanism to be the predominant one.

Therefore, it seems reasonable to assume that the exchange between NaSCN and either isomer of DC18C6 proceeds via the bimolecular mechanism.

5.2.4. General Discussion: Rates and Activation Parameters

The rates of decomplexation were calculated from the τ values by using equation (5.25) in which only the term corresponding to the observed mechanism was considered. It should be noted that for the NaSCN/DA18C6 system the temperature dependence of the proportionality factor $C_{Na}^+/[Na^+]$ has been calculated on the basis of the Van't Hoff plot which is shown on Figure 28 and when the associative-dissociative mechanism was the predominant one. The data were fitted to another form of the Arrhenius equation as shown below.

$$lnk_{T} = lnk_{To} - \left[\frac{E_{a}}{R} \left(\frac{1}{T} - \frac{1}{To} \right) \right]$$
 (5.26)

where To is the temperature at which the dissociation rate is calculated; the other symbols have their usual meaning. Then the free activation energy of decomplexation ΔG^{\dagger} was calculated from the rate according to the transition-state theory of Eyring 142,143 described by the following equation:

$$k = \frac{k_B T}{h} \exp\left(\frac{-\Delta G^{\dagger}}{RT}\right)$$
 (5.27)

where k_B and h are the Boltzmann constant and the Planck constant respectively. The activation enthalpy of decomplexation ΔH^{\ddagger} was calculated from the following expression which only holds for condensed phases (ΔV^{\ddagger} negligible):

$$\Delta H^{\dagger} = E_{o} - RT \qquad (5.28)$$

Finally, the activation entropy of decomplexation was obtained from the following equation:

$$\Delta G^{\dagger} = \Delta H^{\dagger} - T \Delta S^{\dagger} \qquad (5.29)$$

The results are presented in Table 21 along with those obtained by Strasser et al. 141 with ligand 18C6.

By considering the results obtained with DA18C6, we can, now discuss the reasons why two exchange mechanisms are observed with this system.

Table 21 - Activation Parameters and Rates for the Dissociation of NaSCN Complexes in THF^(a)

Crown	T(b)	E _a (c) (kcal/mol)	ΔH _d (d) (kcal/mol)	A8d (d)	ΔG _d (e) (kcal/mol)	$k_{\mathbf{d}}$ (f) $(\underline{\mathbf{M}}^{-1},\mathbf{sec}^{-1})$	Mechanism(g)
DA18C6	25.0	1.93 ± 0.22	1.33 ± 0.15	-38.6 ± 0.5	12.85 ± 0.03	(2.34 ± 0.09) x 10 ³	=
	0.0	1.93 ± 0.22	1.38 ± 0.15	-38.5 ± 0.6	11.89 ± 0.02	$(1.74 \pm 0.05) \times 10^3$	=
	-40.0	8.5 ± 1.0	8.0 ± 0.8	- 2.2 ± 3.9	8.53 ± 0.02	$(4.91 \pm 0.14) \times 10^4$	-
18C6(h)	25.0	3.4 ± 0.4	2.8 ± 0.4	-27:0 ± 1.0	10.68 ± 0.01	(9.16 ± 0.12) x 104	-
DC18C6 cis-anti-cis	25.0	2.80 ± 0.19	2.21 ± 0.15	-26.9 ± 0.5	10.22 ± 0.01	(19.83 ± 0.28) x 10 ⁴	_
DC18C6 cis-syn- cis	25.0	2.58 ± 0.37	1.99 ± 0.28	-24.2 ± 1.0	9.22 ± 0.02	$(10.88 \pm 0.33) \times 10^5$	-

(a) Obtained with NaSCN 0.010 M - The errors represent one standard deviation; (b) ± 0.1°C; (c) Arrhenius activation energy; (d) Δ H_d and when mechanism II applies; (g) I = bimolecular mechanism and II = associative-dissociative mechanism; (h) Reference 141 - Obtained with NaSCN 0.050 M.

This is best explained in terms of free activation energy of decomplexation ΔG_d^{\dagger} . The Arrhenius activation energy has been generally shown not to describe the threshold energy for reaction 144 and, therefore, is of little interest in this case. An extrapolation of the data describing mechanism II gives ΔG_{-2}^{\mp} = 10.36 kcal/mol at -40°C. Thus, it is clear that the system chooses a lower energy pathway with mechanism I for which the free energy barrier to decomplexation is only $\Delta G_1^{\dagger} = 8.53 \text{ kcal/mol at -40°C.}$ At low temperature, the contribution of mechanism I, which theoretically requires a collision between identically charged species, is not surprising since we know that NaSCN solvated or complexed is mainly present as contact ion pairs in THF solutions. In that case, mechanism I is better represented by a collision between neutral species. The slower decomplexation rate for mechanism II is also consistent with the results obtained with the NaBPh₄/18C6 system in THF¹⁴¹ for which $k_d = 53 \text{ sec}^{-1}$. In our case, the rate is faster because of the ion pairing which destabilizes the complex while the solvent separated ion pairs of NaBPh4 do not give significant crown-anion repulsion resulting in a more stable sodium complex.

Regarding the results obtained with DC18C6, we see that the two isomers give results which are very similar to those obtained with the $18C6^{141}$ showing that the assumption of the bimolecular mechanism for these two systems is valid. The faster rates obtained with DC18C6 are probably related to the presence of the two cyclohexyl substituents on the ligand which destabilize the DC18C6 complexes and give a faster bimolecular exchange. These faster decomplexation rates are directly related to the lower free energy barriers for decomplexation, ΔG_1 , and to the lower Arrhenius activation energies, E_8 , compared with those obtained with the 18C6.

Since the temperature dependence of the formation constant of the

DA18C6 complex is known, we can derive the activation parameters and the rates for the formation of the activated complex from the solvated species when mechanism II applies. A computer fit of the data, shown in Figure 28, gave $\Delta H_F = -5.63 \pm 1.33$ kcal/mol and $\Delta S_F = -1.1 \pm 8.4$ e.u. where ΔH_F and ΔS_F are the enthalpy and entropy of formation of the DA18C6 complex respectively. Although the error on these data is fairly large, it is still interesting to get the activation parameters and the rates for the formation of the complex to get the order of magnitude of these values. The results are presented in Table 22. The most surprising result is that the formation of the activated complex from the solvated species is enthalpy stabilized while its formation from the complex is enthalpy destabilized. This may be due to the polarization of the N-H bonds of the ligand upon complexation. In the solvated state of DA18C6, these two bonds probably interact weakly with the solvent molecules but when complexation occurs, their polarization gives more positive interactions with THF which is a good donor (DN = 20.0). As a result, more solvent molecules interact with the ligand in the activated state resulting in a better solvation. This increase in ligand solvation is also reflected in the large negative value of ΔS_f . On the other hand, when decomplexation occurs, the polarization of the N-H bonds of the ligand decreases, resulting in a destabilization of the ligand-solvent interactions as shown by the positive value of ΔH_{-2}^{\ddagger} . This is confirmed by the results obtained for the bimolecular mechanism. In this case, all the ligand is in the complexed state and the exchange occurs between two identical states containing a solvated complex and a solvated ion pair. This exchange results in a larger activation enthalpy of decomplexation due to the larger barrier which is necessary to activate stable polarized solvated species. Another observation is that the rate of

Table 22 - Activation Parameters and Rates for the Formation of the NaSCN-DA18C6 Complex in THF(a)

L(p) (°C)	25.0	0.0
$\Delta H_{\mathbf{f}}^{\dagger}$ (c) (kcal/mol)	-4.3 ± 2.6	-4.2 ± 2.6
$\Delta S_{\mathbf{f}}^{\sharp}$ (d) (e.u.)	-39.7 ± 8.4	-39.5 ± 8.4
$_{\Delta G_{\mathbf{f}}}^{\sharp}$ (e) (kcal/mol)	7.5 ± 3.6	6.6 ± 3.5
$k_{\mathbf{f}}^{(\mathbf{f})} \ (\underline{\mathbf{M}}^{-1}.\mathrm{sec}^{-1})$	$(1.82 \pm 0.92) \times 10^7$	$(3.2 \pm 1.6) \times 10^7$

(a) Obtained with NaSCN 0.010 \underline{M} . The errors represent one standard deviation; (b) \pm 0.1°C; (c) ΔH_f^{\ddagger} is the activation enthalpy of formation obtained from $\Delta H_f^{\ddagger} = \Delta H_F + \Delta H_d^{\ddagger}$; (d) ΔS_f^{\ddagger} is the activation entropy of formation obtained from $\Delta S_f^{\ddagger} = \Delta S_F + \Delta S_d^{\ddagger}$; (e) $\Delta G_f^{\ddagger} = \Delta H_f^{\ddagger} - T\Delta S_f^{\ddagger}$; (f) $k_f = K_F \times k_d$.

formation of the DA18C6 complex is far below the diffusion-controlled limit ($\sim 10^{10}~{\rm M}^{-1}.{\rm sec}^{-1}$), probably because the complexation involves a dipole-dipole attraction rather than the typical charge-dipole attraction usually pictured for complexation reactions involving crown ethers.

5.3 Conclusion

The exchange kinetics of the sodium thiocyanate with some 18 member ring crown ethers in THF solutions have been studied. The results obtained with the two major isomers of DC18C6 compared with those obtained with the 18C6¹⁴¹ did not give very large variations of the activations parameters and of the exchange rates showing that disubstitution with cyclohexyl rings does not significantly influence the kinetics. The bimolecular exchange mechanism obtained with these three crowns is probably governed by the ion pairing as already reported¹⁴¹. On the other hand, substitution of donor atoms, such as with DA18C6, drastically changes the exchange kinetics. The complexation of NaSCN by this ligand proceeds via associative-dissociative mechanism down to -20°C. This is the first time that this mechanism is observed for the complexation of the tight NaSCN ion pair with an 18 member ring crown ether in THF. This mechanism has been observed with NaBPh₄/18C6 in THF probably because of the solvent separated ion pair of this salt¹⁴¹. In our case, observation of the associative-dissociative mechanism may be due to several reasons such as: the soft donor nitrogen atoms, compared with the 18C6, compete less effectively than SCN- for Na+ resulting in less ligand-anion repulsion; the two hydrogen atoms born by the nitrogen atoms become positively polarized upon complexation and, in a "boat" conformation of the ligand, these hydrogens could interact with the SCN⁻ anion therefore stabilizing the complex. At $-35\,^{\circ}$ C and below, the bimolecular mechanism, which presents a lower energy pathway to the system, becomes predominant. The polarization of the two N-H bonds of the ligand is a good model for explaining the observed activation enthalpies ΔH^{\ddagger} and entropies ΔS^{\ddagger} of formation and decomplexation for both mechanisms. It shows again the very significant part played by the solvent in the exchange kinetics in condensed phases. However, more work has to be done to explain the quite interesting phenomenon observed with the NaSCN/DA18C6 system in THF.

5.4 Future Work

We have seen that no large differences exist between the exchange kinetics of NaSCN with the two isomers of DC18C6 and those of NaSCN with 18C6 in THF. Ion pairing probably governs the exchange and the anion-crown repulsion upsets the stability of the complex and increases the dissociation rates resulting in a fast exchange on the ²³Na NMR time scale with the three crowns. It is therefore reasonable to believe that DC18C6 would give the same results than 18C6 with NaBPh4 in THF, i.e., an associative-dissociative mechanism with slow decomplexation rates 141. On the other hand, we have seen that DA18C6 behaves quite differently compared to 18C6 and the most logical continuation of this work is to study the NaBPh₄/DA18C6 system in THF in order to find out the main kinetic differences between this crown and 18C6 toward NaBPh₄ in THF. A preliminary variable temperature study has been done with this system and the spectra are shown in Figure 33. We see that below -20.0°C the signal corresponding to the complex broadens out into the baseline and if the frequency difference ($\nu_A - \nu_B$) is not too large, this system could be studied with the approximate method of Schori and co-workers 24 .

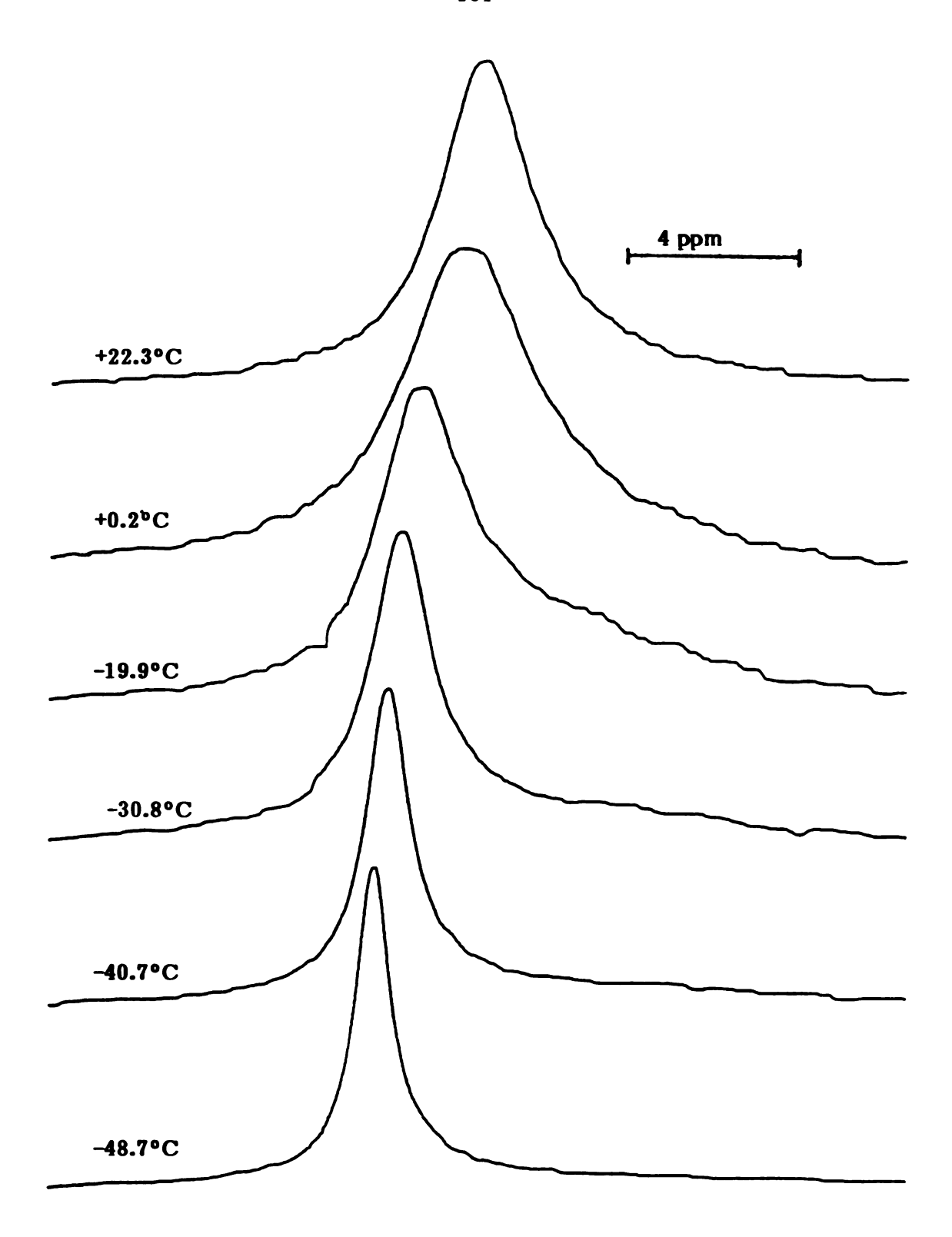


Figure 33 Sodium-23 NMR spectra for a THF solution containing NaBPh₄ (0.050 $\underline{\text{M}}$) and DA18C6 (0.025 $\underline{\text{M}}$) at various temperatures

Another interesting study would be the investigation of the change in the kinetics and the mechanisms when the two N-H groups of DA18C6 are replaced by two N-CH₃ groups, the other parameters such as anion, cation and solvent being kept constant. In order to find out if the polarization of these N-H bonds upon complexation and consequently their interactions with solvent molecules influence the kinetic results, this study should be performed in a good donor solvent such as pyridine (DN = 33.1) and in a poor donor solvent such as nitromethane (DN = 2.7). The length of the substituents on the nitrogen atoms could also be varied without, however, introducing donor atoms in them, since the two sites exchange model would not hold anymore in such a case.

APPENDIX I

USE OF THE NTCDTL SUBROUTINE OF THE NICOLET NTCFTB-1180 PROGRAM FOR TRANSFERING NMR SPECTRA FROM THE BRUKER WH-180 NMR SPECTROMETER ONTO A FLOPPY DISK

After collection of an FID, Fourier transformation and phasing, the NMR spectrum is expanded in the region of interest with the zoom command ZO and CONTROL E until a satisfactory result is obtained. The frequency scale of the expanded region, i.e., the number of Hertz between two data points, is then calculated by dividing its full width by (N-1), N being the total number of data points describing the expanded region. The full width is obtained in the ZO/CONTROL E mode with the right end and the left end of the region displayed on the scope as F_1 and F_2 respectively. The total number of data points is obtained by exiting the ZO mode with RETURN and using the full scale FS routine which gives the number of points displayed in the ZO/CONTROL E mode. Finally, by using the NTCDTL subroutine, the expanded region is transferred to a floppy disk located in a PDP-11 computer conditioned to accept a file. The use of this subroutine is shown

below.

>RUN NTCDTL
DATA-TRANSFER PROGRAM
VERSION # 10903
COMMAND:
BI,BO,CP,AP,AR,KB,LP,LR,MO,PR,TL,TT?
BO
WHAT FORMAT (A=ASCII, B=BINARY)? A
WHAT PARITY (E,O,M,N)? N
MAXIMUM RECORD LENGTH = 64
PROMPT = 12
ENTER TERMINAL MODE (Y,N)? N
COMMAND:
BI,BO,CP,AP,AR,KB,LP,LR,MO,PR,TL,TT?
MO

After answering N to the ENTER TERMINAL MODE question, the LINE FEED key of the PDP-11 computer must be pressed in order to achieve the transfer. The final answer MO is used to exit NTCDTL and to go back to the main NTCFTB program.

NOTE: The frequency scale as well as the total number of points must be known for the next steps of the transfer which are described in section 2.4.3.

APPENDIX II

TRANSFER OF NMR SPECTRA FROM A MAGNETIC TAPE INTO PERMANENT MEMORY ON A CIBER CDC-6500 COMPUTER

A typical program for this transfer is shown below.

PNC CARD POPOV.TP,JC2500. REQUEST, TAPE, VRN=TMP272, AS, Z, HD. FILE.TAPE,RT=F,BT=E,CM=YES,FL=80,RB=10,MBL=800. SKIPF, TAPE, 16, 17. HAL CRMCOPY, I=TAPE, O=FILE1, NPAR=1. CATALOG, FILE1, CAC01, RP=999. HAL CRMCOPY, I=TAPE, O=FILE2, NPAR=1. CATALOG, FILE2, CAC02, RP=999. HAL CRMCOPY, I=TAPE, O=FILE3, NPAR=1. CATALOG.FILE3.CAC03.RP=999. HAL CRMCOPY, I=TAPE, O=FILE4, NPAR=1. CATALOG.FILE4.CAC04.RP=999. HAL CRMCOPY, I=TAPE, O=FILE5, NPAR=1. CATALOG, FILE5, CAC05, RP=999. HAL CRMCOPY, I=TAPE, O=FILE6, NPAR=1. CATALOG, FILE6, CSC01, RP=999. HAL CRMCOPY, I=TAPE, O=FILE7, NPAR=1. CATALOG, FILE7, CSC02, RP=999. HAL CRMCOPY, I=TAPE, O=FILE8, NPAR=1. CATALOG, FILE8, CSC03, RP=999. HAL CRMCOPY, I=TAPE, O=FILE9, NPAR=1. CATALOG, FILE9, CSC04, RP=999. HAL CRMCOPY, I=TAPE, O=FILE10, NPAR=1. CATALOG,FILE10,CSC05,RP=999. HAL CRMCOPY, I=TAPE, O=FILE11, NPAR=1. CATALOG, FILE 11, KIO87, RP=999. HAL CRMCOPY, I=TAPE, O=FILE12, NPAR=1. CATALOG, FILE12, KI088. RP=999. HAL CRMCOPY.I=TAPE.O=FILE13.NPAR=1. CATALOG, FILE 13. KI089. RP=999. HAL CRMCOPY, I=TAPE, O=FILE14, NPAR=1. CATALOG.FILE14.KI090.RP=999. HAL CRMCOPY, I=TAPE, O=FILE15, NPAR=1. CATALOG.FILE15.KI091,RP=999. HAL CRMCOPY, I=TAPE, O=FILE16, NPAR=1. CATALOG, FILE 16. KI 092. RP=999. HAL CRMCOPY, I=TAPE, O=FILE17, NPAR=1. CATALOG.FILE17.KI093,RP=999. HAL CRMCOPY, I=TAPE, O=FILE18, NPAR=1. CATALOG.FILE18.KI094.RP=999. HAL CRMCOPY, I=TAPE.O=FILE19.NPAR=1. CATALOG, FILE 19. KI 095. RP=999. HAL CRMCOPY, I=TAPE, O=FILE20, NPAR=1. CATALOG,FILE20,KI096,RP=999. PFLIST. 8

In this program, the first four cards and the final 6789 card must always be included.

In the third REQUEST card, TMP272 represents the MSU-assigned magnetic tape visual reel name. The code number 272 may vary.

The program shown above will skip the first 16 files on the tape. This is done with the fifth SKIPF card where 16 represents the number of files to be skipped. If this card is not included, the program will transfer the files starting at the first one.

The next forty cards are used to transfer 20 files starting at the seventeenth one. FILE1-FILE20 are the temporary names used for this transfer. For the transfer of one file, two cards which are HAL, CRMCOPY and CATALOG must be used. For a given set of these two cards, the temporary name must be the same although its designation may be changed by the user.

CAC01-CAC05, CSC01-CSC05 and KI087-KI096 are the permanent names assigned by the user to the files transferred into permanent memory. These names can contain 1-40 characters and may be changed. The PFLIST card is used to get an output listing all the permanent files stored in memory on the user's account number. This card may not be included.

APPENDIX III

KINFIT SUBROUTINE EQUATION FOR AN NMR LORENTZIAN LINESHAPE CORRECTED FOR DELAY TIME, LINE BROADENING AND ZERO-ORDER DEPHASING IN THE ABSENCE OF CHEMICAL EXCHANGE

```
PNC CARD
PSPOV.CM45000.RG2.JC1G00,T50.
HAL BANNER.SZCZYGIEL.
2TT4CH.TAPE62.FILE NAME.
REWIND.TAPE62.
ATTACH.READER.READERBINARY.
RETURN. KINFT4. LGO.
HAL. L.DYE. KINFT4=KINFT4.
FIN4, B=LGO.
LOAD. KINFT4.
LOAD. KINFT4.
     <u>L</u>GO.
      18,
                   SUBROUTINE EQN
COMMON KOUNT, ITAPE.JTAPE.INT, LAP.XINCR.NOPT.NOVAR.NCUNK.X.U.ITMAX.
1M TX.TEST, I.AV.RESID.IAR, EPS, ITYP, XX.RXTYP.DX11.FDP.FJ.FU.P.ZL.TO.E
2I GVAL.XST.T.DT, L, M.JJJ.Y.DY, VECT, NCST.CONST.NDAT.JDAT.MOPT.LOPT,
3Y YY.CONSTS
COMMON/FEDT/IMETH
COMMON/FEDT/IMETH
COMMON/FOINT/KOPT.JOPT.XXX
DIMENSIGN X(4.33C).U(20).HTX(4.3DD).XX(4).FDP(3DD).FO(3DD).FU(3DD)
1.P(20.21).VECT(2C.21).ZL(3CD).TO(28).EIGVAL(20).XST(3DD).V(1D).
2DY(10).CONSTS(5D.16).NCST(5D.15MIN(5D).RXTYP(5D).DX11(5D).IRX(5D)
3.MCPT(5D).LOPT(5D).YYY(5D).CONST(16).XXX(15)

1 CONTINUE
1 TAPE=60
JTAPE=61
RETURN
7 CONTINUE
                                                                                                                                                                                                                                                                                                                E 0 N 4
E 0 N 4
E 0 N 4
E 0 N 4
E 0 N 4
                                                                                                                                                                                                                                                                                                                 EGN4
EGN4
                                                                                                                                                                                                                                                                                                                 EON4
EON4
EGN4
                                                                                                                                                                                                                                                                                                                 EON4
EON4
EON4
                                                                                                                                                                                                                                                                                                                EON4
EON4
EON4
EON4
                    7 CONTINUE
NOUNK=5
NOVAR=2
EGN4
                  3 CONTINUE
                                                                                                                                                                                                                                                                                                                ĒQN4
```

```
4 CONTINUE
RETURN
5 CGNTINUE
IF (IMETHONES-1) GO TO 2C
RETURN
20 CGNTINUE
RETURN
9 CONTINUE
RETURN
11 CONTINUE
RETURN
12 CONTINUE
RETURN
12 CONTINUE
RETURN
12 CONTINUE
RETURN
13 CONTINUE
RETURN
14 CONTINUE
RETURN
15 CONTINUE
RETURN
16 CONTINUE
RETURN
17 CONTROL CARD ** WITH 1 IN COLUMN 70 TO READ THE FILE **
TITLE CARD OR BLANK CARD
CONSTANT CARD ** 2 CONSTANTS ARE DEFINED **
BLANK CARD

7 8
9
```

APPENDIX IV

KINFIT SUBROUTINE EQUATION FOR AN NMR LINESHAPE OF AN UNCOUPLED SPIN SYSTEM UNDERGOING CHEMICAL EXCHANGE BETWEEN TWO NONEQUIVALENT SITES CORRECTED FOR DELAY TIME, LINE BROADENING AND ZERO-ORDER DEPHASING

```
PNC CARD
POPO V.CM45000.RG2.JC1000,T50.
HAL BANNER.SZCZYGIEL.
ATTACH, TAPE62.FILE NAME.
REWINO, TAPE62.
ATTACH, READER.READERBINARY.
RETURN, KINFT4, LG0.
HAL. L.DYE, KINFT4=KINFT4.
LOAD, KINFT4.
LOAD, READER.
LOAD, READER.
      8
                       SUBROUTINE EQN

COMMON KOUNT.ITAPE.JTAPE.IUT.LAP.XINCR.NOPT.NOVAR.NOUNK.X.U.ITMAX. EQN4

1W TX.TEST.I.AV.RESID.IAR.EPS.ITYP.XX.RXTYP.DX11.FGP.FD.FU.P.ZL.TO.E EQN4

2I GVAL.XST.T.DT.L.M.JJJ.Y.DT.V.VECT.NCST.CONST.NDAT.JDAT.MOPT.LOPT. EQN4

COMMON/FEDT.IMETH

COMMON/FEDT.IMETH

COMMON/POINT/KOPT.JOPT.XXX

COMPLEX ALPHA.ALPHB.XLAMA.XLAMB.C1.C2.XS.2RUCE.ALEX.AL.FRED

DIMENSION X.(4.300).U.(20).WIX.(4.300).XX.(4.300).FU(300).FU(300)

1.P(20.21).VECT(20.21).ZL(300).TO(20).EIGVAL(20).XST(300).Y(10).

EQN4

1.P(20.21).VECT(20.21).ZL(300).TO(20).EIGVAL(20).XST(300).Y(10).

EQN4

2DV(10).CONSTS(50.16).NCST(50).ISMIN(50).RXTYP(50).DXII(50).IRX(50)

EQN4

GO TO (2.3.4.5.1.7.8,9.10.11.12) ITYP

1.TAPE=60

JTAPE=60

JTAPE=60
                  JTAPE=61
RETURN
7 CONTINUE
NOUNK=5
NOVAR=2
                                                                                                                                                                                                                                                                                                                                                               EON4
EON4
EON4
                                                                                                                                                                                                                                                                                                                                                              EGN4
EGN4
EGN4
EGN4
                    RETURN
8 CONTINUE
RETURN
                                                                                                                 U(1) = K (INTENSITY . UNITLESS)
U(2) = B (BASELINE INTENSITY . UNITLESS)
U(3) = THETA (ZERO GRDER PHASE CORRECTION . RAD.)
U(4) = DELTAM (FREQ. CORR.=2(FI)(DELTAMU) . RAD./SEC.)
U(5) = TAU (EXCHANGE RATE . SEC.)
                                          PARAMETERS
                                                                                                                                                                                              (POP. OF FREE SITE . UNITLESS)

(RELAXATION TIME . SEC./RAD.)

(WA=2(PI)(NUA) . RAD./SEC.)

(POP. OF COMPLEXED SITE . UNITLESS)

(RELAXATION TIME . SEC./RAD.)

(WB=2(PI)(NUB) . RAD./SEC.)

(DELAY TIME . SEC.)

(LINE BROAD.=(PI)(LB(HZ)) . RAD./SEC.)
                                                                                                                 CONST(1) = PA

CONST(2) = T2A

CONST(3) = WA

CONST(4) = PB

CONST(5) = T2B

CONST(6) = W5

CONST(7) = DE

CONST(8) = LB
                                          CONSTANTS
```

```
IF(U(1).GT.0.)GD TO 1CD2
U(1)=1.E+09
1002 CONTINUE
IF(U(5).LT.1.)GD TO 1001
U(5)=.0001
1001 CONTINUE
IF(U(5).GT.0.)GO TO 1000
U(5)=.0001
1000 CONTINUE
PI=2-3.14159
ALPHA=1./CONST(2)+CMPLX(0.,1.)+(CONST(3)-XX(1)+PI+U(4))
ALPHB=1./CONST(5)+CMPLX(0.,1.)+(CONST(6)-XX(1)+PI+U(4))
BRUCE=-(ALPHA+ALPHB+1./U(5))
FRED=(ALPHA+ALPHB+1./U(5))
FRED=(ALPHA+ALPHB+0.NX(14)/U(5)-CONST(1)/U(5))+2
B 0B=4+CONST(1)+CONST(4)/(U(5)+U(5))
ALEX=FRED+B0B
AL=CEXP(CLOG(ALEX)/2.)
XLAMA=(BRUCE+AL)/2.
CI=CMPLX(0.,1.)+(XLAMB+CONST(1)+ALPHA+CONST(4)+ALPHB)/(-XLAMA+1)XLAMB)
C2=CMPLX(0.,1.)+(XLAMA+CONST(1)+ALPHA+CONST(4)+ALPHB)/(XLAMA-1)XLAMB)
C2=CMPLX(0.,1.)+(XLAMA+CONST(1)+ALPHA+CONST(4)+ALPHB)/(XLAMA-1)XLAMB)
C2=CMPLX(0.,1.)+(XLAMA+CONST(1)+ALPHA+CONST(4)+ALPHB)/(XLAMA-1)XLAMB)
                    CI=CHPLX(0.,1.)+(XLAMB+CONST(1)+ALPHA+CONST(4)+ALPHB)/(-XLAMB)

C2=CMPLX(0.,1.)+(XLAMA+CONST(1)+ALPHA+CONST(4)+ALPHB)/(XLAMA-1XLAMB)

XS=-C1+(CEXP((XLAMA-CONST(8))+CONST(7)))/(XLAMA-CONST(8))+

(-C2)+(CEXP((XLAMB-CONST(8))+CONST(7)))/(XLAMB-CONST(8))+

REAP=REAL(XS)

AMAG=AIMAG(XS)

CALC=U(1)+(-REAP+SIN(U(3))+AMAG+COS(U(3)))+U(2)

IF (IMETH-NE.-1) GO TO 35

RETURN

35 CONTINUE

RETURN

4 CONTINUE

RETURN

5 CONTINUE

RETURN

9 CONTINUE

RETURN

10 CONTINUE

RETURN

11 CONTINUE

RETURN

12 CONTINUE

RETURN

13 CONTINUE

RETURN

14 CONTINUE

RETURN

15 CONTINUE

RETURN

16 CONTINUE

RETURN

17 CONTINUE

RETURN

18 CONTINUE

RETURN

19 CONTINUE

RETURN

10 CONTINUE

RETURN

11 CONTINUE

RETURN

12 CONTINUE

RETURN

END
                                                                                                                                                                                                                                                                                                                                                                                                                                                                                                                                                                             EGN4
EGN4
                                                                                                                                                                                                                                                                                                                                                                                                                                                                                                                                                                             EGN4
                                                                                                                                                                                                                                                                                                                                                                                                                                                                                                                                                                              EGN4
EGN4
EGN4
                                                                                                                                                                                                                                                                                                                                                                                                                                                                                                                                                                            789
                                                END
  CONTROL CARD ** WITH 1 IN COLUMN 70 TO READ THE FILE **
TITLE CARD OR BLANK CARD
CONSTANT CARD ** 8 CONSTANTS ARE DEFINED **
INITIAL ESTIMATE CARD ** 5 INITIAL ESTIMATES ARE DEFINED **
BLANK CARD
áL
7
```

APPENDIX V

APPLICATION OF THE COMPUTER PROGRAM KINFIT TO THE CALCULATION OF COMPLEX FORMATION CONSTANTS FROM THE NMR DATA

The KINFIT computer program was used to fit the sodium-23 chemical shift vs. mole ratio data to the equation (5.6) of Chapter V which was used as the SUBROUTINE EQN.

$$\delta_{\text{obs}} = [(K_{\text{F}}C_{\text{M}}^{\text{T}} - K_{\text{F}}C_{\text{L}}^{\text{T}} - 1) + ((K_{\text{F}}C_{\text{L}}^{\text{T}} - K_{\text{F}}C_{\text{M}}^{\text{T}} + 1)^{2} + 4K_{\text{F}}C_{\text{M}}^{\text{T}})^{1/2}] (\frac{\delta_{\text{M}} - \delta_{\text{ML}}}{2K_{\text{F}}C_{\text{M}}^{\text{T}}}) + \delta_{\text{ML}}$$
(5.6)

Equation (5.6) has two unknown quantities, δ_{ML} and K_F . designated as U(1) and U(2) respectively in the FORTRAN code. The two input variables are the analytical concentration of the ligand (C_L^T , \underline{M}) and the observed chemical shift (δ_{ODS} , ppm) which are denoted as XX(1) and XX(2) respectively in the FORTRAN code. Starting with a reasonable estimate for the value of K_F and δ_{ML} , the program fits the calculated chemical shifts (the right hand side of the equation (5.6)) to the observed ones by iteration method.

The first control card contains the number of data points (columns 1-5 (Format I5)), the maximum number of iteration allowed (columns 11-15 (I5)), the number of constants (columns 36-40 (I5)) and the convergence tolerance (0.0001 works well) in columns 41-50 (Format F10.6). The second control card contains any title the user desires. The third control card contains the values of CONST(1) (C_M^T , \underline{M}) in columns 1-10 (F10.6) and CONST(2) (δ_M , ppm) in columns 11-20 (F10.6); other constants can be listed in columns

21-30, 31-40, etc... up to column 80. The fourth and final control card contains the initial estimates of the unknowns $U(1) = \delta_{ML}$ and $U(2) = K_F$, in columns 1-10 and 11-20 (F10.6) respectively. The fifth through the Nth cards are the data cards which contain $XX(1) = C_L^T$ in columns 1-10 (F10.6), the variance on XX(1) in columns 11-20, XX(2) = the chemical shift at XX(1) in columns 21-30 (F10.6) and the variance on XX(2) in columns 31-40 (F10.6). This sequence is repeated in columns 41-80 for the second data point. Each card must contain two data points except the last one which may contain only one. The SUBROUTINE EQN is given below:

```
5 CONTINUE
IF (IMETH.NE.-1) GO TO 20
RETURN
20 CONTINUE
RETURN
9 CONTINUE
RETURN
10 CONTINUE
RETURN
11 CONTINUE
RETURN
12 CONTINUE
RETURN
12 CONTINUE
RETURN
13 CONTINUE
RETURN
14 CONTINUE
RETURN
15 CONTINUE
RETURN
16 CONTINUE
RETURN
17 CONTINUE
RETURN
18 CONTINUE
RETURN
                                                                                                   EGNA
EGNA
EGNA
EGNA
EGNA
                                                                                                   FOLA
  8,
```

APPENDIX VI

CALCULATION AND PROPAGATION OF ERRORS

The equation used to calculate the standard deviation on a result can be found in many texts. They are usually referred to as propagation-of-random-error expression in terms of confidence limits and are 145:

(1) For $F = ax \pm by \pm cz$

$$d^{2}(F) = a^{2}d^{2}(x) + b^{2}d^{2}(y) + c^{2}d^{2}(z)$$
 (VI.1)

(2) For F = axyz (or axy/z or ax/yz or a/xyz)

$$\frac{d^{2}(F)}{F^{2}} = \frac{d^{2}(x)}{x^{2}} + \frac{d^{2}(y)}{y^{2}} + \frac{d^{2}(z)}{z^{2}}$$
(VI.2)

(3) For $F = ax^n$

$$\frac{d^2(F)}{F^2} = n^2 \frac{d^2(x)}{x^2}$$
 (VI.3)

where a, b and c are constants and x, y and z are directly measured experimental quantities are assumed to be mutually independent which is true in our case. d is a confidence limit for each variable and is estimated from the experiment. It is assumed to represent a 68% confidence limit, i.e., d is equal to one standard deviation of the experimental value assumed

to be the mean of a population with an ideal Gaussian distribution.

An example of such calculation is given below. It describes the calculation of the error on the equivalent conductances reported in Chapter IV. They are obtained from equation (4.3) recalled below.

$$\Lambda = \frac{1000K}{R_{SOl} \times C}$$
 (4.3)

 $d(\Lambda)$ is obtained from the following equation.

$$\frac{d^2(\Lambda)}{\Lambda^2} = \frac{d^2(K)}{K^2} + \frac{d^2(R_{sol})}{R^2_{sol}} + \frac{d^2(c)}{C^2}$$
 (VI.4)

 $d(R_{SOI})$ is obtained from equation (VI.5) derived from equation (4.1) as shown below.

$$\frac{1}{R_{SOl}} = \frac{1}{R_{SOl} + SR} - \frac{1}{R_{SR}}$$
 (4.1)

Rearrangement leads to:

$$R_{SOl} = \frac{R_{SR} \times R_{SOl} + SR}{R_{SR} - R_{SOl} + SR}$$

$$\frac{d^{2}(R_{SOl})}{R^{2}_{SOl}} = \frac{d^{2}(R_{SOl})}{R^{2}_{SR}} + \frac{d^{2}(R_{SOl} + SR)}{R^{2}_{SOl} + SR} +$$

$$(R_{SR} - R_{Sol} + SR)^{-2} [d^2(R_{SR}) + d^2(R_{Sol} + SR)]$$
 (VI.5)

d(C) is obtained from equation (VI.7) derived from equation (VI.6) as shown below.

$$C = \frac{1000 \times m}{M \times v}$$
 (VI.6)

where C is the salt concentration in eq/l, m is the analytical mass of salt in grams, M is the equivalent weight of the salt in g/eq and v is the volume of the flask in ml.

$$\frac{d^{2}(C)}{C^{2}} = \frac{d^{2}(m)}{m^{2}} + \frac{d^{2}(M)}{M^{2}} + \frac{d^{2}(v)}{v^{2}}$$
(VI.7)

d(m) and d(v) are obtained from the specifications on the analytical balance and on the Class A Pyrex volumetric flasks respectively. d(K) and d(M) were assumed to be $0.03~cm^{-1}$ and 0.01~g/eq respectively.

APPENDIX VII.

DERIVATION OF THE LINESHAPE OF THE ABSORPTION PART OF THE NMR SPECTRUM CORRECTED FOR DELAY TIME DE, LINE BROADENING LB AND ZERO-ORDER DEPHASING IN THE ABSENCE OF CHEMICAL EXCHANGE

The equation describing a Free Induction Decay (FID) is given by 98:

$$f(t) = K \exp[i(\omega_A - \omega_O)t] \exp(-t/T_{2A})$$
 (VII.1)

where ω_0 is the angular frequency of the radiofrequency pulse in rad/s, t is the time in s., ω_A and T_{2A} are the Larmor angular frequency in rad.s⁻¹ and the transverse (or spin-spin) relaxation time in s.rad⁻¹ of the investigated nucleus in a given site A, respectively. K is an intensity factor.

The transformation from the time domain to the frequency domain is given by the Fourier transformation described by the equation shown below.

$$g(\omega) = \int_{0}^{+\infty} f(t) \exp[-i(\omega - \omega_{O})t] dt$$
 (VII.2)

where ω is the variable frequency.

Since $\exp[-i(\omega - \omega_0)t] = \cos[(\omega - \omega_0)t] - i \sin[(\omega - \omega_0)t]$, we can write the following expression for $g(\omega)$:

$$g(\omega) = \int_{0}^{+\infty} f(t)\cos[(\omega - \omega_{O})t]dt - i \int_{0}^{+\infty} f(t)\sin[(\omega - \omega_{O})t]dt \qquad (VII.3)$$

The separation of $g(\omega)$ into a real and on imaginary part is easily done by developing equation (VII.3), regrouping the real terms as well as the imaginary terms into one real integral and one imaginary integral respectively and simplifying each of them by trigonometric transformations. This leads to the following equations.

$$g(\omega) = A(\omega) - iD(\omega)$$
 (VII.4)

with

$$A(\omega) = K \int_{0}^{+\infty} \exp(-t/T_{2A})\cos[(\omega - \omega_{A})t]dt \qquad (VII.5)$$

and

$$D(\omega) = K \int_{0}^{+\infty} \exp(-t/T_{2A}) \sin[(\omega - \omega_{A})t] dt \qquad (VII.6)$$

where $A(\omega)$ and $D(\omega)$ represent the absorption (or real) part and the dispersion (or imaginary) part of the NMR spectrum respectively.

Applying a Line Broadening (LB) of N Hertz prior to Fourier transformation is equivalent to multiplying the FID by an exponentially decaying function $\exp(-\pi Nt)$. Combining this expression with equation (VII.1) gives:

$$f(t) = K \exp[i(\omega_A - \omega_O)t] \exp(-t/T)$$
 (VII.7)

with

$$T = \frac{T_{2A}}{1 + \pi N T_{2A}}$$
 (VII.8)

where T is the apparent transverse relaxation time after LB and is related to the apparent linewidth at half-height $W_{1/2\mathrm{app}}$ after LB according to the following equation.

$$^{\pi}W_{1/2app} = T^{-1}$$
 (VII.9)

In order to understand the effect of a delay time DE, let us recall some basic principles of pulsed Fourier Transform NMR spectroscopy, the theory of which has been described by Ernst and Anderson¹⁴⁶. Suppose a system of isolated spins in a magnetic field Ho along the z axis is subjected to a sequence of rectangular radiofrequency pulses along the x axis with angular frequency ω_0 , magnetic field amplitude H₁, duration τ_0 and period T₀. These pulses tip the magnetization vectors which have Larmor frequencies ω_i 's such that $\Upsilon H_1/2 \gg \omega_i - \omega_o$, where Υ is the gyromagnetic ratio of the nucleus. The resulting FID is the sum of the time dependences, during the acquisition times τ_{ac} , of the x,y component of the magnetization vectors in a frame rotating with a frequency ω_0 around the z axis. The pulse length τ_0 is short compared to the relaxation times T_1 and T_2 of the nucleus so that relaxation is negligible during the pulse. The usefulness of the delay time DE is to start recording the FID after complete decay of the trigger pulse in order to avoid any interference of the latter. Therefore the relationship DE >> τ_0 must be true. Assuming that the pulse occurs at t = 0, applying DE is equivalent to "miss" the part of the FID between t = 0 and t = DE. Thus, the logical correction for this lack of information is to integrate from DE to infinity instead of from 0 to infinity during Fourier transformation. At this point, the integration up to infinity can be criticized but usually the acquisition time is chosen such as the FID completely decays down to zero before the end of acquisition, i.e., all the magnetization vectors decay back to the z axis.

According to the observations described above, an NMR spectrum for species undergoing no chemical exchange and corrected for LB and DE is

obtained by calculating the following Fourier transformation.

$$A(\omega) = K \int_{DE}^{+\infty} \exp(-t/T)\cos[(\omega - \omega_A)t]dt \qquad (VII.10)$$

$$D(\omega) = K \int_{DE}^{+\infty} \exp(-t/T)\sin[(\omega - \omega_A)t]dt \qquad (VII.11)$$

Integrating both equations by part twice and rearranging gives:

$$A(\omega) = \frac{N}{D} \left\{ -T \sin[(\omega - \omega_A)DE] + \frac{\cos[(\omega - \omega_A)DE]}{(\omega - \omega_A)} \right\}$$
 (VII.12)

$$D(\omega) = \frac{N}{D} \left\{ T\cos[(\omega - \omega_A)DE] + \frac{\sin[(\omega - \omega_A)DE]}{(\omega - \omega_A)} \right\}$$
 (VII.13)

with

$$N = KT(\omega - \omega_A) \exp(-DE/T)$$
 (VII.14)

and

$$D = 1 + T^{2}(\omega - \omega_{A})^{2}$$
 (VII.15)

The absorption part of the NMR spectrum corrected for zero-order dephasing is given by 69:

$$S(\omega) = A(\omega)\cos\theta - D(\omega)\sin\theta \qquad (VII.16)$$

where θ is the zero-order dephasing in rad., and $A(\omega)$ and $D(\omega)$ are the absorption and dispersion part of the spectrum perfectly phased, i.e., θ = 0, described by equations (VII.12) and (VII.13) respectively.

Equation (VII.16), simplified by trigonometric transformations, is given below.

$$S(\omega) = \frac{U}{V} \left\{ \cos[(\omega - \omega_A)DE + \theta] - T(\omega - \omega_A)\sin[(\omega - \omega_A)DE + \theta] \right\} + B (VII.17)$$

with

$$U = KT \exp(-DE/T)$$
 (VII.18)

and

$$V = 1 + T^{2}(\omega - \omega_{A})^{2}$$
 (VII.19)

The final expression of $S(\omega)$ represents the function describing the absorption part of the NMR spectrum corrected for delay time DE, line broadening LB and zero-order dephasing in the absence of chemical exchange. The new factor B is the intensity of the baseline.

REFERENCES

- 1. C.J. Pedersen, J. Am. Chem. Soc., 89, 7017 (1967).
- 2. C.J. Pedersen, J. Am. Chem. Soc., 92, 391 (1971).
- 3. C.J. Pedersen, J. Org. Chem., 36, 254 (1971).
- 4. B. Dietrich, J.-M. Lehn and J.-P. Sauvage, Tetrahedron Lett., 2885 (1969).
- 5. E. Graf and J.-M. Lehn, J. Am. Chem. Soc., 97, 5022 (1975).
- 6. J.-M. Lehn, Acc. Chem. Res., 11, 49 (1978).
- 7. J.-M. Lehn, E. Souveaux and A.K. Willard, J. Am. Chem. Soc., 100, 4916 (1978).
- 8. C. Moore and B.C. Pressmann, Biochem. Biophys. Res. Comm., 15, 562 (1964).
- 9. R.J.P. Williams, Quart. Rev., 24, 331 (1970).
- 10. D.C. Tosteson, Sci. Am., 244, 164 (April 1981).
- 11. A.I. Popov and J.-M. Lehn in "Coordination Chemistry of Macrocyclic Compounds", G.A. Melson ed., Plenum Press (1979), p. 537.
- 12. J.D. Lamb, R.M. Izatt, J.J. Christensen and D.J. Eatough, Ibid., p. 145.
- 13. "Progress in Macrocyclic Chemistry", R.M. Izatt and J.J. Christensen eds., Wiley Interscience (1979).
- 14. I.M. Kolthoff, Anal. Chem., 51, 1R (1979).
- 15. N.S. Poonia and A.V. Bajaj, Chem. Rev., 79, 389 (1979).
- 16. M. Hiraoka, "Crown Compounds: Their Characteristics and Applications", Elsevier ed., New York (1982).
- 17. (a) R.A. Schwind, T.J. Gilligan and E.L. Cussler in "Synthetic Multidentate Macrocyclic Compounds", R.M. Izatt and J.J. Christensen eds., Academic Press (1978), p. 302; (b) C. Sirlin, Bull. Soc. Chim. Fr., II-5 (1984).
- 18. J.-M. Lehn, Struct. Bonding (Berlin), 16, 1 (1973).

- 19. J.D. Lin and A.I. Popov, J. Am. Chem. Soc., 103, 3773 (1981).
- 20. J.M. Ceraso and J.L. Dye, J. Am. Chem. Soc., 95, 4432 (1973).
- 21. Y. Cahen, J.L. Dye and A.I. Popov, J. Phys. Chem., 79, 1292 (1975).
- J.M. Ceraso, P.B. Smith, J.S. Landers and J.L. Dye, J. Phys. Chem., 81, 760 (1977).
- 23. A.I. Popov, Pure Appl. Chem., 51, 101 (1979).
- 24. E. Schori, J. Jagur-Grodzinski, Z. Luz and M. Shporer, J. Am. Chem. Soc., 93, 7133 (1971).
- 25. E. Schmidt, Ph.D. Thesis, Michigan State University, East Lansing, MI (1981).
- 26. G.W. Liesegang and E.M. Eyring in "Synthetic Multidentate Macrocyclic Compounds", R.M. Izatt and J.J. Christensen eds., Academic Press (1978), p. 245.
- 27. Professor M. Chabanel (Université de Nantes France). Personal communication. To be published.
- 28. E.L. Yee, O.A. Gansow and M. Weaver, J. Am. Chem. Soc., <u>102</u>, 2278 (1980).
- 29. B.G. Cox and H. Schneider, J. Am. Chem. Soc., 99, 2809 (1977).
- 30. B.G. Cox, H. Schneider and J. Stroka, J. Am. Chem. Soc., <u>100</u>, 4746 (1978).
- 31. B.G. Cox and H. Schneider, J. Am. Chem. Soc., 102, 3628 (1980).
- 32. B.G. Cox, J. Garcia-Rosas and H. Schneider, J. Am. Chem. Soc., <u>103</u>, 1054 (1981).
- 33. B.G. Cox, J. Garcia-Rosas and H. Schneider, Ber. Busenges. Phys. Chem., 86, 293 (1982).
- 34. B.G. Cox, P. Firman and H. Schneider, Inorg. Chim. Acta, <u>64</u>, L263 (1982).
- B.G. Cox, J. Garcia-Rosas and H. Schneider, Nouv. J. Chim., <u>6</u>, 397 (1982).
- B.G. Cox, J. Garcia-Rosas and H. Schneider, J. Am. Chem. Soc., <u>104</u>, 2434 (1982).
- 37. B.G. Cox, P. Firman and H. Schneider, Inorg. Chim. Acta, 69, 161 (1983).
- 38. B.G. Cox, C. Guminski, P. Firman and H. Schneider, J. Phys. Chem., 87, 1357 (1983).

- 39. B.G. Cox, Ng Van Truong, J. Garcia-Rosas and H. Schneider, J. Phys. Chem., 88, 996 (1984).
- 40. B.G. Cox, Ng Van Truong and H. Schneider, J. Am. Chem. Soc., <u>106</u>, 1273 (1984).
- 41. R. Gresser, D.W. Boyd, A.M. Albrecht-Gary and J.P. Schwing, J. Am. Chem. Soc., 102, 651 (1980).
- 42. J.-M. Lehn, J.-P. Sauvage and B. Dietrich, J. Am. Chem. Soc., <u>92</u>, 2916 (1970).
- 43. E. Mei, J.L. Dye and A.I. Popov, J. Am. Chem. Soc., 99, 5308 (1977).
- 44. E. Mei, A.I. Popov and J.L. Dye, J. Am. chem. Soc., 99, 6532 (1977).
- 45. E. Mei, A.I. Popov and J.L. Dye, J. Phys. Chem., 81, 1677 (1977).
- 46. M. Eigen and L. De Maeyer in "Technique of Organic Chemistry: Rates and Mechanisms of Reactions", Vol. VIII, part II, 2nd ed., S.L. Friess, E.S. Lewis and A. Weissberger eds., Wiley Interscience (1963), p. 895.
- 47. H. Diebler, M. Eigen, G. Ilgenfritz, G. Maass and R. Winkler, Pure Appl. Chem., 20, 93 (1969).
- 48. P.B. Chock, Proc. Nat. Acad. Sci., 69, 1939 (1972).
- 49. B.G. Cox, D. Knop and H. Schneider, J. Am. Chem. Soc., <u>100</u>, 6002 (1978).
- 50. G.W. Liesegang, M.M. Farrow, N. Purdie and E.M. Eyring, J. Am. Chem. Soc., 98, 6905 (1976).
- 51. G.W. Liesegang, M.M. Farrow, F.A. Vasquez, N. Purdie and E.M. Eyring, J. Am. chem. Soc., 99, 3240 (1977).
- 52. L.J. Rodriquez, G.W. Liesegang, R.D. White, M.M. Farrow, N. Purdie and E.M. Eyring, J. Phys. Chem., 81, 2118 (1977).
- 53. G.W. Liesegang, M.M. Farrow, L.J. Rodriquez, R.K. Burnham and E.M. Eyring, Int. J. Chem. Kinetics, X, 471 (1978).
- 54. H. Farber and S. Petrucci, J. Phys. Chem., 85, 1396 (1981).
- 55. C.C. Chen and S. Petrucci, J. Phys. Chem., 86, 2601 (1982).
- 56. K.J. Maynard, D.E. Irish, E.M. Eyring and S. Petrucci, J. Phys. Chem., 88, 729 (1984).
- 57. C. Chen, W. Wallace, E.M. Eyring and S. Petrucci, J. Phys. Chem., <u>88</u>, 2541 (1984).
- 58. P. Jagodzinski and S. Petrucci, J. Phys. Chem., 78, 917 (1974).

- 59. H. Farber and S. Petrucci, J. Phys. Chem., 79, 1221 (1975).
- 60. D. Saar, J. Brauner, H. Farber and S. Petrucci, J. Phys. Chem., <u>84</u>, 341 (1980).
- 61. S. Onishi, H. Farber and S. Petrucci, J. Phys. Chem., 84, 2922 (1980).
- 62. P. Lazlo, Progress in NMR Spectrosc., 13, 257 (1980).
- 63. D. Live and S.I. Chan, J. Am. Chem. Soc., 98, 3769 (1976).
- 64. K.H. Wong, G. Konizer and J. Smid, J. Am. Chem. Soc., 92, 666 (1970).
- 65. K.M. Aalmo and J. Krane, Acta Chem. Scand., A36, 219 (1982).
- 66. J.A.A. de Boer, J.W.H.M. Viterwijk, J. Geevers, S. Harkema and D.N. Reinhoudt, J. Org. Chem., 48, 4821 (1983).
- 67. E. Schmidt and A.I. Popov, J. Am. Chem. Soc., 105, 1873 (1983).
- 68. J. Bouquant, A. Deville, J. Grandjean and P. Lazlo, J. Am. Chem. Soc., 104, 686 (1982).
- 69. J.M. Ceraso, Ph. D. Thesis, Michigan State University, East Lansing, MI (1975).
- 70. M. Shamsipur, Ph.D. Thesis, Michigan State University, East Lansing, MI (1979).
- 71. E. Grell, T. Funck and F. Eggers in "Membranes", G. Eisenmann ed., Vol. III, Dekker, New York (1975), p. 1-171.
- 72. M.S. Gutowsky and A. Saika, J. Chem. Phys., 21, 1688 (1953).
- 73. J.W.H.M. Viterwijk, S. Harkema, B.W. Van De Waal, F. Göbel and H.T.M. Nibbeling, J. Chem. Soc., Perkin II, 1843 (1983).
- 74. J.C. Lassegues, M. Fouassier and J.L. Viovy, Mol. Phys., 50, 417 (1983).
- 75. R. Perrin, C. Decoret, G. Bertholon and R. Lamartine, Nouv. J. Chim., 7, 263 (1983).
- 76. E. Weber, J. Org. Chem., 47, 3478 (1982).
- 77. S.J. McLain, J. Am. Chem. Soc., 105, 6355 (1983).
- 78. A. Kaifer, H.D. Durst, L. Echegoyen, D.M. Dishong, R.A. Schultz and G.W. Gokel, J. Org. Chem, 47, 3197 (1982).
- 79. Y. Nakatzuji, T. Nakamura and M. Okahara, Chem. Lett., 1207 (1982).
- 80. Y. Nakatzuji, T. Nakamura, M. Okahara, D.M. Dishong and G.W. Gokel, Tetrahedron Lett., 23, 1351 (1982).

- 81. D.M. Dishong, C.J. Diamond, M.I. Cinoman and G.W. Gokel, J. Am. Chem. Soc., 105, 586 (1983).
- 82. Y. Nakatzuji, T. Nakamura, M. Okahara, D.M. Dishong and G.W. Gokel, J. Org. Chem., 48, 1237 (1983).
- 83. A. Kaifer, L. Echegoyen, D.A. Gutowski, D.M. Goli and G.W. Gokel, J. Am. Chem. Soc., 105, 7168 (1983).
- 84. G.W. Gokel, D.M. Dishong and C.J. Diamond, Chem. Comm., 1053 (1980).
- 85. F.R. Fronczek, V.J. Gatto, R.A. Schultz, S.J. Jungk, W.J. Colucci, R.D. Gandour and G.W. Gokel, J. Amc. Chem. Soc., 105, 6717 (1983).
- 86. G.W. Gokel, D.J. Cram, C.L. Liotta, H.P. Harris and F.L. Cook, J. Org. Chem., 39, 2445 (1974).
- 87. R.N. Greene, Tetrahedron Lett., 1793 (1972).
- 88. R.M. Izatt, B.L. Haymore, J.S. Bradshaw and J.J. Christensen, Inorg. Chem., 14, 3132 (1975).
- 89. R.M. Izatt, D.P. Nelson, J.H. Rytting, B.L. Haymore and J.J. Christensen, J. Am. Chem. Soc., 93, 1619 (1971).
- 90. C.J. Pedersen, Org. Synth., <u>52</u>, 66 (1972).
- 91. P. Gramain and Y. Frère, Nouv. J. Chim., 3, 53 (1979).
- 92. G.E. Hiegel and K.C. Selk, App. Spectrosc., 33, 528 (1979).
- 93. J.A. Riddick and W.B. Bunger, "Techniques of Chemistry Volume II: Organic Solvents", 3rd edition, A. Weissberger ed., Wiley-Interscience, New York (1970), p. 353.
- 94. S. Khazaeli, Ph.D. Thesis, Michigan State University, East Lansing, MI (1982).
- 95. D. Live and S.I. Chan, Anal. Chem., 42, 791 (1970).
- 96. "Handbook of Chemistry and Physics", The Chemical and Rubber Company, 56th edition (1975-1976).
- 97. G.J. Templeman and A.L. Van Geet, J. Am. Chem. Soc., 94, 5578 (1970).
- 98. M.L. Martin, G.J. Martin and J.J. Delpuech, "Practical NMR Spectroscopy", Heyden and Son Ltd., London (1980).
- 99. E.D. Becker, J.A. Ferretti and P.N. Gambier, Anal. chem., <u>51</u>, 1413 (1979).
- 100. J.C. Lindon and A.G. Ferridge, Prog. in NMR Spectrosc., 14, 27 (1980).

- 101. A.I. Popov and A.J. Smetana, J.-P. Kintzinger and T.T. Nguyen, Helv. Chim. Acta, 63, 668 (1980).
- 102. These programs were designed and written by Dr. Thomas V. Atkinson, Department of Chemistry, Michigan State University, East Lansing, MI.
- 103. V.A. Nicely and J.L. Dye, J. Chem. Educ., 48,443 (1971).
- 104. H.B. Thompson and M.T. Rogers, Rev. Sci. Instr., 27, 1079 (1956).
- 105. G.E. Smith, Ph.D. Thesis, Michigan State University, East Lansing, MI (1963).
- 106. M.P. Faber, Ph.D. Thesis, Michigan State University, East Lansing, MI (1961).
- 107. J. Comyn, F.S. Dainton and K.J. Ivin, Electrochim. Acta, 13, 1851 (1968).
- 108. J. Barthel, F. Feuerlein, R. Neueder and R. Wachter, J. Solution Chem., 9, 209 (1980).
- 109. J.D. Lin, Ph.D. Thesis, Michigan State University, East Lansing, MI (1980).
- 110. S. Boileau and P. Sigwalt, Eur. Polym. J., 3, 57 (1967).
- 111. P. Guerin, P. Hemery, S. Boileau and P. Sigwalt, Eur. Polm. J., <u>7</u>, 953 (1971).
- 112. P. Hemery, S. Boileau and P. Sigwalt, Eur. Polym. J., 7, 1581 (1971).
- 113. C. Carvajal, K.J. Tölle, J. Smid and M. Szwarc, J. Am. Chem. Soc., 87, 5548 (1965).
- 114. D.J. Metz and A. Glines, J. Phys. Chem., 71, 1158 (1967).
- 115. V. Gutmann and E. Wychera, Inorg. Nucl. Chem. Lett., 2, 257 (1966).
- 116. V. Gutmann, "The Donor-Acceptor Approach to Molecular Interactions", Plenum Press, New York (1969).
- 117. Pamela Mosier-Boss, Personal communication. To be published.
- 118. D.N. Bhattacharyya, C.L. Lee, J. Smid and M. Szwarc, J. Phys. Chem., 69, 608 (1965).
- 119. M. Chabanel and Z. Wang, J. Phys. Chem., 88, 1441 (1984).
- 120. J.F. Garst in "Solute-Solvent Interactions", Vol. I, J.F. Coetzee and C.D. Ritchie eds., Marcel Dekker, New York (1969), p. 539.
- 121. G. Tersac and S. Boileau, J. Chim. Phys. Physicochim. Biol., <u>68</u>, 903 (1971).

- 122. M.K. Wong and A.I. Popov, J. Inorg. Nucl. Chem., 34, 3615 (1972).
- 123. S. Boileau, P. Hemery and J.C. Justice, J. Solution Chem., <u>4</u>, 873 (1975).
- 124. E. Schori and J. Jagur-Grodzinski, Isr. J. Chem., 11, 243 (1973).
- 125. T.E. Hogen-Esch and J. Smid, J. Phys. Chem., 79, 233 (1975).
- 126. H.P. Hopkins Jr. and A.B. Norman, J. Phys. Chem., 84, 309 (1980).
- 127. D.F. Evans, S.L. Wellington, J.A. Nadis and E.L. Cussler, J. Solution Chem., 1, 499 (1972).
- 128. M. Della Monica, A. Ceglie and A. Agostiano, Electrochim. Acta, 29, 161 (1984).
- 129. R. M. Fuoss and F. Accascira, "Electrolytic Conductance", Interscience, New York (1972).
- 130. J.D. Lamb, Ph.D. Thesis, Brigham Young University, Provo, UT (1978).
- 131. G. Anderegg, Helv. Chim. Acta., 58, 1218 (1975).
- 132. H.K. Frensdorf, J. Am. Chem. Soc., 93, 600 (1971).
- 133. A. Abragam, "The Principles of Nuclear Magnetism", Oxford University Press, London (1961).
- 134. C. Deverell, Progress in NMR Spectrosc., 4, 278 (1969).
- 135. M. ST. J. Arnold and K.J. Packer, Mol. Phys., <u>10</u>, 141 (1966).
- 136. J.-P. Kintzinger and J.-M. Lehn, J. Am. Chem. Soc., 96, 3313 (1974).
- 137. T.E. Burke and S.I. Chan, J. Mag. Res., 3, 55 (1970).
- 138. R.K. Gupta, T.P. Pitner and R. Wasylishen, J. Mag. Res., 13, 383 (1974).
- 139. B.O. Strasser and K. Hallenga, J. Mag. Res., to be published.
- 140. I. Amdur and G.G. Hammes, "Chemical Kinetics. Principles and Selected Topics", McGraw-Hill, New York (1966), p. 147.
- 141. B.O. Strasser, K. Hallenga and A.I. Popov, J. Am. Chem. Soc., to be published.
- 142. K.J. Laidler, "Chemical Kinetics", McGraw-Hill, New York (1965), p.
- 143. W.F.K. Wynne-Jones and H. Eyring, J. Chem. Phys., 3, 493 (1935).
- 144. M. Menzinger and R. Wolfgang, Angew. Chem. Int. Ed. Engl., 8, 438 (1969).

- 145. D.P. Shoemaker, C.W. Garland and J.I. Steinfeld, "Experiments in Physical Chemistry", 3rd ed., McGraw-Hill, New York (1974), p. 53.
- 146. R.R. Ernst and W.A. Anderson, Rev. Sci. Instr., <u>37</u>, 93 (1966).